EBI2 is a negative modulator of adipose tissue activity

Dissertation zur
Erlangung des Doktorgrades (Dr. rer. nat.)
der
Mathematisch-Naturwissenschaftlichen Fakultät
der
Rheinischen Friedrich-Wilhelms-Universität Bonn

vorgelegt von

Francesca Copperi

aus Ciriè (TO), Italien

Bonn 2020

Angefertigt mit Genehmigung der Mathematisch-Naturwissenschaftlichen Fakultät der Rheinischen Friedrich-Wilhelms-Universität Bonn.

1. Gutachter: Prof. Dr. Alexander Pfeifer

2. Gutachter: Prof. Dr. Evi Kostenis

Tag der Promotion: 04. August 2020

Erscheinungsjahr: 2020

ACKNOWLEDGEMENTS

The path toward this dissertation has been meandering.

My gratitude goes first to my supervisor Prof. Alexander Pfeifer for this opportunity, for his patience, and for his guidance through my Ph.D. study, and whose teachings have extended beyond science. I would also like to thank my second supervisor Prof. Evi Kostenis for the helpful discussions.

Thanks to Dr. Mies-Klomfass and Dr. Thorsten Gnad for revising this thesis, to the whole GRK1873, to the DFG (Deutsche Forschungsgemeinschaft) for funding this project, and of course to the thesis committee members.

I would like to recognize the invaluable assistance of all the people who contributed to this research: Dr. Loren M. Brown for introducing me to the project, Prof. Dieter Lütjohann and Anja Kerksiek for their tireless help, Prof. Giulio Muccioli, Patricia Zehner, Prof. Caroline Pot and Duc Donovan, Prof. Martin Klingenspor and Sabine Mocek, and Dr. Florian Kurschus for his precious support. Thanks to all the students who worked with me and in particular to Inna Schleis.

Heartfelt thanks to Laura for sharing the good and brightening the bad moments of this journey, I could not have asked for a better comrade-in-arms. A special thanks to the great “Office 006” mates Deborah and Ben, to Davide and Gerburg for their help and advices, and to all the friends I found in this working group.

Finally, to all the special people (and cat) in my life who have been there for me during these years: thank you.

TABLE OF CONTENTS

ABBREVIATIONS

%	Percent
°C	Degrees Celsius
µ	Microgram
µl	Microliter
24(S)-HC	24(S)-hydroxycholesterol
25-OH	25-hydroxycholesterol
27-OH	27-hydroxycholesterol
7-kCh	7-ketocholesterol
7TM	Seven-transmembrane domain
7α,25-OHC	7alpha,25-dihydroxycholesterol
7α,25-OHC	7alpha,25-dihydroxycholesterol
7α,27-OHC	7alpha,27-dihydroxycholesterol
7α-OH	7alpha-hydroxycholesterol
7β,25-OHC	7beta,25-dihydroxycholesterol
7β-OH	7beta-hydroxycholesterol
8-Br-cGMP	8-Bromoguanosine 3',5'-cyclic monophosphate
AC	Adenylate cyclase
AD	Alzheimer's disease
AGS	Activator of G protein signaling
ANOVA	Analysis of variance
ATGL	Adipocyte triglyceride lipase
ATP	Adenosine triphosphate
BA	Brown adipocytes
BAT	Brown adipose tissue
BBB	Blood brain barrier
BSA	Bovine serum albumin
CAD	Coronary artery disease
cAMP	3',5'-cyclic adenosine monophosphate
cDNA	Complementary deoxyribonucleic acid
CH25H	Cholesterol 25-hydroxylase
CHO	Chinese hamster ovary cells
CNS	Central nervous system
CYP27A1	Sterol 27-hydroxylase
CYP7B1	25-hydroxycholesterol 7-alpha-hydroxylase
DAG	Diacylglycerol
DIO	Diet induced obesity

DMEM	Dulbecco's Modified Eagle Medium
DMSO	Dimethyl sulfoxide
EBI2	Epstein-Barr virus-induced G protein coupled receptor 2
EBV	Epstein-Barr virus
ECL	Enhanced chemiluminescence
ECLs	Extracellular loops
ER	Endoplasmic reticulum
ERK1/2	Extracellular signal-regulated kinases 1/2
EtOH	Ethanol
Fabp4/aP2	Fatty acid-binding protein 4
FBS	Fetal bovine serum
FDA	Food and drug administration
FFA	Free fatty acids
g	Gram
GAP	GTPase-activating protein
GDI	Guanine nucleotide dissociation inhibitor
GDP	Guanosine diphosphate
GEF	Guanine nucleotide exchange factor
GIRK	G protein-coupled inwardly-rectifying potassium channels
GPCR	G protein-coupled receptor
GRK	G protein-coupled receptor kinase
GTP	Guanosine-5'-triphosphate
h	Hour
HE	Hematoxylin/Eosin
HFD	High fat diet
Hprt	Hypoxanthine-guanine phosphoribosyltransferase
HRP	Horseradish peroxidase
HSL	Hormone sensitive lipase
IBMX	3-isobutyl-1-methylxanthine
IP3	Inositol 1,4,5-trisphosphate
KO	Knockout
M	Molar
mA	Milliampere
mg	Milligram
min	Minutes
ml	Milliliter
mM	Millimolar
mRNA	Messenger ribonucleic acid

NAFLD	Non-alcoholic fatty liver disease
ND	Normal diet
NE	Norepinephrine
NE	Norepinephrine
ng	Nanogram
nM	Nanomolar
NPC	Niemann-Pick type C disease
NST	Non-shivering thermogenesis
PBS	Phosphate-buffer saline
PCR	Polymerase chain reaction
PGC-1α	Peroxisome proliferator-activated receptor-gamma coactivator-1alpha
PGK	Phosphoglycerate kinase
PI3K	Phosphoinositide 3-kinases
PIP2	Phosphatidylinositol 4,5-bisphosphate
PKA	Protein kinase A
PKC	Protein kinase C
PLCβ	Phospholipase C-beta
Pparg/PPARγ	Peroxisome proliferator-activated receptor gamma
PT	Pertussis Toxin
PVAT	Perivascular adipose tissue
rcf	Relative centrifugal force
RGS	Regulators of G protein signaling
RNA	Ribonucleic acid
ROCK	Rho-kinase
ROS	Reactive oxygen species
rpm	Round per minute
RT	Room temperature
RTK	Receptor tyrosine kinase
RT-qPCR	Reverse transcription quantitative polymerase chain reaction
s.e.m.	Standard error of the mean
SNS	Sympathetic nervous system
SVF	Stromal vascular fraction
T2D	Type 2 diabetes
TD-NMR	Time-Domain Nuclear Magnetic Resonance
TG	Triglycerides
TriolCh	Cholestane-3beta,5,6beta-triol
UCP1	Uncoupling protein 1
UV	Ultraviolet

V	Volts
WA	White adipocytes
WAT	White adipose tissue
WATg	Gonadal white adipose tissue
WATi	Inguinal white adipose tissue
WT	Wildtype

TABLE OF FIGURES

1 | INTRODUCTION

1.1 | GPCRs

1.1.1 | Characteristics and mechanism of signal transduction

G protein-coupled receptors (GPCRs), also known as seven-transmembrane domain receptors (7TM receptors) are the largest family of receptors in many organisms, including mice, humans and worms (but not in prokaryotes). GPCRs consist of seven transmembrane spanning segments, which position the N-terminus of the protein outside of the cell and the C-terminus inside, and the ability to bind and interact with G proteins.

GPCRs activity and signaling are involved in regulating multiple fundamental biological processes, from embryonal development to heart and brain function, as well as in many diseases (Wettschureck and Offermanns, 2005). Also for this reason, GPCRs are one of the main families of drug targets: indeed, 34% of the drugs approved by FDA (Food and drug administration) target 108 GPCRs (and 66 are currently in clinical trial), with a global sales volume estimated to be 180 billion of US dollars as of 2018 (Hauser et al., 2018).

GPCRs can bind a large number of ligands, such as proteins, small molecules, hormones and photons. The ligands bind at the receptors' N-terminus and extracellular loops (ECLs) or at the transmembrane region (Basith et al., 2018), thus initiating a conformational change of the receptor and the propagation of the signal intracellularly. The effectors of the GPCRs activation are the heterotrimeric G proteins, consisting of three subunits named G_α, G_β and G_γ. G_α and G_γ are typically anchored to the cell membrane by the N-terminus, whereas G_β is anchored to G_γ by hydrophobic interaction (Higgins and Casey, 1994; Vögler et al., 2008). G_α subunits are small GTPases able to catalyze the hydrolysis of GTP to GDP. The activated GPCRs act as guanine nucleotide exchange factors (GEFs) and exchange GDP to GTP in the G_α subunit. Upon activation, G_α changes its conformation and separates from the $G_{\beta\gamma}$ dimer. The subunits are then free to interact with downstream targets. When G_α hydrolyzes GTP to GDP it becomes inactivated and thus able to re-associate with $G_{\beta\gamma}$. This process represents a full GPCR G protein cycle (Figure 1).

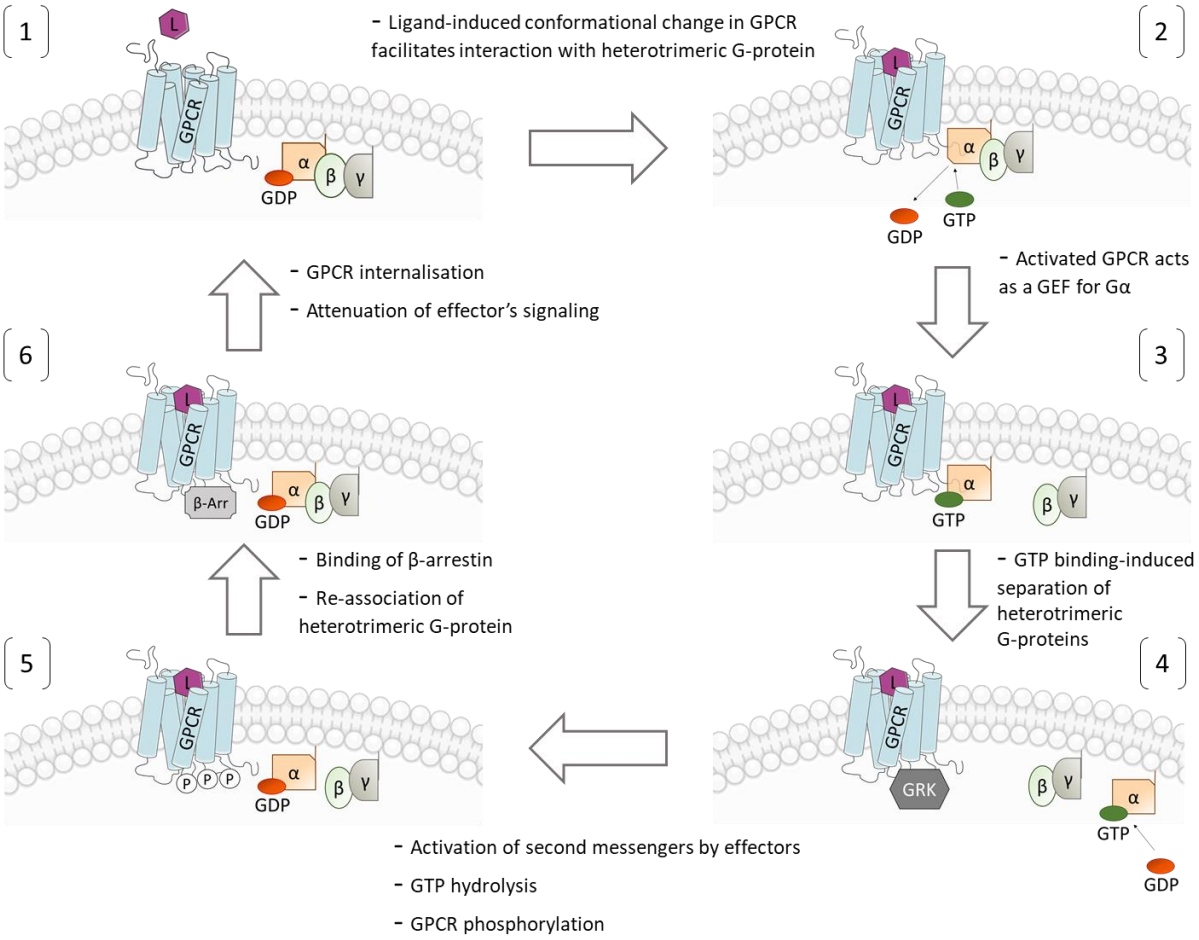

Figure 1: GPCR cycle

(1*) The inactive GPCR binds its ligand, which induced conformational changes and allows the interaction with heterotrimeric G-proteins. (2) The GPCR acts as GEF on the Gα subunit, promoting the exchange of GDP with GTP. (3) The biding of the Gα subunit with GTP induces the separation of the Gα subunit from the Gβγ dimer. (4,5) Gα subunit separates from the GPCR and hydrolyses GTP to GDP, promoting downstream signaling cascade through second messengers. GRK binds the GPCR and phosphorylates. (6) β-arresting binds to phosphorylated GPCR and induces GPCR internalization. The GDP-bound Gα subunit binds to the Gβγ dimer, forming again the inactive heterodimer. Adapted from* Hanlon and Andrew, 2015.

G_α proteins are divided in four subclasses, each targeting a specific downstream signaling cascade (Wettschureck and Offermanns, 2005): $G_{\alpha s}$, $G_{\alpha i/o}$, $G_{\alpha q/11}$, and $G_{\alpha 12/13}$. Previous models have suggested that each GPCR interacts with only one type of G_α subunits, but it is now established that a single GPCR can interact with multiple G_α proteins, albeit with specific preferences for one (Cerione et al., 1985).

Since G_α proteins are weak GTPases, the process of GTP hydrolysis can be accelerated by regulators of G protein signaling (RGS) molecules, which are a type of GTPase-Activating Protein

(GAP) (De Vries et al., 2000). Conversely, activators of G protein signaling (AGS) can act as GEFs to G_α to prolong the signaling (Vögler et al., 2008). G_α can also be activated by other GEFs non associated with GPCR signaling pathways (e.g. the receptor tyrosine kinase (RTK) pathway) (Garcia-Marcos et al., 2015). Additionally, some AGS proteins act as guanine-nucleotide-dissociation inhibitors (GDIs), causing G_α to remain in a GDP-bound state and preventing reassociation of the $G_{\beta\gamma}$ subunit with the G_α. Finally, the GPCRs conformational changes upon ligand binding allows accessibility for phosphorylation by G protein-coupled receptor kinases (GRKs) (Palczewski et al., 1991). $G_{\beta\gamma}$ is able to recruit a GRK to the GPCR, thus establishing a negative-feedback loop (Luttrell et al., 1999). The phosphorylation induced by GRKs results in the binding of β-arrestin, which then promotes the receptor internalization (Drake et al., 2006). GPCRs are divided into two classes depending upon how strongly they maintain β-arrestin binding: class A GPCRs lose β-arrestin following internalization and can be dephosphorylated and recycled back to the cell surface (Oakley et al., 2000); class B receptors maintain β-arrestin binding, which stimulates ubiquitylation of the GPCR and drives it to the lysosomes for degradation (Figure 1).

1.1.2 | Downstream signaling

GPCRs can activate different downstream signaling cascades: the four types of G_α subunits signal via three different signaling pathways, whereas the $G_{\beta\gamma}$ subunit can have multiple effectors and work exclusively or synergistically with the G_α subunit (Clapham and Neer, 1997).

$G_{\alpha s}$ and $G_{\alpha i/o}$: The effector of both the $G_{\alpha s}$ and $G_{\alpha i/o}$ pathways is the cyclic-adenosine monophosphate (cAMP)-generating enzyme adenylate cyclase (AC), which catalyzes the conversion of cytosolic adenosine triphosphate (ATP) to cAMP. The interaction of the AC with $G_{\alpha s}$ subunits stimulates the production of cAMP, whereas $G_{\alpha i/o}$ has an inhibitory effect. cAMP is a ubiquitous second messenger and it can work by activating protein kinase A (PKA), by regulating the function of ion channels such as the HCN channels and other cyclic nucleotide-binding proteins such as Epac1 and RAPGEF2.

$G_{\alpha q/11}$: The effector of the $G_{\alpha q/11}$ pathway is phospholipase C-β (PLCβ). PLCβ cleaves the membrane-bound phosphatidylinositol 4,5-bisphosphate (PIP2) into the second messengers inositol (1,4,5) trisphosphate (IP3), and diacylglycerol (DAG). IP3, through the IP3 receptors on the endoplasmic reticulum (ER), elicits Ca^{2+} release from the ER, while DAG diffuses along the plasma membrane where it activates a second ser/thr kinase called protein kinase C (PKC). The increase of Ca^{2+} itself can activate as well PKC, together with other proteins as calmodulins.
$G_{\alpha 12/13}$: The effectors of $G_{\alpha 12/13}$ are three RhoGEFs (p115-RhoGEF, PDZ-RhoGEF, and LARG), which in turn activate the small GTPase Rho. Once activated, Rho can activate various proteins responsible for cytoskeleton regulation such as Rho-kinase (ROCK) (Dhanasekaran and Dermott, 1996).

$G_{\beta\gamma}$: As mentioned previously, the effectors of $G_{\beta\gamma}$ are various and not yet fully investigated. The most common effectors are ion channels, such as G protein-regulated inwardly rectifying K^+ channels (GIRKs) (Logothetis et al., 1987), P/Q- and N-type voltage-gated Ca^{2+} channels (Ikeda, 1996), as well as some isoforms of AC and PLC (Li et al., 2000; Tang and Gilman, 1991), along with some phosphoinositide-3-kinase (PI3K) isoforms (Li et al., 2000; Stephens et al., 1997).

1.2 | Oxysterols

1.2.1 | Characteristics of oxysterols and oxysterol metabolism

Oxysterols are 27-carbons molecules made of a steroid backbone and a 6-methylheptan-2-yl side chain. The carbon in position 3 of the steroid part can be substituted either by a hydroxyl group or by a ketone group. Additionally, the 3-hydroxyl group can be esterified or sulfurized. Traditionally, oxysterols are identified as hydroxylated forms of cholesterol, and thus also called hydroxycholesterols: however, not only hydroxylated compounds belong to the oxysterol family, but also oxysterols with a ketone group, epoxides, or with two different groups (e.g. hydroxyl and ketone group).
Oxysterols can be formed from cholesterol or from other oxysterols by free radical oxidation or by enzymatic mechanisms. The free radical oxidation occurs when a hydrogen atom is abstracted from position C-7 by reactive oxygen species (ROS) such as $OH^{\bullet}$ or reactive nitrogen species such

as $ONOO^-$ (Iuliano, 2011; Yin et al., 2011). Also the carbons C-20 and C-25 have been shown *in vitro* to be prone to free radical oxidation (Yin et al., 2011), but no reports suggest this reaction could happen *in vivo*. On the other hand, the enzymatic mechanisms leading to oxysterols formation are multiple and complex, and lead to a large variety of different oxysterols. Three main groups of enzymes carry the enzymatic reactions involved in oxysterols metabolism: oxidoreductases (i.e. cytochromes P450, cholesterol hydroxylase, hydroxysteroid dehydrogenases and squalene epoxidase), hydrolases (i.e. cholesterol epoxide hydrolase, cholesterol esterase) and transferases (i.e. hydroxysteroid sulfotransferases, acyl-CoA cholesterol transferase, lecithin-cholesterol acyltransferase).

Because of this complex system of multiple non-enzymatic and enzymatic reactions, the metabolism of oxysterols cannot be oversimplified in a linear and simple series of reactions: indeed many enzymes can catalyze the formation of a given oxysterol, the same oxysterol can be formed from different substrates (e.g. 7-ketocholesterol can be formed from cholesterol, dehydrocholesterol, and 7β-OH), and for some oxysterols (e.g. 7α-OH) part of their origin can be explained by both enzymatic and non-enzymatic (ROS).

1.2.2 | Oxysterols in human diseases

Several oxysterols are important mediators in many pathological conditions. Far from being considered only as intermediate metabolite between cholesterol and bile acids, oxysterol levels have been studied and linked to several diseases.

Metabolic syndrome and obesity: Numerous studies have underlined the role of cholesterol metabolism in the development of obesity and related comorbidities (Lupattelli et al., 2011; Van Rooyen et al., 2013). Since oxysterols are one of the main cholesterol metabolites, the interest in investigating their influence as treatment or markers in such conditions increased in the last few years. Recent studies characterized the changes of oxysterols and the enzymes involved in their production both in obese mouse models and in obese humans (Guillemot-Legris et al., 2016a; Tremblay-Franco et al., 2015; Wooten et al., 2014). Profound changes were identified in oxysterols levels in multiple organs and tissues such as liver, adipose tissue, hypothalamus and

plasma during and after the development of obesity (Guillemot-Legris et al., 2016a; Wooten et al., 2014). Additionally, a markedly different profile of oxysterols was observed between lean and obese patients (Tremblay-Franco et al., 2015). Thus, oxysterols emerged as possible players in the development of metabolic syndrome and obesity, but the specific role of single oxysterols in the development of such pathological conditions as well as their possible use in treatments has not been investigated so far.

Coronary artery disease (CAD) and atherosclerosis: Atherosclerosis is a chronic inflammatory condition of arterial tree that may lead to intimal destruction, arterial thrombosis and end-organ ischemia (Zmysłowski and Szterk, 2017). Extensive research has been conducted on the role of oxysterols in the initiation and progression of this disease, indicating that oxysterols from autoxidized cholesterol induce significant apoptosis or necrosis in vascular cells (Ares et al., 2000; Lizard et al., 1996; Yuan et al., 2000). Moreover, oxysterols concentrations have been found up to 100 times higher in atherosclerotic plaques than in human plasma (Brown and Jessup, 1999). To date, many diagnostic tools are available to identify the presence of atherosclerosis and CAD, from imaging tests to blood tests. However, there is currently a lack of markers that could potentially be used to identify atherosclerosis and CAD at the very early stages: thus, oxysterols have been proposed for this purpose.

Niemann-Pick type C disease (NPC): NPC is a rare neurovisceral disorder (1 in 120 000-150 000 people) characterized by progressive hepatosplenomegaly and CNS neurodegeneration (Chang et al., 2005). In NPC cholesterol accumulates in late endosomal/lysosomal structures (Ory, 2000), where it gets oxidized by enzymatic and non-enzymatic reactions (Ribas et al., 2012). Two specific oxysterols, cholestane-3β,5,6β-triol (triolCh) and 7-ketocholesterol (7-kCh), are increased in the plasma of NPC patients (Jiang et al., 2011; Tint et al., 1998). TriolCh and 7-kCh are currently proposed as early biomarkers for NPC and as primary test in confirming of suspicious NPC (Reunert et al., 2016; Vanier et al., 2016).

1.3 | EBI2 and its ligand 7α,25-dihydroxycholesterol

The G protein-coupled receptor Epstein-Barr virus induced gene 2 (EBI2), also known as GPR183, was identified in 1993 as a highly upregulated gene in B-cells upon infection with Epstein-Barr virus (Birkenbach et al., 1993). In the years following its identification, EBI2 has been shown to be expressed in many other cell types of the hematopoietic lineage such as T cells, natural killer cells, monocytes, macrophages, dendritic cells, neutrophils, eosinophils, platelets and osteoclasts (Amisten et al., 2008; Heinig et al., 2010; Nevius et al., 2015; Novershtern et al., 2011; Rutkowska et al., 2015; Shen et al., 2015).

In 2006 EBI2 was shown to be a $G_{\alpha i}$ coupled receptor: cells transfected with the receptor were found to have a decreased production of forskolin induced cAMP and a reduced activity of the transcription factor cAMP response element binding protein in a Pertussis toxin-sensitive manner (Rosenkilde et al., 2006). Later, EBI2 was shown also to induce ERK1/2 phosphorylation and to recruit β-Arrestin (Benned-Jensen et al., 2011, 2013; Hannedouche et al., 2011; Liu et al., 2011).

For many years after its identification, the receptor remained orphan, i.e. no endogenous ligand able to activate it was known. In 2011 the EBI2 ligand was identified independently by two groups from Novartis and Johnson & Johnson (Hannedouche et al., 2011; Liu et al., 2011). By treating cells with extract from septic sheep liver and rat spleen respectively, they were able to induce EBI2-specific signaling. With chromatography and mass spectrometry techniques, they identified EBI2 ligands to be oxysterols. The three most potent oxysterol ligands for EBI2 were determined by both groups to be 7α,25-dihydroxycholesterol (7α,25-OHC), 7α,27-OHC, and 7β,25-OHC. The EC50-values for these ligands were calculated via GTPγS assays on CHO cells to be 0.14, 1.3, and 2.1 nM, respectively. Together with these oxysterols, other oxysterols as 7α-OH and 25-OH were able to activate EBI2 as well, but with considerably lower potencies.

The biosynthetic pathway of 7β,25-OHC is poorly characterized, whereas the reactions and enzymes leading to the formation of 7α,25-OHC and 7α,27-OHC are well known. 7α,25-OHC is generated through the subsequent action of two hydroxylases (Figure 2): the first hydroxylation is catalyzed by the enzyme CH25H, that forms 25-OH from cholesterol, and the second by CYP7B1, an enzyme of the cytochrome P450 superfamily that converts 25-OH in 7α,25-OHC. Similarly, 7α,27-OHC is generated stepwise by the enzymes CYP27A1 and CYP7B1 (Figure 2, below) (Russell,

2003). Since different immune cells upregulate EBI2, CH25H and CYP7B1 when treated with lipopolysaccharides (LPS), whereas the levels of CYP27A1 decrease, 7α,25-OHC and not 7α,27-OHC was hypothesized to be the main ligand of EBI2 (Liu et al., 2011). This hypothesis was confirmed by using mice deficient for CH25H (Hannedouche et al., 2011) or treated with clotrimazol, a CYP7B1 inhibitor (Liu et al., 2011): in both cases, the effects on B cells were comparable to the effects on EBI2 knockout mice, thus indicating that 7α,25-OHC is the main endogenous ligand of EBI2.

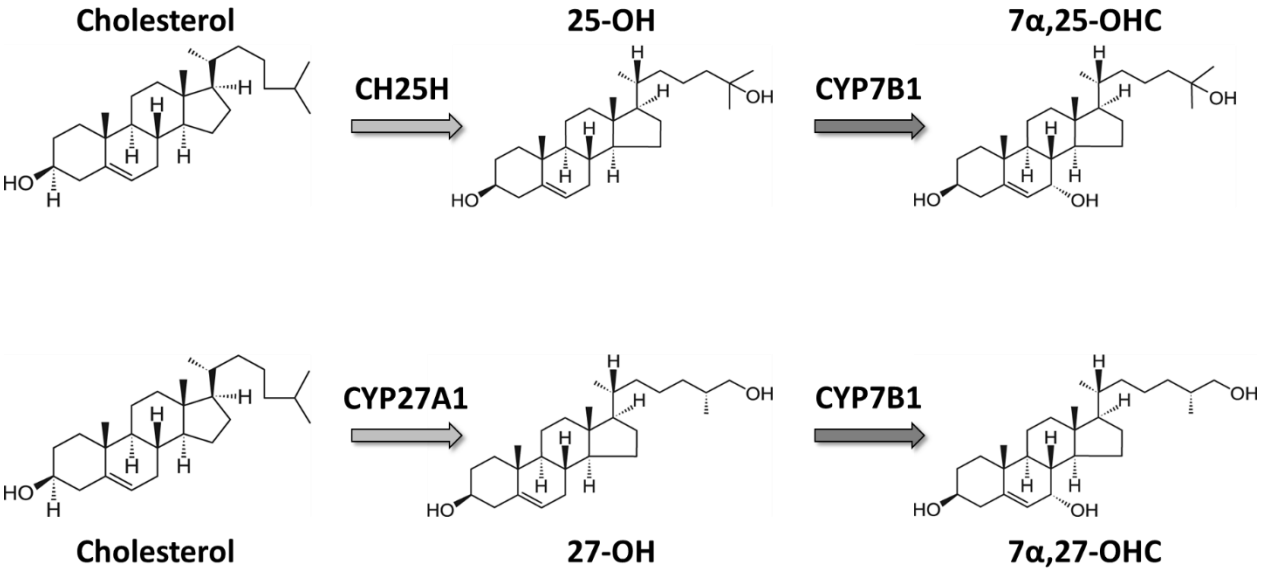

Figure 2: Biosynthetic pathway of 7α,25-OHC and 7α,27-OHC

Biosynthetic pathway leading to the formation of 7α,25-OHC (above) and 7α,27-OHC (below) from cholesterol.

Besides its endogenous ligand, a number of small molecules has been developed to agonize and antagonize EBI2 (Ardecky et al., 2010; Benned-Jensen et al., 2011, 2013; Deng et al., 2016): among the others, a potent and selective antagonist named NIBR189 was identified (Gessier et al., 2014).

1.4 | Adipose tissues and metabolic diseases

1.4.1 | Characteristics of adipocytes and adipose tissues

In mammals, three types of adipose tissue can be found, the white adipose tissue (WAT), the brown adipose tissue (BAT), and an intermediate type named “beige” or “brite” (for brown-in-white) adipose tissue, which have different morphology, distribution, gene expression, and function.

BAT is present in almost all mammals, and especially active in newborns and hibernating animals (Gesta et al., 2007). Originally, BAT was thought to be present in humans during the neonatal period only. However, further studies proved that adults retain some metabolically active depots of BAT that respond to cold and sympathetic activation of the nervous system (Cypess et al., 2009; van Marken Lichtenbelt et al., 2009; Nedergaard et al., 2007; Virtanen et al., 2009; Zingaretti et al., 2009). In adult humans, it localizes mostly in the supraclavicular, paravertebral, mediastinal, para-aortic and suprarenal areas (van Marken Lichtenbelt et al., 2009). The BAT consists of brown adipocytes (BA) and the remaining stromal vascular fraction (SVF), formed by preadipocytes, fibroblasts, vascular endothelial cells and immune cells such as adipose tissue macrophages. BA are characterized by multilocular morphology, abundancy of small lipid droplets, high number of mitochondria and enrichment of uncoupling protein-1 (UCP1) (Aherne and Hull, 1966; Cannon and Nedergaard, 2004). The main function of BAT is to dissipate the stored energy in form of heat in a process called non-shivering thermogenesis (NST).

WAT consists mostly of two subtypes: subcutaneous and visceral. Subcutaneous and visceral fat have different molecular, cellular, and anatomical features (Wajchenberg, 2000): subcutaneous adipose tissue presents higher levels of leptin compared to visceral, it is less sensitive to insulin effect and has smaller capacity to mobilize free fatty acids (Hellmér et al., 1992; Montague et al., 1997).

Subcutaneous WAT can also undergo a process called “browning” or “beiging” in response to β-adrenergic stimulus (e.g. during cold), modifications of gut microbiota (Carrière et al., 2014; Li et al., 2017), exercise (Knudsen et al., 2014; Schlein et al., 2016), and endogenous modulators as parathyroid hormone and bile acids (Kir et al., 2014; Worthmann et al., 2017). In response to one

or more of these stimuli, WAT acquires intermediate characteristics between white and brown fat (e.g. by expressing UCP1 and increasing mitochondrial biogenesis) (Cousin et al., 1992; Harms and Seale, 2013; Ikeda et al., 2018; Young et al., 1984).

The main cell type present in WAT are white adipocytes (WA). WA present variable size, in general between 25 and 200 μM, a unilocular lipid droplet, a peripheral and flat nucleus, few mitochondria and low oxidative rate, and great capacity of storing energy in form of triglycerides (TG) (Jeanson et al., 2015; Tan and Vidal-Puig, 2008). In addition to adipocytes, WAT contains macrophages, leukocytes, fibroblasts, cell progenitors, and endothelial cells.

1.4.2 | Lipid metabolism and mobilization in adipose tissue

One of the main function of ATs is to provide energy to the organism when needed. Indeed, ATs can store triglycerides (TGs) in a process called lipogenesis, and release free fatty acids (FFAs), a processed called lipolysis. Systemically, the lipogenic pathway is induced by feeding, while the lipolytic by fasting (Figure 3).

Lipogenesis comprises both *de novo* FFAs synthesis and TGs synthesis. During feeding, the pancreas releases insulin. Insulin stimulates glucose uptake in the adipocytes, activates glycolytic and lipogenic enzymes, and stimulates the expression of genes required for cholesterol, fatty acids, TG and phospholipid synthesis (Assimacopoulos-Jeannet et al., 1995; Ferré and Foufelle, 2007). The glucose from the circulation, following insulin stimulus, provides both Acetyl-coA and glycerol for FFAs and TGs synthesis. FFAs are synthetized with the addition of two carbon units to Acetyl-CoA. TGs synthesis occurs by esterification of FFAs, from the circulation or *de novo* synthetized, to glycerol. The lipogenesis process does not only provide the organism with a fuel reservoir, but also clears the plasma from FFAs and TGs avoiding them to deposit in other organs (e.g. skeletal muscle and liver), and buffers lipotoxicity and insulin resistance (Frayn, 2002).

Lipolysis, oppositely to lipogenesis, is induced by fasting and supplies glycerol for hepatic gluconeogenesis, and free fatty acids for oxidation according to energy needs in other organs and for ketone body formation in case of low glucose intake. Decreased levels of insulin during fasting suppresses lipogenesis and activates lipolysis, as well as increased levels of glucagon. Lipolysis in mediated by the release of catecholamines by the sympathetic nervous system (SNS) and activate

β-adrenergic receptors on adipocytes. As a consequence of these stimuli, the increase of intracellular cAMP and PKA activation in the adipocytes leads to the metabolism of TGs to glycerol and FFAs by adipocyte triglyceride lipase (ATGL) and hormone-sensitive lipase (HSL) (Haemmerle et al., 2002; Zimmermann et al., 2004). Glycerol and FFAs are then released in the blood flow, whereas FFAs only can undergo to further β-oxidation and be used by BAs as substrate for thermogenesis.

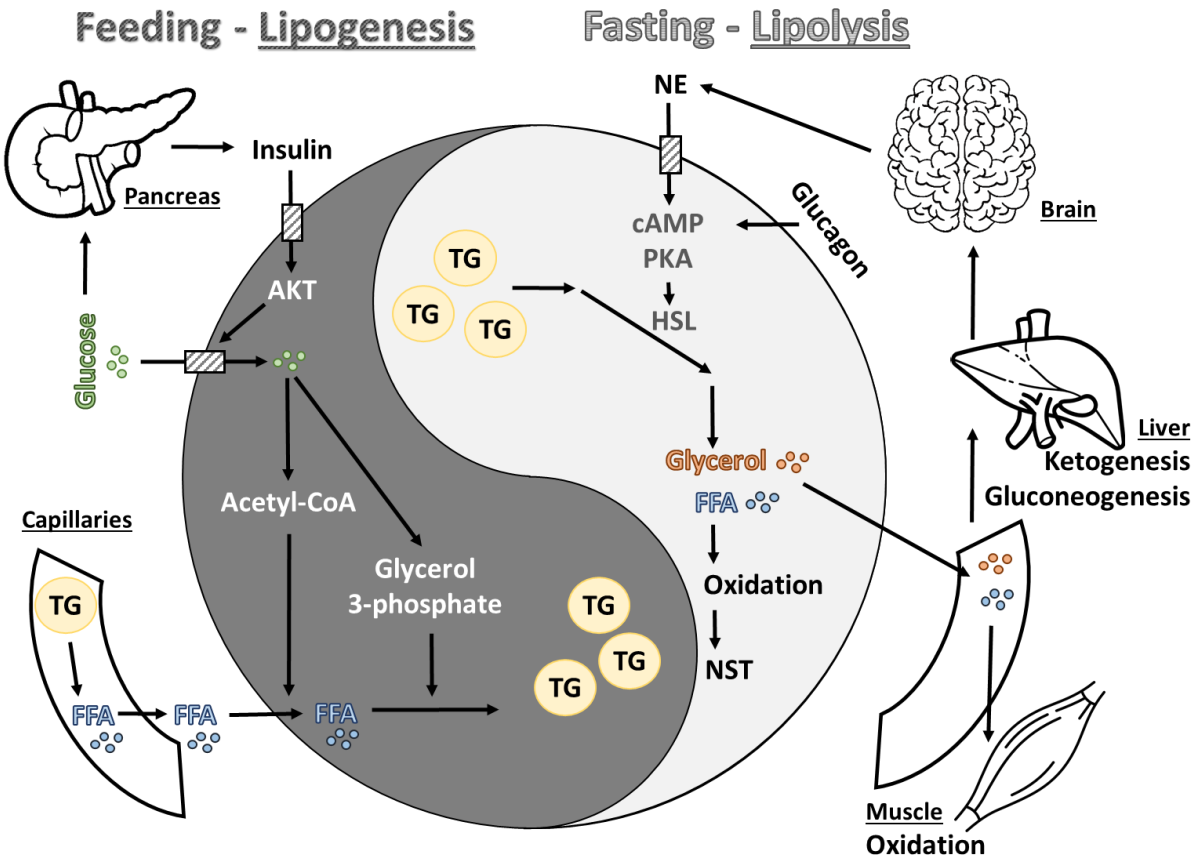

Figure 3: Schematic representation of lipogenesis and lipolysis in adipocytes

Graphical representation of lipogenesis (left part) and lipolysis (right part) in adipocytes. Lipogenesis: Increase of glucose induces release of insulin from the pancreas. Insulin activates its receptors and promotes glucose uptake in adipocytes and its metabolism to Acetyl-CoA and Glycerol 3-phosphate. Meanwhile, TG are metabolized to FFAs and uptaken by adipocytes, where, together with Acetyl-CoA and Glycerol 3-phosphate promotes the synthesis of TGs. Lipolysis: Stimuli from the brain lead to SNS activation and release of NE. NE promotes increase of cAMP intracellular levels in adipocytes, PKA is activated and through HSL TGs are metabolized to glycerol and FFAs. Glycerol and FFAs can be released in the blood flow and serve as substrate for oxidation in muscle or ketogenesis and glucogenesis in the liver, or used for oxidation and NST in adipocytes, especially BA. TG: triglycerides; FFAs: free fatty acids; NE: norepinephrine; cAMP: cyclic adenosine monophosphate; PKA: protein kinase A; HSL: hormone sensitive lipase. NST: non-shivering thermogenesis. Modified from Luo and Liu, 2016.

1.4.3 | Thermogenic function of adipose tissue and implications for metabolic health

One of the main features of brown and beige ATs is the ability to dissipate energy in the form of heat through a processed called non-shivering thermogenesis (NST). The NST is induced by SNS activation. The sympathetic fibers that innervate the ATs release norepinephrine (NE) that binds to the β_3-adrenergic receptors on the adipocytes, initiating the process of lipolysis described in the previous chapter. The FFAs produced activate a protein on the mitochondrial inner membrane called uncoupling protein-1 (UCP1) or thermogenin (Fedorenko et al., 2012; Rial et al., 1983). This causes an influx of H^+ into the matrix of the mitochondrion along proton gradient and bypasses the ATP synthase channel. Consequently, oxidative phosphorylation is uncoupled, and the energy from the proton motive force is dissipated as heat. Together with UCP1 activation, *Ucp1* gene expression increases through cAMP-induced modulation of the Peroxisome proliferator-activated receptor-g coactivator-1α (PGC-1α) (Villarroya et al., 2017).

Because of the ability of BAT to dissipate energy in form of heat, brown and beige ATs have been proposed as therapeutic targets to treat obesity and related diseases, such as type 2 diabetes. Even though in humans the contribution of BAT in the resting metabolic rate is estimated to be about 1-5%, it is speculated to reach up to 16% when stimulated (Moonen et al., 2019): for this reason, the interest in understanding new mechanisms to modulate BAT activity increased in the last few years, aiming to find new pharmacological therapies to modulate energy expenditure. Approaches to increase BAT activation via noradrenergic stimulation had so far very limited success due to multiple reasons: differences in the binding characteristics of β_3-adrenergic receptor of selective agonists between humans and rodents, poor oral availability and pharmacokinetic, and time-limited efficacy (Arch, 2008; Clapham and Arch, 2007; Larsen et al., 2002). However, β_3-adrenergic receptor agonists continue to be of great interest, with new molecules such as mirabegron (Cypess et al., 2015).

The advancement in understanding new pathways for BAT activation increased also the attention on non-adrenergic pharmacological targets. Valuable examples are the mesodermal growth factor BMP-7 and FGF-21, which can stimulate BAT growth and reduce weight gain when expressed in mice (Kharitonenkov et al., 2005; Schlein et al., 2016; Tseng et al., 2008).

However, only a very limited number of drugs is currently approved for obesity treatment in humans (González-Muniesa et al., 2017), thus increasing the interest in finding new modulators of ATs activity.

2 | AIM AND OBJECTIVES

The aim of this research is to elucidate the role of EBI2, the receptor for the oxysterol 7α,25-OHC, in brown adipocytes and adipose tissue. Thus, the following questions will be addressed:

1. Does EBI2 activation or lack of EBI2 affect brown adipocytes *in vitro*? Through which mechanism and signaling pathway does EBI2 regulate brown adipocytes activity?
2. Does EBI2 activation or lack of EBI2 affect adipose tissues activity *ex vivo*?
3. What is the effect of EBI2 activation or lack of EBI2 on the whole-body metabolism of mice? Is EBI2 involved in adipose tissue activation in response to cold? Does EBI2 affect the development of diet-induced obesity?

To investigate these aspects, the endogenous EBI2 ligand 7α,25-OHC and its antagonist NIBR189 will be used, as well as a genetic mouse model lacking for EBI2 (EBI2 global knockout mice).

3 | MATERIALS AND METHODS

3.1 | Common materials and equipment

- 96-well plates (Sarstedt, Cat. No. 83.3924)
- Acetic acid (Carl Roth, Cat. No. KK62)
- Autoclave, Varioklav 135 T (Faust)
- Bovine Serum Albumin, BSA (Carl Roth, Cat. No. 8076)
- Calcium chloride, $CaCl_2$ (Carl Roth, Cat. No. A119)
- Centrifuge (Eppendorf, Cat. No. 5415R)
- Centrifuge cell culture
- Chloroform (Carl Roth, Cat. No. Y015)
- Conical tubes, 15 ml and 50 ml volume (Sarstedt, Cat. No. 62.554.502, 62.547.254)
- D-(+)-Glucose (Sigma Aldrich, Cat. No. G8270)
- Dimethyl sulfoxide, DMSO (Carl Roth, Cat. No. 7029)
- Disodium phosphate, Na_2HPO_4 (Carl Roth, Cat. No. P030)
- EnSpire™ Multimode Plate Reader (Perkin Elmer)
- Ethanol, EtOH (Carl Roth, Cat. No. 9065)
- Ethylenediaminetetraacetic acid, EDTA (Carl Roth, Cat. No. 8040)
- EVOS® FL Cell Imaging System (Thermo Fisher Scientific)
- Glycerol (Sigma Aldrich, Cat. No. G5516)
- Glycine (Carl Roth, Cat. No. 3908)
- HEPES (Sigma Aldrich, Cat. No. PHG0001)
- Incubator, HERAcell® 150 (Heraeus)
- Isopropanol (Carl Roth, Cat. No. AE73)
- Laminar air flow, HerasafeTM (Heraeus)
- Magnesium chloride, $MgCl_2$ (Carl Roth, Cat. No. KK36)
- Methanol (Carl Roth, Cat. No. 0082)
- Minispin centrifuge (Sigma Aldrich, Cat. No. Z606235)

- Monopotassium phosphate, KH_2PO_4 (Carl Roth, Cat. No. 3904)
- NaCl 0.9% saline solution (B. Braun)
- Nonidet™ P 40 Substitute, NP-40 (Sigma Aldrich, Cat. No. 74385)
- Paraformaldehyde, PFA (Carl Roth, Cat. No. 0964)
- Pipetboy acu 2 (Integra)
- Potassium chloride, KCl (Carl Roth, Cat. No. 6781)
- Potassium hydroxide, KOH (Carl Roth, Cat. No. 7986)
- Reaction tube 1.5 mL (Sarstedt, Cat. No. 72706)
- Scissors, forceps (Fine science tools)
- Serological pipettes 5 ml, 10 ml, 25 ml (Sarstedt, Cat. No. 86.1253.001, 86.1254.001, 86.1685.001)
- Sodium chloride, NaCl (Carl Roth, Cat. No. 3953)
- Sodium dodecyl sulfate (Carl Roth, Cat. No. 0183)
- Thermomixer comfort (Eppendorf, Cat. No. 2050-120-04)
- Tris-HCl (Carl Roth, Cat. No. 9090)
- Triton® X 100 (Carl Roth, Cat. No. 3051)
- Xylol (Carl Roth, Cat. No. 9713)

3.2 | Cell culture

Materials and equipment

- 10 cm^2 TC dishes (ThinCertTM; Greiner, Cat. No. 664160)
- 10 cm^2 TC dishes, Standard (Sarstedt, Cat. No. 83.3902)
- 12-well TC plates (Greiner, Cat. No. 662160)
- 12-well TC plates, Standard (Sarstedt, Cat. No. 83.3921)
- 12-well TPP plates (TPP Techno Plastic Products AG, Cat. No. 92412)
- 3,3',5-Triiodo-L-thyronine sodium salt (Sigma Aldrich, Cat. No. T6397)
- 30 µM and 100 µM nylon meshes (Millipore, Cat. No. NY3002500, NY1H00010)
- 3-Isobutyl-1-methylxanthine, IBMX (Sigma Aldrich, Cat. No. I5879)

- 6-well tissue culture (TC) plates (Sarstedt, Cat. No. 83.3920)
- 6-well TPP plates (TPP Techno Plastic Products AG, Cat. No. 92406)
- Cannulas (Braun, Sterican 0,90 x 40 mm, Cat. No. 4657519)
- Collagenase, Type II (Worthington, Cat. No. CLS2)
- Countess Automated Cell Counter (Invitrogen, Cat. No. C10227)
- Cryogenic vials (Sarstedt, Cat. No. 72.379.992)
- D(+)-Biotin (Novabiochem, Cat. No. 58-85-5)
- Dexamethasone (Sigma Aldrich, Cat. No. D4902)
- DMEM, high glucose, GlutaMAX(TM), pyruvate (Gibco, Cat. No. 31966)
- DMEM, high glucose, GlutaMAX(TM) (Gibco, Cat. No. 61965)
- Fetal Bovine Serum, FBS (Biochrom, Cat. No. S0015)
- Insulin solution human (Sigma Aldrich, Cat. No, I9278)
- Pantothenate (Sigma Aldrich, Cat. No. P5155)
- Penicillin/streptomycin (P/S; Merck, Cat. No. A2213)
- Rosiglitazone (Sigma Aldrich, Cat. No. R2408)
- Sodium ascorbate (Carl Roth, Cat. No. 3149)
- Syringe filter 0.22 µm (VWR, Cat. No. 514-0061)
- Syringes 5 ml (BD Discardit II, Cat. No. 309050)
- T175 tissue culture flasks (Sarstedt, Cat. No. 83.3912.002)
- Trypan Blue Stain (Gibco, Cat. No. 15250)
- Trypsin-EDTA (0.05 %), phenol red (Gibco, Cat. No. 25300054)

3.2.1 | Cell culture of brown adipocytes

Brown adipocytes isolation

Isolation buffer	
$CaCl_2$	1.3 mM
Glucose	5 mM
HEPES	100 mM

KCl	5 mM
NaCl	123 mM
H_2O	
pH was adjusted to 7.4 and sterile filtered	

Digestion buffer	
BSA	1.5 %
Collagenase II	2 mg/ml
BSA and Collagenase II were dissolved in isolation buffer and sterile filtered	

BA isolation culture medium	
FBS	10 %
HEPES	10 nM
Insulin	4 nM
P/S	1 %
Sodium Ascorbate	25 µg/ml
T3	4 nM
All substances were added to DMEM, high glucose, GlutaMAX™ (Gibco, Cat. No. 61965)	

Dissected interscapular BAT from newborn mice was finely chopped into small pieces using surgical scissors in 3 ml of the digestion buffer. The tissue was digested for 30 min in a water bath at 37 °C, shaking every 5 min to ensure complete digestion of the tissue. Once digested, the tissue was filtered using a 100 µm nylon-mesh and incubated on ice for 30 min. The middle-phase was collected and filtered a second time using a 30 µm nylon-mesh. The obtained samples were

centrifuged at 700 rcf for 10 min. After centrifugation, the pellet was resuspended in 2 ml of BA isolation culture medium and plated in a 6-well TC plate and cultured at 37 °C, 5 % CO_2 for 24 h. Immortalization of the obtained preadipocytes was achieved by using 200 ng of Simian Virus 40 (SV40) large T-antigen under the control of phosphoglycerate kinase (PGK) promoter per well.

Expansion of immortalized brown adipocytes

BA growth medium	
FBS	10 %
P/S	1 %
All substances were added to DMEM, high glucose, GlutaMAX™ (Gibco, Cat. No.61965)	

PBS	
KH_2PO_4	1.4 mM
KCl	2.7 mM
NaCl	137 mM
Na_2HPO_4	8 mM
All substances were dissolved in H_2O, the pH adjusted to 7.4 and the solution autoclaved.	

Immortalized cells were maintained in BA growth medium until reaching 80-90 % confluency. Cultured cells were washed PBS and detached from the well by adding Trypsin-EDTA and incubated at 37°C until complete detachment. Trypsin was inactivated by adding BA growth medium. The obtained cell suspension was centrifuged at 1000 rpm for 5 min. After resuspending the pellet in BA growth medium, cells from three mice were pooled and reseeded in three 10-cm^2 TC (passage 1). Cells were further expanded in a 1:10 ratio following the same procedure until passage 4. Storage of cells in cryogenic vials in BA growth medium containing 10% DMSO was performed at passage 2 ($1*10^6$ cells/cryo) and passage 4 ($3*10^6$ cells/cryo). Cells were counted

before freezing using Trypan Blue Stain and Countess Automated Cell Counter. The cryogenic vials were stored for few weeks at -80°C and at -150°C for longer-term storage.

Differentiation of BA

BA differentiation medium	
FBS	10 %
P/S	1 %
Insulin	1 nM
T3	20 nM
All substances were added to DMEM, high glucose, GlutaMAX™ (Gibco, Cat. No. 61965)	

BA induction medium	
FBS	10 %
P/S	1 %
Insulin	1 nM
T3	20 nM
Dexamethasone	1 µM
IBMX	0.5 mM
All substances were added to DMEM, high glucose, GlutaMAX™ (Gibco, Cat. No. 61965)	

Preadipocytes were seeded (day -4) in BA Growth medium in a density of $1*10^6$ cells/plate, in 6-well or 12-well plates. After two days of incubation at 37°C, 5 % CO_2, medium was replaced by BA Differentiation medium (day -2). After another two days, induction of the adipogenic program was started by replacing the medium with BA Induction medium (day 0). Afterwards, cells were maintained in BA Differentiation medium until day 7, and medium was refreshed every two days (day 2 to day 7). Mature BA were analyzed at day 7. Preadipocytes were analyzed at day -2. Sustained stimulation was performed from day -2 to day 7, if not otherwise stated.

3.2.2 | Cell culture of WA

WA isolation

WA were isolated from 8-12 weeks old C57BL/6J mice.

Digestion buffer	
BSA	0.5 %
Collagenase II	1.5 mg/ml
BSA and Collagenase II were dissolved in DMEM, high glucose, GlutaMAX™, pyruvate (Gibco, Cat. No. 31966)	

WA growth medium	
FBS	10 %
P/S	1 %
All substances were added to DMEM, high glucose, GlutaMAX™, pyruvate (Gibco, Cat. No. 31966)	

Dissected WAT was washed with ice cold PBS and minced with surgical scissors. Approximately 1 g of tissue from 2-3 different mice was digested with 7 ml of WA Digestion buffer in a water bath at 37°C, shaking every 5 min. After 30-45 min, 7 ml of WA Growth medium was added to stop collagenase action. Following 30 min incubation at RT, cells were centrifuged at 1000 rpm for 10 min. Pellets were resuspended in 2 ml of WA Growth medium and filtered through a 100 µm nylon mesh. The filtered solution was seeded in T175 culture flask in WA Growth medium. 24 h after seeding, cells were washed with RT PBS and maintained with WA Growth medium in the incubator at 37°C, 5 % CO_2. Medium was refreshed every second day for 1 week or until cells reached approximately 80% confluency. Afterwards cells were washed twice with RT PBS and detached from the flask by adding Trypsin and incubated at 37° C, 5 % CO_2 until complete detachment. Trypsinization was stopped by adding WA Growth medium. Cells were collected and

centrifuged at 1000 rpm for 10 min. The obtained pellet was resuspended in WA Growth medium containing 10 % DMSO and stored in cryogenic vials at -80°C for short term storage, or at -150°C for long term storage.

Differentiation of WA

WA maintenance medium	
FBS	5 %
P/S	1 %
Insulin	0.172 mM
T3	1 nM
Sodium ascorbate	50 mg/ml
Pantothenate	17 mM
D-biotin	1 mM
All substances were added to DMEM, high glucose, GlutaMAX™, pyruvate (Gibco, Cat. No. 31966)	

WA induction medium	
Dexamethasone	0.25 mM
IBMX	0.5 mM
Rosiglitazone	1 µM
All substances were added to WA maintenance medium	

Primary white preadipocytes were seeded in 12-well TPP plates in a density of ~80000 cells per well. Cells were grown to confluency in WA Growth medium, changing the medium every second day. Once confluent (day -3), cells were maintained in WA Growth medium for 72 h. After these three days (day 0), preadipocytes were induced for 48 h (day 2) by changing the medium to WA Induction medium. From day 2 until day 10, cells were maintained in WA Maintenance medium, refreshing it every second day. All experiments were performed using day 10-13 WA.

3.3 | RNA analysis

Materials and equipment

- Diethyl pyrocarbonate, DEPC (Carl Roth, Cat. No. K028.1)
- InnuSOLV RNA Reagent (Analytik Jena AG, Cat. No. 845-SB-2090100)
- LightCycler 480 SYBR Green I Master (Roche, Cat. No. 04707516001)
- Nanodrop200 Spectrophotometer (Thermo Fisher Scientific)
- ProtoScript® II First Strand cDNA Synthesis Kit (New England Biolabs, Cat. No. E6560S)
- Reaction tube 1.5 mL (Sarstedt, Cat. No. 72706)
- Real-time PCR machine, HT7900 (Applied Biosystems)
- SpeedVac Concentrator, 5301 (Eppendorf)
- SYBR-Green PCR master mix (Applied Biosystems, Cat. No. 4309155)

3.3.1 | RNA isolation

Isolation of RNA from cells or tissues was performed by using innuSOLV RNA Reagent. 1 ml of ice-cold reagent was added to the well to lyse the cells. The cell lysate was transferred to an autoclaved 1.5 ml reaction tube and 200 µl of chloroform was added to each sample. The samples were manually shacked for 15 seconds and incubated for 5 on ice, then centrifuged for 10 min, 13000 rpm at 4°C. The upper phase containing the RNA (~500 µl) was transferred to a new 1.5 ml reaction tube and mixed with 500 µl of isopropanol to precipitate the RNA. Pelleting of the RNA was achieved by 10 min of centrifugation, 13000 rpm at 4°C. After removing the supernatant, the RNA pellet was washed four times with 1 ml of 75% EtOH followed by centrifugation step (5 min, 4°C, 13000 rpm). Finally the RNA pellet was dried in SpeedVac at 30°C for 30 min and was dissolved in 30-50 µl H_2O.

3.3.2 | Synthesis of complementary DNA (cDNA)

of RNA was quantified using Nanodrop Spectrophotometer. Following the manufacturer's instructions, 500 ng or 1000 ng of RNA were transcribed using a First Strand cDNA Synthesis Kit with the following program:

Step	Temperature (°C)	Time (s)
1	25	300
2	42	3600
3	80	300

The cDNA was finally diluted in H_2O to a of 2.5 ng/µL.

3.3.3 | Real-time PCR (RT-qPCR)

mRNA expression was assessed by RT-qPCR using a HT7900 instrument from Applied Biosystems. The reaction was performed using the fluorescent dye SYBR-Green PCR master mix (Applied Biosystems) and the following program:

Step	Temperature (°C)	Time (s)	Repetitions
1	95	600	
2	95	15	
3	60	60	To step 2 for 40 times
4	95	1	
5	65	15	
6	95	∞	

Quantification of mRNA levels was performed based on the crossing point values of the amplification curves using the second derivative maximum method. Hprt (Hypoxanthine-guanine

phosphoribosyltransferase) was used as an internal control for the cell samples and β-Actin (Actb) was used for the tissue samples. The primer sequences used to amplify the target genes are shown in the following table:

Name	Primer sequence (5'->3')	Species
Actb forward	CAT TGC TGA CAG GAT GCA GAA GG	mouse
Actb reverse	TGC TGG AAG GTG GAC AGT GAG G	mouse
Adrb3 forward	CCT TCA ACC CGG TCA TCT AC	mouse
Adrb3 reverse	GAA GAT GGG GAT CAA GCA AGC	mouse
Cidea forward	TGC TCT TCT GTA TCG CCC AGT	mouse
Cidea reverse	GCC GTG TTA AGG AAT CTG CTG	mouse
Cox8b forward	TGT GGG GAT CTC AGC CAT AGT	mouse
Cox8b reverse	AGT GGG CTA AGA CCC ATC CTG	mouse
Ebi2 forward	CAG CTT TAC CCA CTC GGA TA	mouse
Ebi2 reverse	AAG AAG CGG TCT TGC TCA A	mouse
Fabp4 forward	TGA AAG AAG TGG GAG TGG GCT TTG C	mouse
Fabp4 reverse	CAC CAC CAG CTT GTC ACC ATC TCG T	mouse
Hprt forward	ACA TTG TGG CCC TCT GTG TGC TCA	mouse
Hprt reverse	CTG GCA ACA TCA ACA GGA CTC CTC GT	mouse
Pgc1a forward	TAT GGA GTG ACA TAG AGT GTG CT	mouse
Pgc1a reverse	CCA CTT CAA TCC ACC CAG AAA	mouse
Pparg forward	TCC GTA GAA GCC GTG CAA GAG ATC A	mouse
Pparg reverse	CAG CAG GTT GTC TTG GAT GTC CTC G	mouse
Prdm16 forward	ACA CGC CAG TTC TCC AAC CTG T	mouse
Prdm16 reverse	TGC TTG TTG AGG GAG GAG GTA	mouse
Ucp1 forward	GGT GAA CCC GAC AAC TTC CGA AGT G	mouse
Ucp1 reverse	GGG TCG TCC CTT TCC AAA GTG TTG A	mouse

3.4 | Protein analysis

Materials and equipment

- BioPhotometer D30 (Eppendorf)
- Cell scraper (Labomedic, Cat. No. 2015217)
- Centrifuge 5430R (Eppendorf)
- Complete protease inhibitor cocktail (Roche, Cat. No. 04693116001)
- Coomassie brilliant blue G-250 (Merck, Cat. No. 1.15444.0025)
- PBS (as described at p. 17)

- Phosphoric acid (Carl Roth, Cat. No. 9076)
- Sodium deoxycholate (Sigma Aldrich, Cat. No. D6750)
- Sodium fluoride, NaF (Carl Roth, Cat. No. 4530)
- Sodium orthovanadate, Na_3VO_4 (Carl Roth, Cat. No. 0735)
- Syringe filter 0.22 µm (VWR, Cat. No. 514-0061)
- Ultra-Turrax® T8 (IKA)

3.4.1 | Isolation of proteins

Cells were washed two times with cold PBS and lysed with cold lysis buffer. Cells were scraped from the wells and transferred to a 1.5 ml reaction tube, then centrifuged for 30 min at 4°C, 13000 rpm. The clear phase was transferred to a new sterile reaction tube and stored at -20°C or directly used. For tissue samples, approximately 30 mg of tissue was placed in sterile reaction tubes and an appropriate amount of lysis buffer was added. The tissue was homogenized by using Ultra-Turrax® and centrifuged for 20 min at 4°C, 13000 rpm. The clear phase was transferred to a new sterile reaction tube and stored at -80°C or directly used.

RIPA buffer	
Sodium deoxycholate	0.1%
NaCl	150 mM
NP-40	1%
SDS	0.1%
Tris-HCl (pH 7.5)	50 mM
All substances were added to Millipore H_2O and solution was sterile filtered and stored at 4°C	

Lysis buffer	
Complete protease inhibitor cocktail	40 µl/ml

NaF	10 mM
Na_3VO_4	1 mM
All substances were added fresh to RIPA buffer prior to use	

3.4.2 | Bradford assay and protein quantification

Coomassie solution	
Coomassie brilliant blue G-250	0.01%
EtOH	5%
Phosphoric acid	8.5%
All substances were dissolved in H_2O and the solution was stored at 4°C	

2 µl of the sample was diluted with 98 µl 0.15 M NaCl solution. Next, 1 ml of Coomassie solution was added to each sample. The absorbance was measured at 595 nm using Eppendorf BioPhotometer D30. Protein concentration was calculated from the BSA standard calibration curve established with known BSA standard concentrations.

3.4.3 | SDS-PAGE and Western Blot

Materials and equipment

- Ammonium Persulphate, APS (GE Healthcare, Cat. No. GE17-1311-01)
- B-Mercaptoethanol (Sigma Aldrich, Cat. No. M6250)
- Bromophenol blue (Carl Roth, Cat. No. 6558)
- Enhanced chemiluminescence (ECL) Western Blotting Detection Reagent (Amersham Bisociences, Cat. No. RPN2106)
- Image Quant LAS 4000 mini (Life sciences, Cat. No. 28-9558-10)
- Milk powder (Sigma Aldrich, Cat. No. 70166)
- Mini-PROTEAN Tetra Cell electrophoresis system (BioRad)

- N,N,N',N'-Tetramethylethylenediamine, TEMED (Sigma Aldrich, T9281)
- Nitrocellulose membrane, Amersham Protran 0.45 NC (GE Healthcare Life Sciences, Cat. No. 10600002)
- Odyssey® Fc Imaging System (LI-COR)
- PageRuler Prestained Protein Ladder (Thermo Scientific, Cat. No. 26616)
- Power supply, Consort EV 202 (Sigma Aldrich, Cat. No. Z654418)
- Primary and secondary antibodies (See list below)
- Roller Mixer SRT6 (Stuart)
- Rotiphorese®Gel 30 "Acrylamide" (Carl Roth, Cat. No. 3029)
- Trans-Blot Turbo Transfer System (BioRad)
- Tween® 20 (Carl Roth, Cat. No. 9127)

SDS-PAGE

After quantifying protein concentration, an appropriate amount of sample was mixed with 3x Laemmli buffer. The protein samples were then incubated for 10 min at 98°C and analyzed using SDS-PAGE and Western blot.

Laemmli buffer 3x	
Bromphenol blue 0.015 %	0.015%
Glycerol	20%
SDS	17%
Tris-HCl (pH 6.8)	150 mM
B-mercaptoethanol	10%
All substances were dissolved in H_2O and the solution was stored at -20°C	

Proteins were separated according to the electrophoretic mobility using SDS-PAGE gels. SDS-PAGE gels were prepared combining an upper stacking gel and a bottom resolving gels. Different percentage of resolving gels were prepared according to the molecular mass of the protein of interest, while the stacking gel was always the same (See tables below).

Resolving gel	8%	10%	12%	15%
H_2O	4.6 ml	4 ml	3.3 ml	2.3 ml
Acrylamide	2.7 ml	3.3 ml	4 ml	5 ml
Tris-HCl (pH 8.8)	2.5 ml	2.5 ml	2.5 ml	2.5 ml
20% APS	50 µl	50 µl	50 µl	50 µl
TEMED	4 µl	4 µl	4 µl	4 µl

Stacking gel	
H_2O	3.4 ml
Acrylamide	830 µl
Tris-HCl (pH 8.8)	630 µl
20% APS	25 µl
TEMED	5 µl

Electrophoresis was performed at 180 V in RT electrophoresis buffer using Mini-PROTEAN Tetra Cell electrophoresis system.

Electrophoresis buffer 10x	
Tris-HCl	250 mM
Glycine	2 M
SDS	0.1%
All substances were dissolved in H_2O and pH adjusted to 8.3. Before to use the buffer was dilute to a of 1x in H_2O	

Western blot and protein detection

Following SDS-PAGE, proteins were transferred to a nitrocellulose membrane by semi-dry western blotting using a Trans-Blot Turbo Transfer System (BioRad) with Towbin buffer. Proteins

were transferred at 25 V, 1.0 A maximum, for 30 min, according to the Standard SD Bio-Rad programmed protocol.

Towbin buffer	
Tris-HCl	25 mM
Glycine	192 mM
Methanol	20%
All substances were dissolved in H_2O and pH adjusted to 8.3	

After transferring, the membranes were briefly washed in TBST and blocked for at least 1 h in 5 % BSA solution or 5 % milk (according to manufacturer indication) under constant agitation at RT. After blocking, membranes were briefly washed in TBST and incubated overnight with the primary antibody in 5 % BSA solution or 5 % milk (according to manufacturer indication) at 4°C.

TBS 10x	
Tris-HCl	100 mM
NaCl	1.4 M
SDS	0.1%
All substances were dissolved in H_2O and pH adjusted to 8.0	

TBST	
Tween-20	0.1%
Tween-20 was dissolved in 1xTBS and stored at RT protected from light	

5% BSA solution	
BSA	5%
BSA was dissolved in TBST prior to use	

5% milk solution	
Milk powder	5%
Milk powder was dissolved in TBST prior to use	

Following incubation with the first antibody, membranes were washed 3 times for 10 min each in TBST and incubated with a secondary horseradish peroxidase (HRP)-conjugated or fluorescent antibody (800 nm or 680 nm wavelength absorbance) in TBST for at least 1 h at RT under constant agitation (in the dark if fluorescent antibody were used). Membranes were then washed 3 times for 5 min each in TBST. When HRP- conjugated secondary antibody was used, the membranes were covered in ECL reagent for 1 min according to the manufacturer's instructions prior to detection. Protein levels were detected in the ImageQuant LAS 4000 mini and quantified by densiometric analysis (Image J software) in case of the HRP-conjugated secondary antibody, or detected and quantified with the Odyssey® Fc Imaging System in case of fluorescent secondary antibody.

List of primary antibodies used

- Calnexin (Novus Biologicals, Cat. No. NB300-518)
- HSL and pHSL (Cell signaling, Cat. No. 4107 and 4137)
- UCP1 (Sigma Aldrich, Cat. No. sc-6529)
- Tubulin (Dianova, Cat. No. MS-719-P0)
- ERK1/2 and pERK1/2 (Cell signaling, Cat. No. 9102 and 9101)

List of secondary antibodies used

- DyLight™ 680-conjugated anti-mouse (Cell Signaling, Cat. No. 5470)
- DyLight™ 680-conjugated anti-rabbit (Cell Signaling, Cat. No. 5366)
- DyLight™ 800-conjugated anti-mouse (Cell Signaling, Cat. No. 5257)
- DyLight™ 800-conjugated anti-rabbit (Cell Signaling, Cat. No. 5151)
- HRP-conjugated anti -rabbit (Cell Signaling, Cat. No. 7074)
- HRP-conjugated anti-goat (Dianova, Cat. No. 705-035-147)

- HRP-conjugated anti-mouse (Dianova, Cat. No. 115-035-146)

3.5 | Lipolysis assays

Materials and equipment

- 24-well plates (Sarstedt, Cat. No. 83.3921)
- Bovine serum albumin “BSA”, fatty acids free (Sigma Aldrich, Cat. No. A7030)
- Dulbecco's Modified Eagle Medium (DMEM) (Gibco, Cat. No. 21063)
- EnSpire™ Multimode Plate Reader (Perkin Elmer)
- Free glycerol reagent (Sigma Aldrich, Cat. No. F6428)
- Glycerol standard (Sigma Aldrich, Cat. No. G7793)
- Norepinephrine, NE (Sigma Aldrich, Cat. No. A9512)

3.5.1 | In vitro lipolysis

Lipolysis assay

Mature BA were washed twice with warm (37°C) lipolysis medium. The compounds were pre-mixed at the final desired concentration in lipolysis medium and 400 µl were added to each well (12-well plate). The cells were then incubated for 2 hours at 37°C, 5% CO_2. After incubation, 40 µl of the plate lipolysis medium supernatant was pipetted in a 96-well plate together with 60 µl of Free glycerol reagent. The standard solution was prepared mixing 5 µl of the glycerol standard solution with 95 µl of the Free glycerol reagent, whereas the blank was prepared with 40 µl of the lipolysis medium and 60 µl of Free glycerol reagent. All the samples, standard and blank were made in duplicates. Samples were incubated at 37° C, 5 % CO_2 for 5 min and absorption was measured at 540 nm and 600 nm as reference wavelength using EnSpire™ Multimode Plate Reader (Perkin Elmer). The total glycerol release was calculated as indicated by the manufacturer after normalization to the protein concentration for each sample.

Lipolysis medium	
Fatty acids free BSA	2%

BSA was dissolved in DMEM (Gibco, Cat. No. 21063)

Protein quantification

Proteins were isolated and quantified as in p. 26.

3.5.2 | Ex vivo lipolysis

Fat pads were isolated from newborn or 8 weeks old mice, weighed (approximately 5 mg of BAT and 30 mg of WATi or WATg was used) and incubated with 400 µl of lipolysis medium (see p. 32) in a 12 well plate, with or without 1 µM NE and 7α,25-OHC 1 µM at 37°C, 5% CO2 for 2h. After incubation, 40 µl of the lipolysis medium was pipetted to a 96-well plate. 60 µl of Free glycerol reagent was added to each sample.

The standard solution was prepared by mixing 5 µl of the glycerol standard solution together with 95 µl of the Free glycerol reagent. The blank was obtained by pipetting 40 µl of the lipolysis medium used for the samples and 60 µl of the free glycerol reagent. Samples were incubated at 37°C, 5% CO2 for 5 min and absorption was measured at 540 nm, using 600 nm as reference wavelength, with an EnSpire™ Multimode Plate Reader (Perkin Elmer). The total glycerol release was calculated from the values obtained for the blank and the standard and normalized to the weight of tissue in mg of each sample.

3.6 | cAMP ELISA

Materials and equipment

- Direct cAMP ELISA kit (Enzo Life Sciences, Cat. No. ADI-900-066/ ADI-901-066)

BA or WA were seeded $1*10^6$ cells per plate in 12 well plates and differentiated according to the protocol. After differentiation, the cells were pretreated with IBMX 0.5 mM for 30 min, then the treatments performed, in presence of IBMX, for 20 min at 37°C, 5% CO_2. The cells were then washed with ice cold PBS and frozen at -80°C or used immediately.

The cAMP ELISA was performed accordingly to manufacturer instruction. Briefly, BA or WA were lysed in 600 µl/well or 250 µl/well of 0.1 M HCl respectively for at least 10 min. The samples were then centrifuged at 13 000 rpm for 10 min. Neutralizing reagent, standards, samples, blue conjugate and yellow antibody were pipetted in duplicate in the cAMP ELISA kit plate as indicated by the manufacturer. The plate was then incubated for 2 h on a plate shaker at 500 rpm at RT. Following the incubation, the plate was washed 3 times with wash buffer and the blue conjugated for the total activity and the substrate solution pipetted. After a final incubation of 1 h at RT, the stop solution was added and the absorbance measured at 405 nM.

3.7 | *In vitro* respirometry

Materials and equipment

- Cytation 5 Cell Imaging Multi-Mode Reader (BioTek)
- D-(+)-Glucose (Sigma Aldrich, Cat. No. G8270)
- Hoechst 33258 solution (Sigma Aldrich, Cat. No. 94403)
- Indomethacin (Sigma Aldrich, Cat. No. I7378)
- L-Glutamine (Sigma Aldrich, Cat. No. G8540)
- Seahorse XF Cell Mito Stress Test Kit (Agilent, Cat. No. 103015-100)
- Seahorse XF DMEM medium (Agilent, Cat. No. 103575-100)
- Seahorse XFe24 Analyzer (Agilent)
- Seahorse XFe24 FluxPak (Agilent, Cat. No. 102340-100)
- Sodium pyruvate (Sigma Aldrich, Cat. No. P5280)

BA differentiation

Immortalized primary BA were seeded in Seahorse 24-well plates 40 000 cells/well in 100 µl of BA Growth Medium (See p.17). The following day, after reaching confluency, the differentiation was induced with the high induction medium.

High induction medium	
Dexametasone	1 µM
IBMX	100 µM
Rosiglitazone	1 µM
Indomethacin	125 nM
All substances were dissolved in BA differentiation medium (See p.17).	

The high induction medium was replaced after two days with 500 µl of BA differentiation medium (See p.17) and the respirometry assay was performed the following day (three days after induction of differentiation).

Respirometry assay

The day before the assay, the Seahorse cartridges were hydrated overnight in Seahorse calibrant solution at 37°C in a non-CO_2 controlled chamber as indicated by the manufacturer.
The day of the assay, the Seahorse complete medium was prepared as follow:

Seahorse complete medium	
D-(+)-Glucose	25 mM
L-Glutamine	2 mM
Sodium Pyruvate	2 mM
All substances were dissolved in Seahorse XF DMEM medium.	

The cells were washed once with Seahorse complete medium and equilibrated for 1 hour at 37°C in a non-CO_2 controlled chamber in 500 µl of Seahorse complete medium. In the meantime, the cartridge was loaded with the Mito Stress assay treatments as follow:

Mito stress treatments

NE	Final conc. 1 µM	Port A (56 µl)
Oligomycin	Final conc. 2 µM	Port B (62 µl)
FCCP	Final conc. 1 µM	Port C (69 µl)
Rotenone	Final conc. 0.5 µM	Port D (72 µl)
Antimycin A	Final conc. 0.5 µM	
Hoechst staining	Final conc. 10 µg/ml	
All substances were dissolved in Seahorse XF DMEM medium with vehicle (DMSO) or 7α,25-OHC 1 µM		

After equilibration, the cells were treated for 15 min with either vehicle (DMSO). The Mito Stress assay and following was performed according to manufacturer (Agilent) instruction.
Following respirometry data acquisition, the cells were washed twice with PBS and the number of cells labelled with Hoechst staining was calculated with Cytation 5 Cell Imaging Multi-Mode Reader for normalization.

3.8 | ROS assay

Materials and equipment

- Cellular ROS assay kit (Abcam, Cat. No. ab186027)

BA were differentiated in 10 cm plates according to the protocol. At day 7 of differentiation, the cells were detached and resuspended in Differentiation medium to a of $4*10^5$ cells/ml. According to manufacturer instruction, the cells were seeded on a black plate with clear bottom 96 well plate and let attaching during overnight incubation at 37°C, 5 % CO_2. The following morning, the assay was carried out according to manufacturer instruction. Briefly, 100 µl of ROS Red Working Solution were added to each well and the plate was incubated for 1 h at 37°C, 5 % CO_2. After the incubation time, the plate fluorescence was recorded to acquire a background value, then treated with 11X compounds (NE 1 µM, 7α,25-OHC 1 µM, NIBR189 10 µM or H_2O_2 30 %, in HBSS). The fluorescence increase was measured at different time points at Ex/Em = 520/605 nm at bottom read mode with a EnSpire™ Multimode Plate Reader (Perkin Elmer).

3.9 | Animal models

3.9.1 | Animals

WT male C57Bl/6J mice 8weeks old were purchased from Charles River Laboratories. EBI2 knockout mice were kindly provided by Prof. Caroline Pot (Lausanne University Hospital CHUV, Lausanne). All studies were approved by the Landesamt für Natur, Umwelt und Verbraucherschutz, Nordrhein-Westfalen, Germany, Animal protocol No. 84-02.04.2017.A311.
All animals were housed at 23°C±1°C at the Haus für experimentelle Therapie, UKB Universitätsklinikum Bonn, or at the Department of Pharmacology and Toxicology, UKB Universitätsklinikum Bonn, during experiments.
Unless otherwise specified they were given access to chow diet and water *ad libitum*.

3.9.2 | Genotyping of wildtype (WT) and EBI2 KO littermates

Materials and equipment

- Agarose Standard (Carl Roth, Cat. No. 9012-36-6)
- Casting platforms (EmbiTech)
- Electrophoresis chamber (Peqlab)
- Ethidium bromide solution 10 mg/ml (Carl Roth, Cat. No. 2218.1)
- GelDoc®XR (BioRad)
- Microwave oven (Panasonic)
- Phire Tissue Direct PCR Master Mix (Thermo Scientific, Cat. No. F-170)
- QuantityOne® Software (BioRad)
- Thermocycler Biometra T-One (Analytik Jena)

To genotype EBI2 WT and KO littermates, a small biopsy was collected from the ears with an ear puncher. The genotype was assessed through PCR method using Thermo Fisher Scientific Phire Tissue Direct PCR Master Mix.

Before beginning, a heat block was warmed at 98°C. The small tissue was placed in 20 µl of Dilution Buffer and 0.5 µl of DNA Release Additive. The samples were mixed briefly by vortexing and the solution was spinned down by short centrifugation. The reaction was incubated 2-5 min at room temperature and then placed in the pre-heated block at 98°C for 2 min. The samples were frozen at -20°C if not processed immediately.

A reaction mix was prepared as follow:

Component	**Volume**
2X Phire Tissue Direct PCR Master Mix	10 µl
EBI2 WT primer	1 µl (final conc. 0.5 µM)
EBI2 Neo primer	1 µl (final conc. 0.5 µM)
EBI2 Tg primer	1 µl (final conc. 0.5 µM)
Sample	1 µl
H_2O	6 µl (final volume of 20 µl)

The following primers were used:

Name	**Sequence (5'->3')**
EBI2 WT	CATGGAGTATCCAAACTTTGAAGGG
EBI2 Neo	GGGCCAGCTCATTCCTCCCACTCAT
EBI2 Tg	CAGGATGAACACGACAATGATGAGG

The following cycling protocol was used, with the extracted DNA and reaction mix described previously:

Step	**Temperature (°C)**	**Time (s)**	**Repetitions**
1	98	30	
2	98	5	
3	65, -0.5°C/cycle	5	
4	72	10	To step 2 for 10 times
5	98	5	

6	60	5	
7	72	10	To step 5 for 48 times
8	72	60	
9	4	∞	

To visualize the RT-PCR products, agarose gel electrophoresis was used. A 2.5% gel was prepared dissolving agarose in TAE buffer under sustained heating in a microwave oven.

TAE buffer 50x	
Acetic acid	5.71%
Na_2-EDTA	50 mM
Tris-HCl	2 M
All substances were dissolved together in H_2O.	

After dissolving completely the agarose, 800 ng/ml of Ethidium bromide was added to the agarose solution. The agarose solution was poured into cassettes and left to solidify at RT.

The PCR product was directly added to the 2.5% gel. Electrophoresis was performed in an electrophoresis chamber filled with TAE buffer at 120 V. Separated PCR products were visualized under the UV light 366 nm using a UV light transilluminator (GelDoc®XR) in combination with QuantityOne® Software

The PCR products were detected at the following sizes: WT 230 bp; KO 390 bp.

3.10 | *In vivo* experiments

3.10.1 | Diet induced obesity experiment

Materials and equipment

- DIO - 10 kJ% fat (Ssniff Spezialdiäten, Cat. No. D12450)
- DIO - 60 kJ% fat (Ssniff Spezialdiäten, Cat. No. D12492)

8 weeks old males were randomly assigned to control (ND, 10 kJ% fat) or high fat diet (HFD, 60 kJ% fat) fed group. The mice were fed for 12 weeks with *ad libitum* with ND or HFD, with free access to water. The body weight was recorded weekly. At the end of the 12 weeks, body composition, glucose tolerance and whole body metabolism were analyzed (see below, chapters 3.10.2 | 3.10.4 | 3.10.5 |).

3.10.2 | Glucose tolerance test

Materials and equipment

- Accu-Check Nano (Roche)
- Accu-Check Test Strips (Roche)
- Omnifix® 100 Solo 1 ml syringe (B. Braun, Cat. No. 9161708V)
- Sterican® 27G needle (B. Braun, Cat. No. 4665406)

Animals were fasted for 5 hours with free access to water. The weight of the mice was recorded and the basal fasting levels of glucose measured from the blood collected from a small cut on the tail. The mice were then injected with glucose solution i.p., 8 µl/g body weight and the blood glucose was measured after 30, 60, 90 and 120 minutes following the same procedure. The mice were let recovering for 3 days in standard housing conditions before to perform any other experiment.

Glucose solution
Glucose 2.5 g/ml
Glucose was dissolved in sterile NaCl 0.9% saline solution prior to use

3.10.3 | 7α,25-OHC injections

Materials and equipment

- 7α,25-dihydroxycholesterol (Tocris, Cat. No. 62-771-0, or Avanti Polar Lipids, Cat. No. 700080P)
- Omnifix® 100 Solo 1 ml syringe (B. Braun, Cat. No. 9161708V)
- Sterican® 27G needle (B. Braun, Cat. No. 4665406)

8 weeks old male mice were injected daily for 7 days (see p. 80) or once (see p. 77) with 7α,25-OHC, 5 mg/kg. 7α,25-OHC powder was dissolved in sterile DMSO at 10 mM concentration (stored at -20°C according to manufacturer instruction), and further diluted in NaCl 0.9% saline solution prior to inject. The maximum DMSO concentration for each injection was 10%. All injections were performed i.p. with a 27G needle. At the end of the experiment (i.e. after the 7^{th} injection or following the first injection) the whole body metabolism of the mice was analyzed (see p. 41 and p. 41).

3.10.4 | Body composition analysis

Materials and equipment

- Minispec Whole Body Composition Analyzer (Bruker)

The whole-body composition (fat mass, lean mass and free water) of mice was measured with TD-NMR in a Bruker minispec.

3.10.5 | Indirect calorimetry

Materials and equipment

- Phenomaster (TSE Systems)

The mice were housed in single cages with free access to food and water, on a daily cycle of 12 h light (06:00 to 18:00) and 12 h darkness (18:00 to 06:00), at the desired temperature (23°C or 4°C) and 45% humidity. Following 24 h of acclimatization, the O_2 and CO_2 consumption, the RER and locomotor activity were recorded. The locomotor activity was recorded with an Infrared Motion Sensor (InfraMot, TSE System) and normalized to control group mice.

3.11 | Lipids quantifications

3.11.1 | Cholesterol measurement

Materials and equipment

- Cholesterol Quantitation Kit (Sigma Aldrich, Cat. No. MAK043)

Approximately 10 mg of liver was homogenized with 200 µl of chloroform:isoporpanol:IGEPAL (7:11:0.1). The insoluble material was removed by centrifugation for 10 min at 13 000 rpm. The organic phase was transferred in a new tube and air dry at 50°C to remove the chloroform, followed by 30 min under vacuum to remove any residue or organic solvent. The dried lipids were resuspended in 200 µl of Cholesterol Assay Buffer and vortexed to obtain an homogenous mixture.

The serum samples were used to perform the assay without any prior purification.

The reaction mix was prepared as indicated in the Cholesterol Quantitation Kit. 50 µl of samples and 50 µl of reaction mix were loaded in the 96-well plate and incubated for 60 min at 37°C. The absorbance was measured at 570 nm.

All the samples were run in duplicate.

3.11.2 | Free fatty acids measurement

Materials and equipment

- Free Fatty Acid Quantitation Kit (Sigma Aldrich, Cat. No. MAK044)

Approximately 10 mg of liver was homogenized with 200 µl of 1% w/v Triton X-100 in chloroform solution. The insoluble material was removed by centrifugation for 10 min at 13 000 rpm. The organic phase was transferred in a new tube and air dry at 50°C to remove the chloroform, followed by 30 min under vacuum to remove any residue or organic solvent. The dried lipids were resuspended in 200 µl of Fatty Acid Assay Buffer and vortexed for 5 min to obtain an homogenous mixture.

The serum samples were used to perform the assay without any prior purification.

The reaction mix was prepared as indicated in the Free Fatty Acids Quantitation Kit. 50 µl of samples and 50 µl of reaction mix were loaded in the 96-well plate, briefly shacked and incubated for 30 min at 37°C protected from light. The absorbance was measured at 570 nm.

All the samples were run in duplicate.

3.11.3 | Triglycerides measurement

Materials and equipment

- Serum Triglyceride Determination Kit (Sigma Aldrich, Cat. No. TR0100)

Approximately 300 mg of liver was dissolved overnight at 55°C in 350 µl ethanolic KOH (30% KOH 1:1 EtOH). The following day, the tissue was vortexed until completely dissolved and 650 µl of H_2O:EtOH (1:1) were added. Samples were centrifuged for 5 min at 13 000 rpm and the supernatant moved to a new tube. 200 µl of H_2O:EtOH (1:1) were added and mixed by vortexing. 200 µl were moved to a new tube with 215 µl of $MgCl_2$ 1 M. After 10 min on ice, the samples were newly centrifuged for 5 min at 13 000 rpm and the supernatant moved to a new tube.

The serum samples were used to perform the assay without any prior purification.

78 µl of Free Glycerol Reagent, 20 µl of reconstituted Triglycerides Reagent and 2 µl of samples were loaded in the 96-well plate. The plate was incubated for 5 min at 37°C and the absorbance read at 540 nM.

3.12 | Histochemistry

3.12.1 | Tissues preparation

Materials and equipment

- Microtome HM315 (Microm)

Isolated BAT, WATi, WATg and liver pads were fixed in a 4% solution of PFA in PBS. After 24 h, samples were dehydrated in increasing concentrations of ethanol: 50%, 70%, 95% and 100%. Samples were soaked while shaking in each solution for 3 times, 20 min each. The tissues were then incubated in xylol for 3 times, 10 min each time. Afterwards, samples were transferred to liquid paraffin, where they were maintained 2 times for 1 h at 60°C, and then incubated in the liquid paraffin overnight. Finally, tissues were embedded in paraffin and left to solidify at room temperature. 5 µm sections of the tissues were cut using a microtome and dried on histological glass slides at 37° C overnight.

3.12.2 | Hematoxylin/Eosin (HE) staining

Materials and equipment

- Eosin Y-solution “Eosin”, (Merck, Cat. No. 1.09844)
- Mayer´s hemalun solution “Hematoxylin” (Merck, Cat. No. 1.09249)
- Roti®-Histokitt (Carl Roth, Cat. No. 6640)

Tissue sections were washed for 2 min in xylol to remove the paraffin. Rehydration was achieved by incubating the slides in decreasing EtOH concentrations: 100%, 95%, 90%, 75% and 50%, 2 min each, followed by 2 min in water. Next, slides were stained with hematoxylin for 2 s and rapidly washed with distilled water, then for 15 min under running water. Staining with eosin was performed by incubating the tissue section in eosin for 2 min and washed for 4 min with distilled water. Tissue was dehydrated by immersing the slides in increasing EtOH concentrations: 75%, 90%, 95 % and 100 %, for 2 min each, washed for 2 min in xylol and mounted using Roti®-Histokitt.

3.12.3 | UCP1 staining

Materials and equipment

- Anti-rabbit, HRP-conjugated secondary antibody (Cell Signaling, Cat. No. 7074)
- DAB peroxidase HRP-substrate kit (Vector laboratories, Cat. No. SK-4100)
- Mayer´s hemalun solution "Hematoxylin" (Merck, Cat. No. 1.09249)
- UCP1 primary antibody (Sigma Aldrich, Cat. No. sc-6529)

Tissue sections were washed 2 times for 2 min in xylol to remove the paraffin. Rehydration was achieved by incubating the slides in decreasing EtOH concentrations: 100%, 95%, 90%, 75% and 50%, 2 times for 2 min, followed by 2 times in water for 5 min. Slides were next incubated in 20 mM sodium citrate (pH 6) for 5 min, followed by another 5 min incubation with 10 mM sodium citrate (pH 6) at 75-80 °C. Next, slides were washed in 3% hydrogen peroxide for 10 min and again in water for 5 min. In order to reduce unspecific antibody binding, blocking was performed with 2.5% goat serum in PBST for 1 h at RT. Incubation with UCP1 antibody (1:75 in 0.25 % goat serum in PBST) was performed overnight at 4 °C. The following day, slides were washed 3 times for 5 min with PBST. Incubation with the secondary antibody (1:200 in 0.25 % goat serum in PBST) was performed for 1 h at RT. Slides were washed 3 times for 5 min in PBST. Sections were visualized using 3,3'-Diaminobenzidine (DAB) substrate according to manufacturer instruction.

3.12.4 | Oil Red O staining

Materials and equipment

- Oil Red O (Sigma Aldrich, Cat. No. O0625)

Mature BA were washed 2 times with PBS at RT and fixed for 10 min with 4% PFA at RT. The PFA was removed and the cells were further washed for 2 times with RT PBS, then incubated for 2 to

3 hours at RT in Oil Red O solution. After staining, the plate was washed with abundant distilled water and picture of each well was acquired.

Oil Red O stock solution	
Oil Red O	0.5 g
Isopropanol	100 ml
Oil Red O stock solution was stirred overnight and stored at RT	

Oil Red O working solution	
Oil Red O stock solution	60%
Oil Red O stock solution was diluted in H2O and filtered two times with filter papers prior to use	

3.13 | Statistical analysis

Data are represented as mean ± standard error of the mean (s.e.m). Statistical analyses were performed using one-way or two-way analysis of variance (ANOVA) with Bonferroni post-hoc test (multiple comparisons) or two-tailed student's t-test (single comparison). All calculations and analysis were performed using GraphPad Prism 6 software.

"n" represents individual experiments with cells independently seeded or derived from different mice for the *in vitro* experiments, or different individual mice for the *ex vivo* and *in vivo* experiments.

4 | RESULTS

4.1 | EBI2 expression in adipocytes and adipose tissue

EBI2 has been identified as an important chemo-attractant receptor in immune cells (Hannedouche et al., 2011; Liu et al., 2011), mediating migration of B cells (Pereira et al., 2009) and T cells (Chalmin et al., 2015), and other immune cell types (Gatto et al., 2013; Nevius et al., 2015; Preuss et al., 2014; Rutkowska et al., 2015). Thus, EBI2 has been reported to be expressed in multiple tissues and organs: however, no data are available about its presence in adipocytes and adipose tissue. EBI2 was expressed in both BA and WA, and its expression level increased significantly (3.5 fold increase) during differentiation in BA but not in WA. Mature BA expressed significantly higher level of EBI2 than mature WA (+74%) (Figure 4A), suggesting a specific role of EBI2 in thermogenic active adipocytes. EBI2 mRNA was also expressed in all the different depots of adipose tissue (i.e. BAT, WATi, WATg and PVAT) (Figure 4B) and its level was comparable to those of other organs in which it has been reported to have a role, such as brain (Rutkowska et al., 2015, 2018; Wanke et al., 2017), lung (Jia et al., 2018; Shen et al., 2017) and intestine (Emgård et al., 2018; Wyss et al., 2019). These data suggest a possible role of EBI2 in adipocytes and adipose tissue biology.

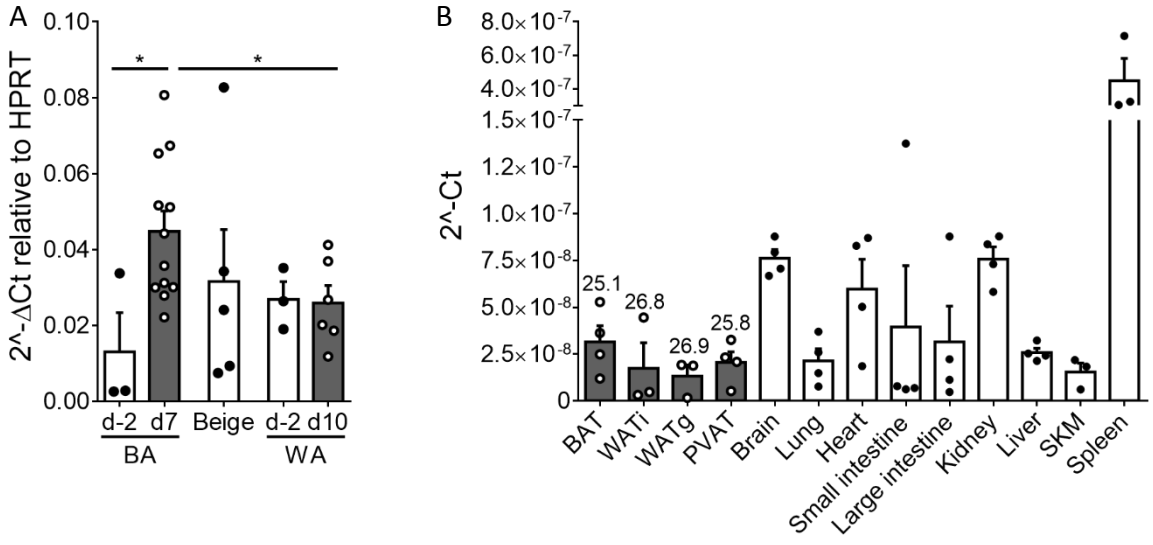

Figure 4: EBI2 expression in adipocytes and tissues

(A) Relative expression to HPRT of EBI2 in pre (d-2) and mature (d7) BA, beige adipocytes and pre (d-2) and mature (d10) WA. n=3-6. (B) Absolute expression of EBI2 in adipose tissues and other organs. n=4. Mean ± s.e.m.

4.2 | *In vitro* effects of EBI2 activation and depletion

4.2.1 | EBI2 couples to $G_{\alpha i}$ in BA

EBI2 has been previously reported to be a $G_{\alpha i}$ coupled receptor in different cell types (Benned-Jensen et al., 2011; Hannedouche et al., 2011; Rosenkilde et al., 2006); however, its coupling in BA has not been tested so far. To test whether EBI2 couples to $G_{\alpha i}$ in BA as well, the sensitivity of its downstream signaling pathway activation to pertussis toxin (PT) was tested. ERK1/2 phosphorylation has been reported to be induced after activation of every type of G_{α} subunit, as well as $G_{\beta\gamma}$ subunit and β-arrestin (Eishingdrelo, 2013), and thus was chosen as readout for testing EBI2 coupling. Additionally, previous studies in astrocytes and CHO cells showed EBI2 activation increases ERK1/2 phosphorylation (Benned-Jensen et al., 2013; Rutkowska et al., 2015). Differentiated BA were treated with the EBI2 agonist 7α,25-OHC (1 μM) for 5 min, 10 min, 20 min, 30 min or 60 min (Figure 5A). The peak in p-ERK1/2 was reached after 5 min of treatment, and the phosphorylation rapidly reached basal level at 10 min (Figure 5B). Thus, 5 min of treatment with 7α,25-OHC was chosen as time point to test EBI2 $G_{\alpha i}$ coupling. Differentiated BA were then pre-treated with PT (200 ng/ml) for 10 min, then for 5 min with 7α,25-OHC. Furthermore, to test the specificity of 7α,25-OHC effect, the highly specific EBI2 antagonist NIBR189 was used (Gessier et al., 2014). As shown in Figure 5C, the increase in ERK1/2 phosphorylation due to 7α,25-OHC treatment was completely blunted by PT, as well as by NIBR189 (10 μM), indicating that EBI2 couples to $G_{\alpha i}$ and it is selectively activated by 7α,25-OHC.

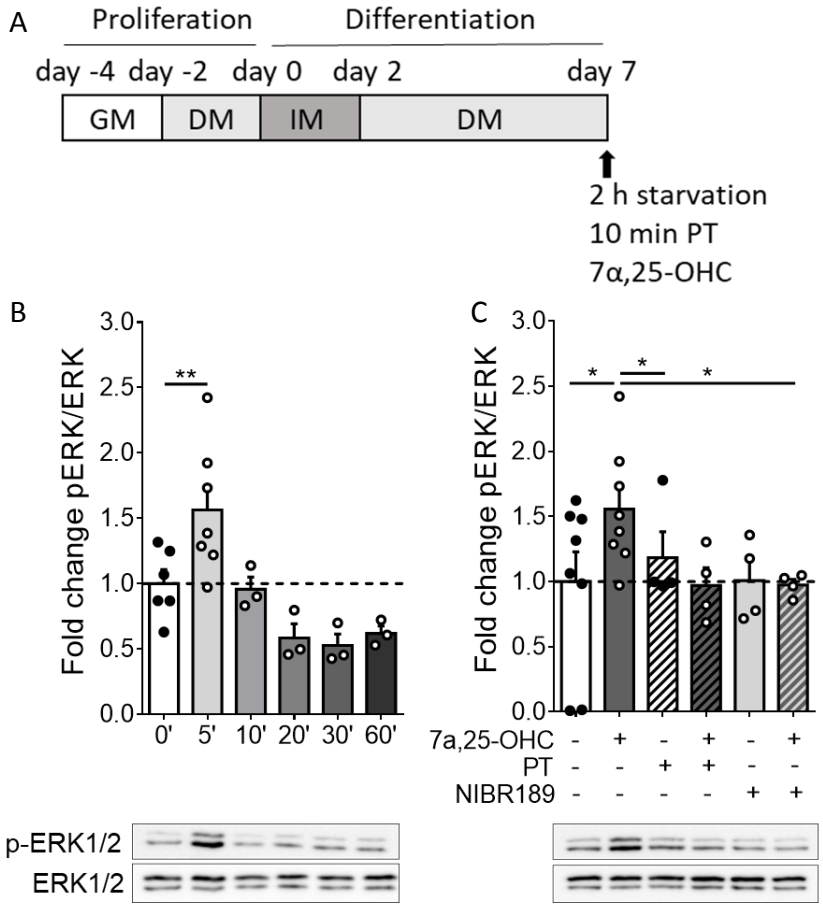

Figure 5: Effect of EBI2 activation on ERK1/2 phosphorylation and $G_{\alpha i}$ coupling

*(A) Schematic representation of BA differentiation and treatment. (B) Relative quantification (above) and representative immunoblot of p-ERK1/2 in BA treated for different times with the endogenous ligand 7α,25-OHC (1 µM). n=3-6. (C) Relative quantification (above) and representative immunoblot of p-ERK1/2 in BA treated for 5 min with 7α,25-OHC (1 µM), pertussis toxin (PT, 200 ng/ml) or the EBI2 antagonist NIBR189 (10 µM). n=4-7. Mean ± s.e.m. ANOVA, * p≤ 0.05, **p≤0.01.*

4.2.2 | EBI2 influences acutely BA activation

Previous studies have shown that 7α,25-OHC can potently decrease intracellular cAMP (IC50 2nM) in cell line stably expressing human EBI2 (Liu et al., 2011). To test whether 7α,25-OHC can affect the cAMP level in adipocytes, BA were treated with 7α,25-OHC (1 nM for 30 min) in presence or absence of NE. Consistently with the literature and the $G_{\alpha i}$ coupling of EBI2, the intracellular levels of cAMP were decreased by 7α,25-OHC treatment (Figure 6A). This effect was

concentration dependent, showing a bell-shaped dose-response curve (Figure 6B) characteristic of many chemotactic GPCRs (Allegretti et al., 2016), with $IC50_1$ 6.60 pM and $IC50_2$ 59.80 nM. cAMP activates PKA, thus inducing phosphorylation of the hormone-sensitive lipase (HSL), which mobilizes the stored fat in the adipocytes. Consistently, also the NE-induced phosphorylation of HSL was decreased by 7α,25-OHC treatment (1 µM for 10 min) (Figure 6C).

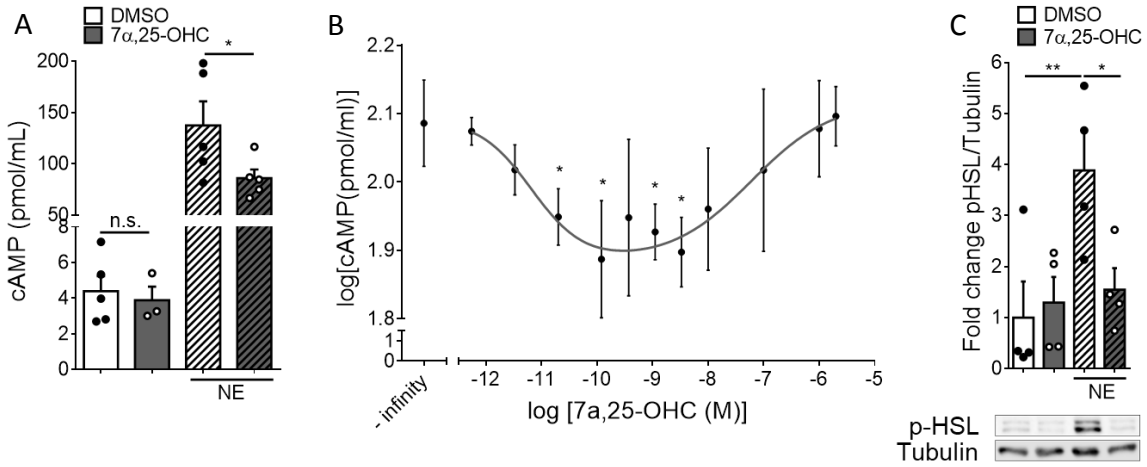

Figure 6: Effects of acute EBI2 activation on intracellular cAMP, p-HSL and thermogenic markers

*(A) Intracellular cAMP levels of BA treated with 7α,25-OHC (1 nM) and/or NE (1 µM). n=3-5. (B) Intracellular cAMP levels of BA treated with increasing concentrations of 7α,25-OHC and NE (1 µM). n=6. (C) Relative quantification (above) and representative immunoblot (below) of p-HSL in BA treated for 10 min with 7α,25-OHC (1 µM) and/or NE (1 µM). n=6. Mean ± s.e.m. t- test and ANOVA, * p≤ 0.05, **p≤0.01, *** p≤0.001.*

$G_{\alpha i}$ coupled receptors have been previously reported to be able to decrease lipolysis in adipocytes (Ge et al.; Liu et al., 2009). Through lipolysis, triglycerides are hydrolyzed into glycerol and free fatty acids. To test whether EBI2 activation was able to inhibit *in vitro* lipolysis, mature BA were treated with NE (30 nM), the EBI2 ligand 7α,25-OHC (1 µM) or the EBI2 antagonist NIBR189 (10 µM). The basal levels of lipolysis were not influenced by the treatment of BA with 7α,25-OHC. However, when lipolysis was induced by NE treatment, the activation of EBI2 significantly decreased the glycerol released by adipocytes, indicating a reduction in lipolysis and further confirming the EBI2 coupling with $G_{\alpha i}$ (Figure 7A). This effect was blunted by the presence of NIBR189. Moreover, BA deficient of EBI2 did not show differences when treated with 7α,25-OHC. Together, the pharmacological inhibition of EBI2 with NIBR189 and the use of EBI2 KO BA indicated the specificity of 7α,25-OHC in activating EBI2 (Figure 7A). Dose response analysis

showed that the NE-induced lipolysis was potently decreased by 7α,25-OHC in a concentration dependent manner, with an IC50 of 1.48 nM (Figure 7B).

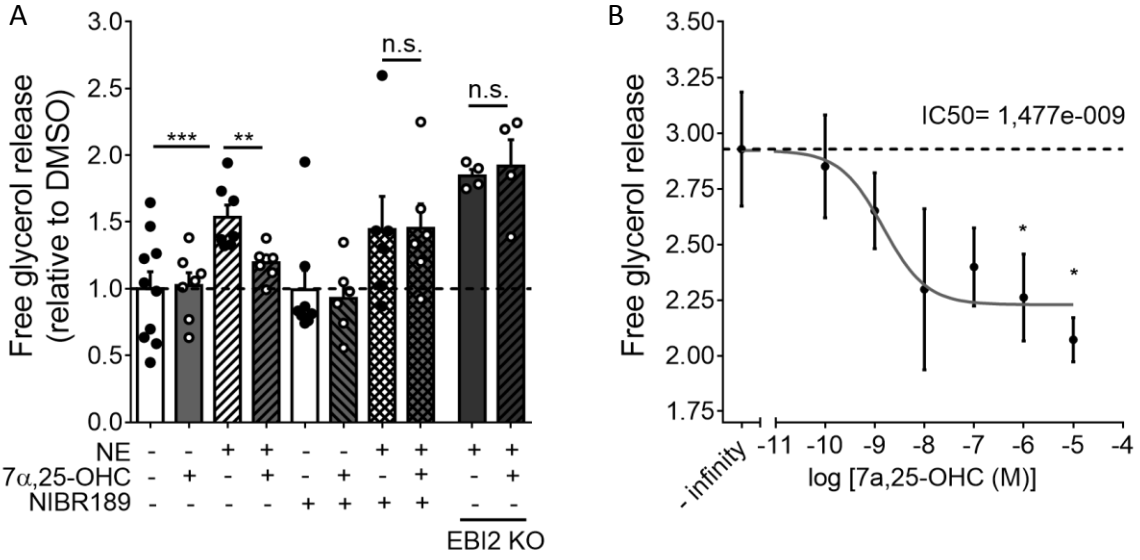

Figure 7: Effect of EBI2 activation on NE-induced lipolysis in BA

*(A) In vitro lipolysis measured as relative glycerol release from BA treated with NE (30 nM), 7α,25-OHC (1 µM) or NIBR189 (10 µM). n=4-10. (B) In vitro lipolysis measured as relative glycerol release from BA treated with NE (30 nM) and increasing concentrations of 7α,25-OHC. n=4. Mean ± s.e.m. ANOVA, * p≤ 0.05, **p≤0.01, *** p≤0.001.*

4.2.3 | EBI2 influences WA activation

The effect of EBI2 activation was also tested in WA. Fully differentiated WA were treated with NE (1 µM for cAMP ELISA, 30 nM for lipolysis) and the EBI2 ligand 7α,25-OHC (1 nM for cAMP ELISA, 1 µM for lipolysis), similarly to the experiments performed in BA. Also in WA, the activation of EBI2 did not influence basal intracellular cAMP levels (Figure 8A) nor lipolysis (Figure 8B). In presence of NE the 7α,25-OHC treatments reduced cAMP and lipolysis, albeit not significantly (Figure 8A,B). Thus, EBI2 also reduces lipolysis in WA, albeit not significantly.

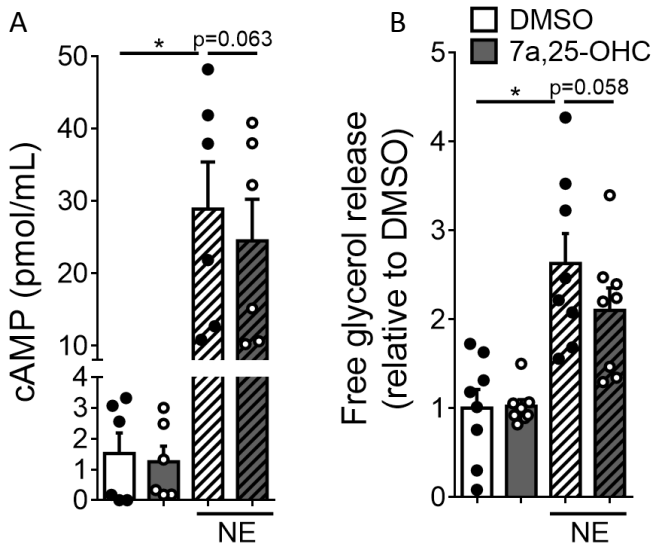

Figure 8: Effect of EBI2 activation on WA lipolysis and intracellular cAMP

*(A) Intracellular cAMP levels of WA treated with 7α,25-OHC (1 nM) and/or NE (1 µM). n=6. (B) In vitro lipolysis measured as relative glycerol release from WA treated with NE (30 nM), 7α,25-OHC (1 µM) or NIBR189 (10 µM). n=8. Mean ± s.e.m. One-way ANOVA, * p≤ 0.05.*

4.2.4 | Acute EBI2 activation decreases mitochondrial maximal respiration of BA

Together with lipolysis, oxygen consumption is a key measure of BA activation. To investigate if mitochondrial respiration was affected by EBI2 activation, the complete respiratory profile of BA was analyzed (Figure 9).

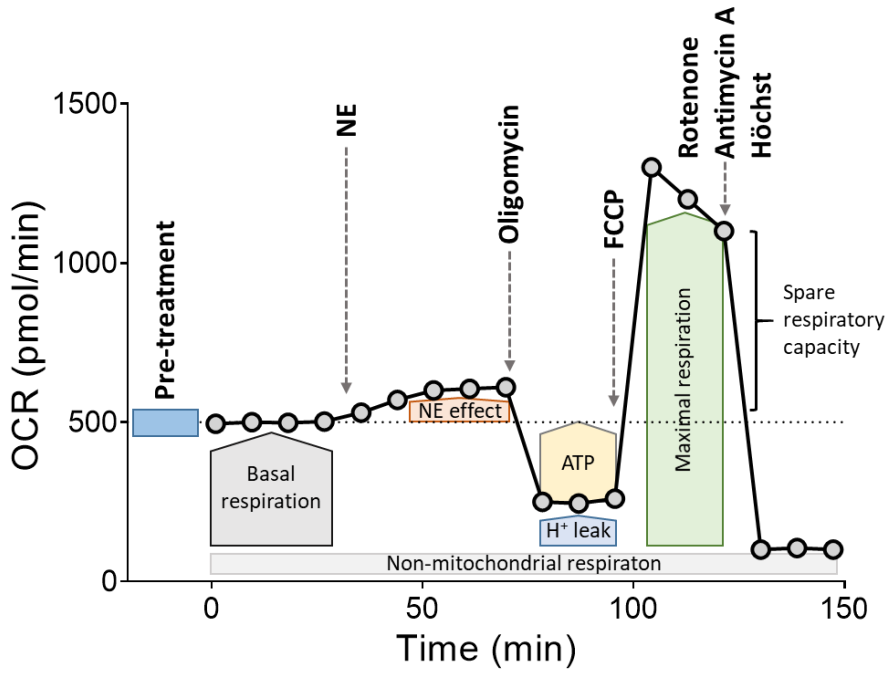

Figure 9: Schematic representation of Oxygen Consumption Rate (OCR) and treatment of BA

Murine BA were pre-treated for 15 min with DMSO or 7α,25-OHC (1 µM). The basal respiration, non-mitochondrial respiration, NE-effect, ATP-dependent respiration (ATP), proton leak (H^+ leak), maximal respiration and spare respiratory capacity were calculated from the OCR.

BA were pretreated with either vehicle (DMSO) or the EBI2 ligand 7α,25-OHC (1 µM) for 15 min. After determining basal respiration, the cells were treated with NE (1 µM) and the NE-induced respiration was measured. The adenosine triphosphate (ATP) synthase inhibitor oligomycin (2 µM) was then added, to distinguish between oxygen consumption from ATP synthesis (coupled respiration) and proton leak (uncoupled respiration). Next, the ionophore uncoupling agent carbonyl cyanide-4-(trifluoromethoxy)phenylhydrazone (FCCP) (1 µM) was used to assess the maximal respiratory capacity and the spare respiratory capacity, indicating the ability of the cells to respond to increased energy demand or under stress. Finally, rotenone and antimycin A (0.5 µM each) were added to block the electron transport chain. The remaining oxygen consumption was calculated as non-mitochondrial respiration (Figure 10).

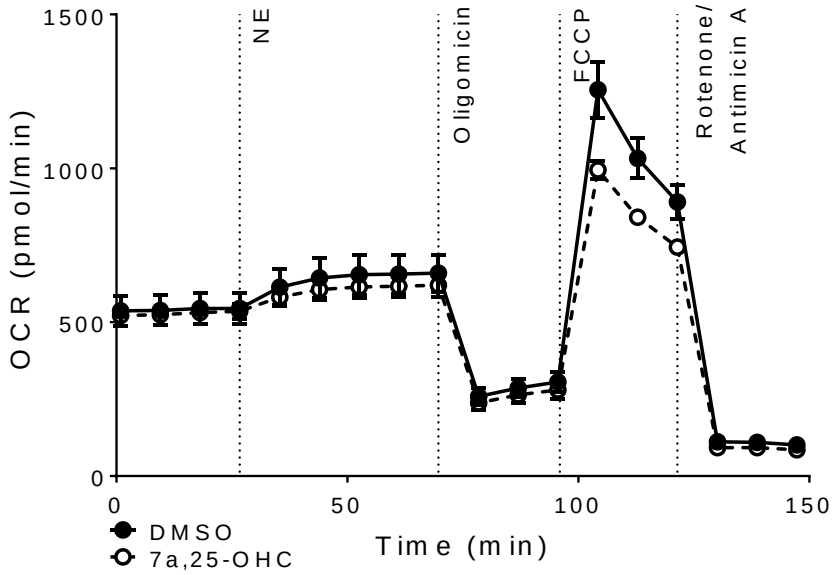

Figure 10: Respirometry trace of BA following pretreatment with 7α,25-OHC

Time course of oxygen consumption rates (OCR) of BA pre-treated for 15 min with vehicle (DMSO) or 7α,25-OHC (1 μM) before energetic profiling.

When pretreated with 7α,25-OHC BA showed a significantly lower response to NE-induced oxygen consumption compared to DMSO treated BA (Figure 11B), as well as markedly reduced maximal respiration and spare respiratory capacity (Figure 11E,F). No differences were observed in the basal respiration, ATP production, proton leak and non-mitochondrial respiration (Figure 11A,C,D,G). These results suggest that EBI2 activation negatively influences the ability of BA to respond to noradrenergic stimulation and to high demand of energy from mitochondria.

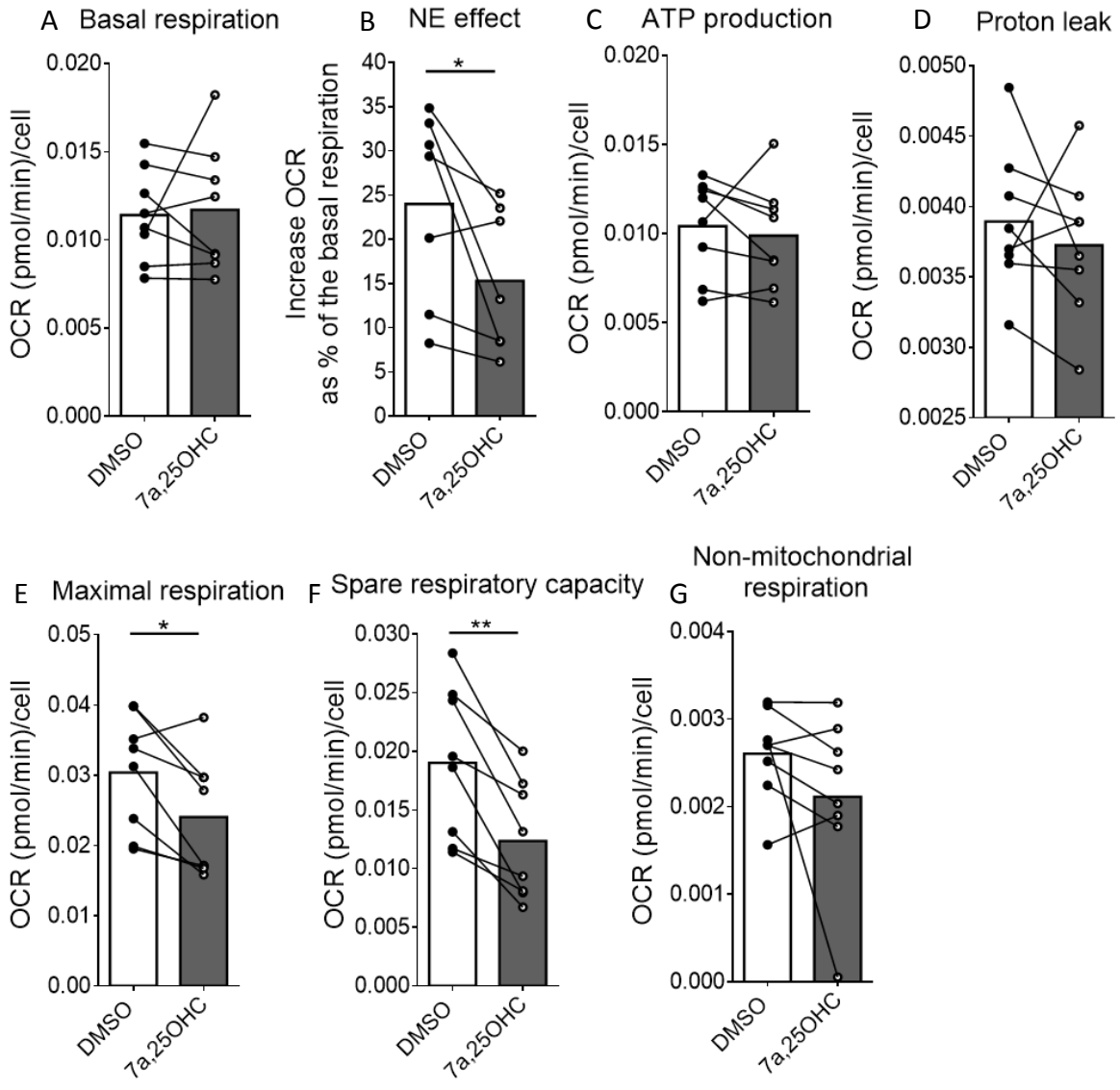

Figure 11: Mitochondrial respiration of BA following pretreatment with 7α,25-OHC

*(A-G) Basal respiration (A), NE-induced respiration increase (B), ATP-production (C), proton leak (D), maximal respiration (E), spare respiratory capacity (F) and non-mitochondrial respiration (G) of murine BA pre-treated for 15 min with vehicle (DMSO) or 7α,25-OHC. n=8. Mean ± s.e.m. t- test, **p≤0.01.*

4.2.5 | EBI2 activation increases NE-induced ROS production in BA

The decrease in the maximal respiration and spare respiratory capacity observed in BA following treatment with 7α,25-OHC and NE suggests that energy might also be dissipated through a mechanism independent of ATP-synthase and UCP1. Previous publications reported that treatment of BA with NE acutely increases ROS production, and that ROS production is

responsible for decrease in maximal respiration (Chouchani et al., 2016; Lettieri-Barbato, 2019; Shabalina et al., 2014) and spare respiratory capacity in endothelial cells (Dranka et al., 2010). To investigate if the activation of EBI2 could influence the production of ROS, BA were treated with 7α,25-OHC (1 µM), NE (1 µM) and NIBR189 (10 µM), and the kinetic of ROS production was measured. The NE treatment increased ROS production, albeit not significantly, reaching a plateau after 60 min of treatment (Figure 12A). 7α,25-OHC alone had no effect in ROS production, however significantly increased ROS level in presence of NE (Figure 12A), with a peak at 60 min (Figure 12B) and then reaching levels comparable to NE alone after 4 hours (Figure 12A). The 7α,25-OHC effect in presence of NE was completely blunted by the presence of the EBI2 antagonist NIBR189, thus indicating that the effect was mediated by EBI2 (Figure 12A,B). This results indicate that 7α,25-OHC is able to increase NE-induced ROS production in BA.

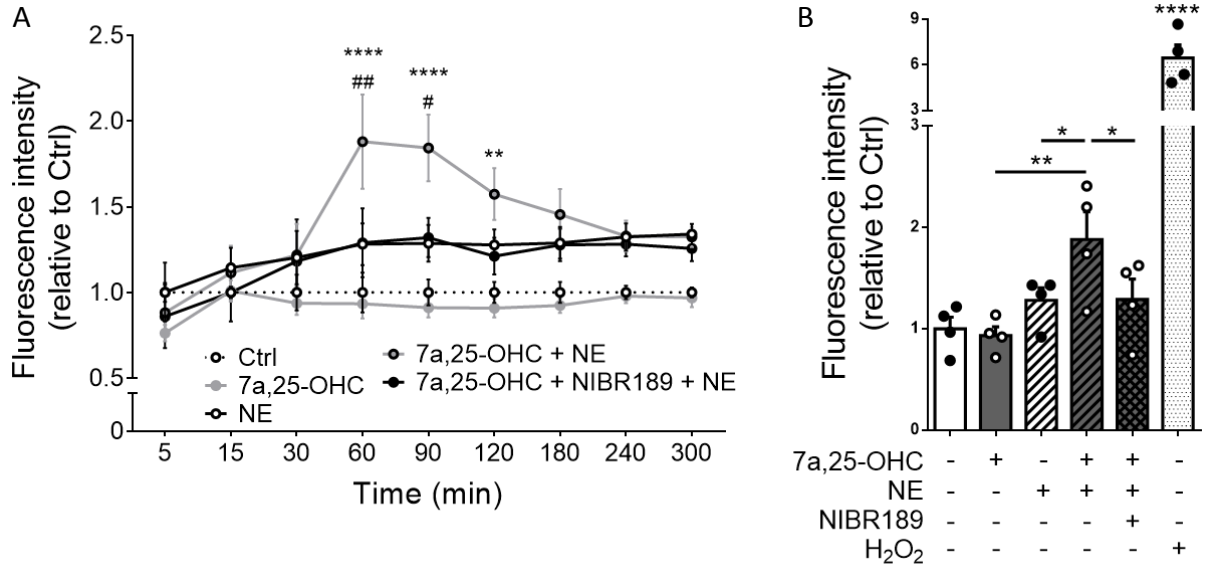

Figure 12: BA ROS production following NE and 7α,25-OHC treatment

(A*) BA ROS production measured as fluorescence intensity at different time points following NE (1 µM), 7α,25-OHC (1 µM) and NIBR189 (10 µM). (B) BA ROS production measured as fluorescence intensity after 60 min of treatment. H_2O_2 3%. n=4. Mean ± s.e.m. One-way and two-way ANOVA, *p≤0.05, **p≤0.01, ****p≤0.0001.*

4.2.6 | Chronic EBI2 activation and EBI2 loss do not affect BA differentiation

BA undergo a process of proliferation and differentiation before acquiring morphological and phenotypical characteristics of mature BA. To investigate the influence of chronic activation of EBI2 on the differentiation of BA, cells were treated chronically from the day of confluency (day -2) with 7α,25-OHC (1 µM). In parallel, BA were treated with 8-Br-cGMP (200 µM), a positive regulator of adipocytes differentiation (Hoffmann et al., 2015), to ensure the responsiveness of the cells to pharmacological treatments (Figure 13A). At the end of the differentiation process, BA treated with 7α,25-OHC showed comparable Oil Red O staining (Figure 13B), levels of thermogenic (*Ucp1*) and adipogenic markers (*Pparg*, *Fabp4*) (Figure 13C) to the control, indicating that EBI2 activation does not significantly influence the differentiation of BA.

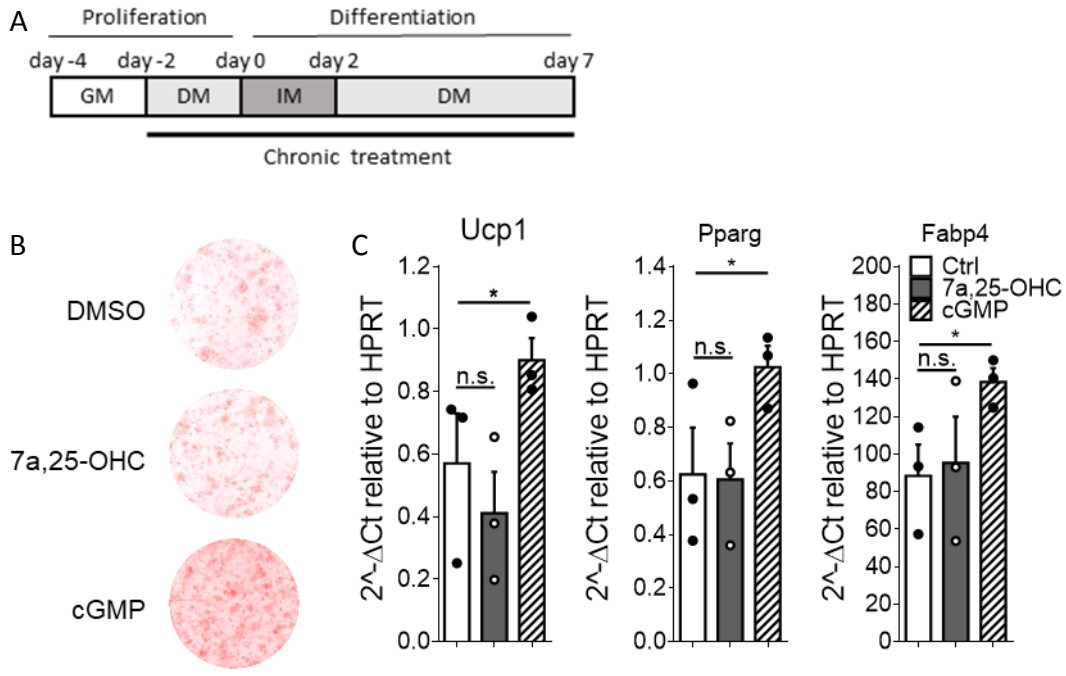

Figure 13: Effect of chronic EBI2 activation of BA differentiation

*(A) Schematic representation of BA differentiation and chronic treatment. (B) Representative Oil Red O stain of murine BA, differentiated in the presence of DMSO (1 µl/ml) as control, 7α,25-OHC (1 µM) or 8-Br-cGMP (200 µM). (C) Relative expression to HPRT of the thermogenic marker Ucp1 (left), and adipogenic markers Pparg (middle) and Fabp4 (right) in BA treated with 7α,25-OHC (1 µM) or 8-Br-cGMP (200 µM) during differentiation. n=3. Mean ± s.e.m. t- test and ANOVA, * p≤ 0.05.*

To test whether EBI2 loss could influence BA differentiation, primary BA were isolated from EBI2 WT and KO littermates and the expression of thermogenic (i.e. *Ucp1*, *Cidea* and *Pgc1a*) and adipogenic marker genes (i.e. *Pparg* and *Fabp4*) analyzed. EBI2 WT and KO BA presented comparable levels of both thermogenic and adipogenic genes, and similar response to chronic treatment with 8-Br-cGMP (200 µM) (Figure 14A). EBI2 WT and KO BA showed similar amount of lipid droplets (Figure 14B). Finally, EBI2 KO BA responded similarly to NE treatment (Figure 14C).

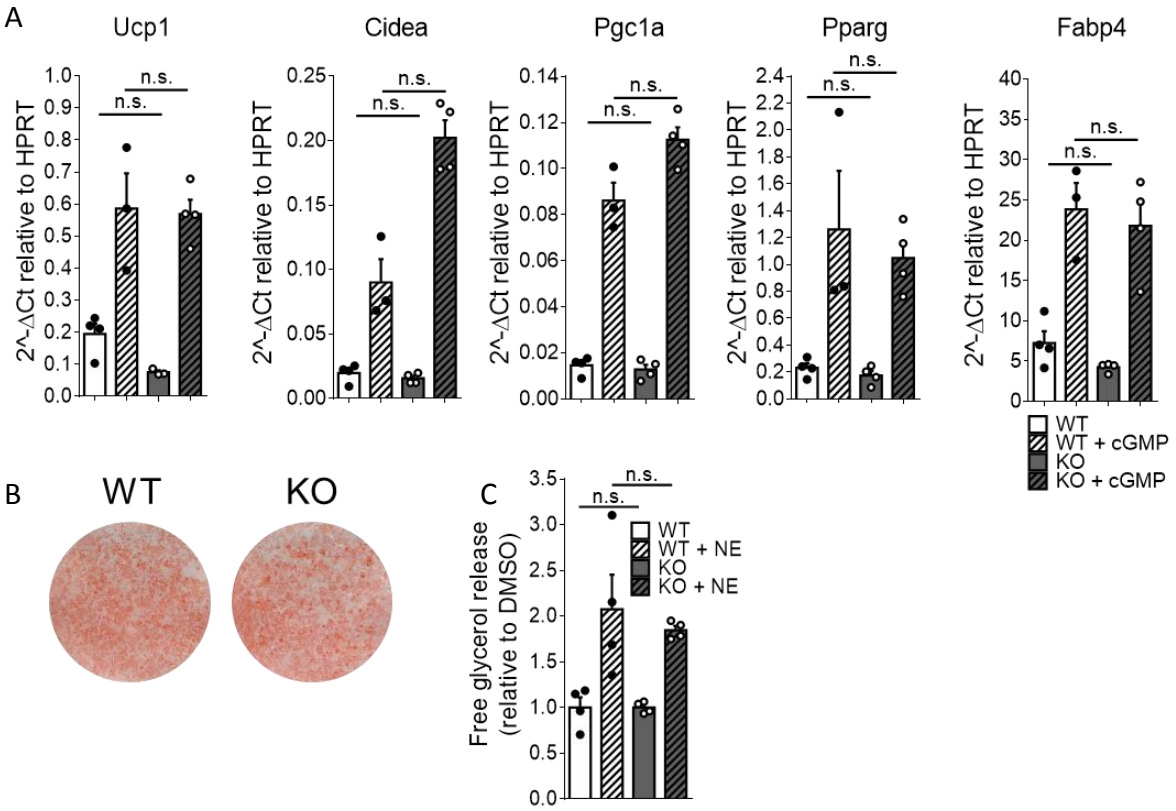

Figure 14: Activation and differentiation in EBI2 WT and KO BA

(A) Relative expression to HPRT of the thermogenic and adipogenic marker genes in EBI2 WT and KO BA, in presence or absence of chronic treatment with 8-Br-cGMP (200 µM). (B) Representative Oil Red O stain of EBI2 WT and KO BA. (C) In vitro lipolysis measured as relative glycerol release from EBI2 WT and KO BA treated with NE (1 µM). n=3-4. Mean ± s.e.m.

4.3 | *Ex vivo* effects of EBI2 activation and depletion

4.3.1 | EBI2 activation influences lipolysis of BAT from newborn mice and WATi from adult mice

Brown adipose tissue is particularly active in newborn mice (Napolitano and Fawcett, 1958). For this reason, BAT was harvested from 1-2 days old newborn WT mice and treated with the EBI2 ligand 7α,25-OHC (1 µM) alone or in combination with NE (1 µM), similarly to the *in vitro* experiment performed with immortalized BA (Figure 7). Consistently with what was observed *in vitro*, the treatment with the EBI2 ligand 7α,25-OHC decreased the effect of NE-induced lipolysis (Figure 15A).

The same experimental setup was used to investigate the effect of 7α,25-OHC on NE-induced lipolysis in WAT from adult mice (8 weeks old). The treatment with 7α,25-OHC was able to decrease the lipolysis in WATi stimulated with NE (Figure 15B), but no effect was measured in WATg (Figure 15C). Thus, these data suggest that EBI2 activation through its endogenous ligand 7α,25-OHC is able to decrease BAT and WATi lipolysis following NE stimulation. The difference between WATi and WATg might be explained by the lower levels of expression of EBI2 in WATg.

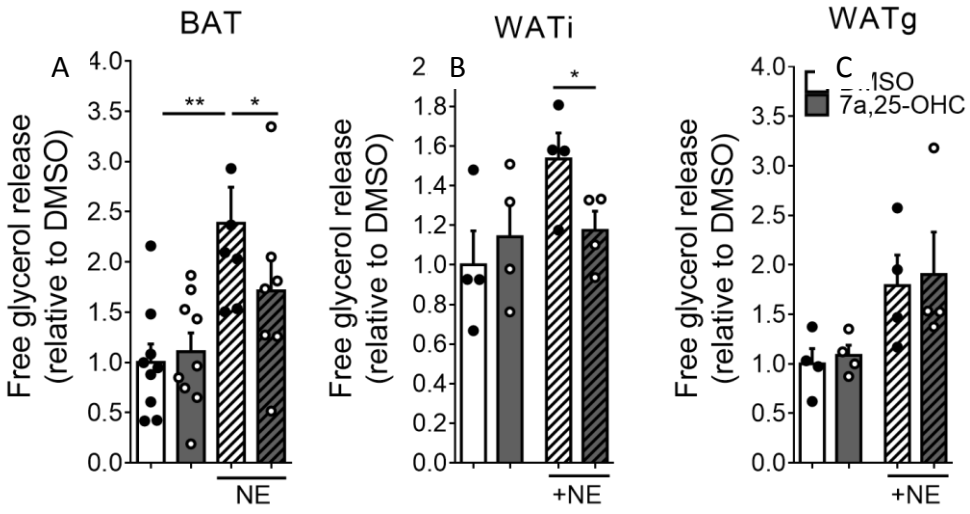

Figure 15: Effect of EBI2 activation on NE-induced lipolysis in ATs

*Ex vivo lipolysis measured as relative glycerol release from newborns BAT (A), 8 weeks old mice WATi (B) and 8 weeks old mice WATg (C) treated with NE (1 µM) and/or 7α,25-OHC (1 µM). n=4-9. Mean ± s.e.m. t- test, * p≤ 0.05.*

4.3.2 | Loss of EBI2 partially influences basal and NE stimulated lipolysis in ATs

To investigate whether the loss of EBI2 influences the ability of ATs to perform lipolysis, BAT, WATi and WATg were harvested from 8 weeks old WT and EBI2 KO littermates and lipolysis assay was performed. ATs from WT and EBI2 KO mice had similar basal level of lipolysis, besides a small but significant increase in EBI2 KO WATi compared to WT (Figure 16A). When WATi or WATg were stimulated with NE (1 µM), the relative NE-responses were comparable between WT and KO in WAT (Figure 16B, middle and right). In contrast, whereas the relative NE-induced increase in lipolysis was stronger in BAT from EBI2 KO mice than WT (Figure 16B, left), suggesting that EBI2 might be involved in regulating the response to noradrenergic stimulus in brown adipose tissue.

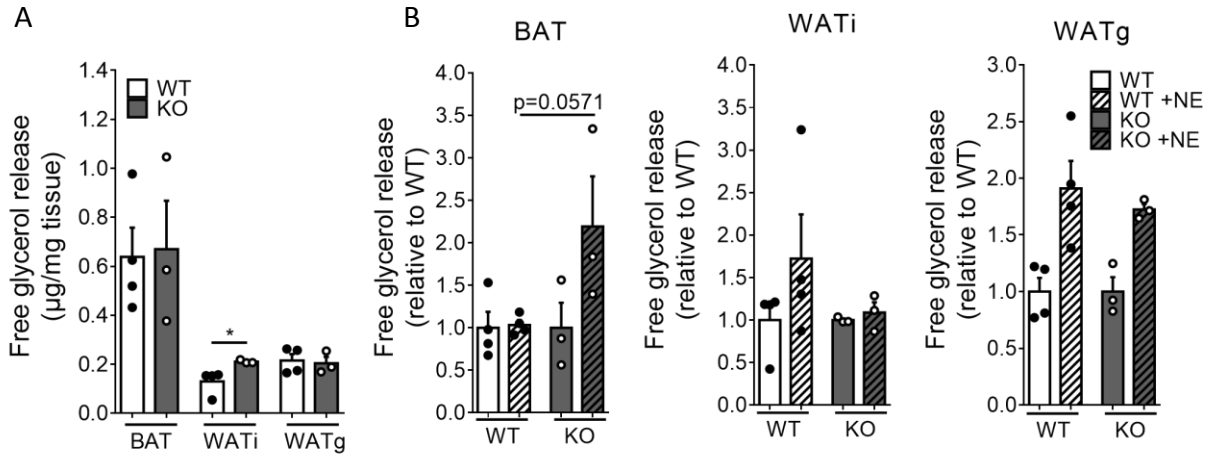

Figure 16: Effect of EBI2 depletion on lipolysis in ATs

*(A) Basal ex vivo lipolysis measured as relative glycerol release from ATs of WT and EBI2 KO mice. (B) Ex vivo lipolysis of BAT (left), WATi (middle) and WATg (right) of adult (8 weeks old) WT and EBI2 KO mice stimulated with NE (1 µM). n=4. Mean ± s.e.m. t- test, * p≤ 0.05.*

4.4 | Effects of EBI2 KO in diet-induced obesity mouse model

4.4.1 | Loss of EBI2 does not affect high fat diet-induced weight gain

In order to investigate the effect of EBI2 in obesity, EBI2 knockout mice were used. 8 weeks old mice were fed for 12 weeks with a high fat diet (HFD, 60% fat) or a control diet (ND) and their body weight was recorded weekly (Figure 17).

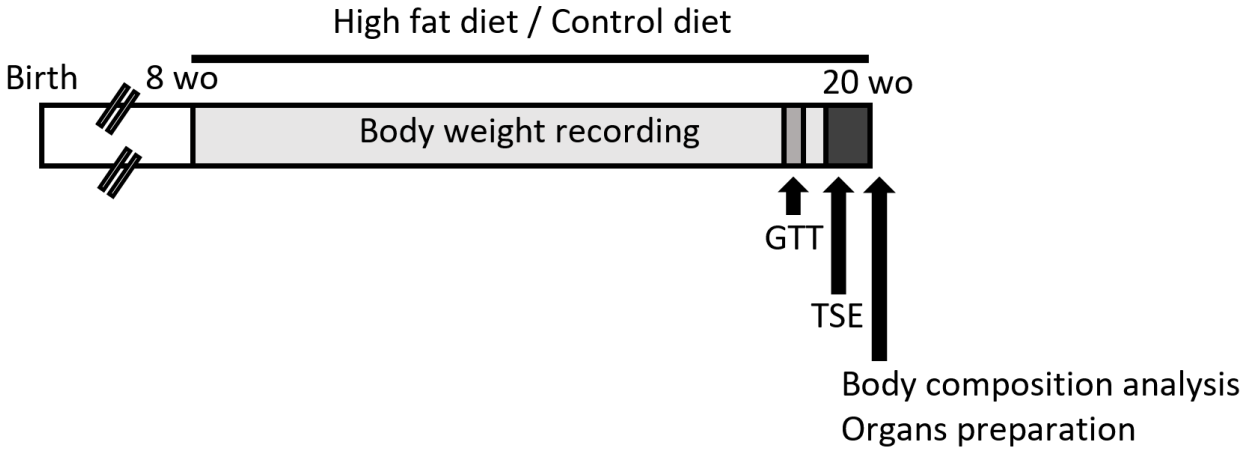

Figure 17: High fat diet experiment setup

Schematic representation of 12 weeks high fat diet/control diet experiment followed by glucose tolerance test (GTT) and metabolic cages (TSE) measurement.

EBI2 WT and KO mice showed no significant differences in the body weight at the start of the experiment (8 weeks old), as well as at the end (20 weeks old), neither in ND (Figure 18A) nor in HFD (Figure 18C). In HFD conditions, both the genotypes gained ~65% of their initial body weight. At the end of the 12 weeks of diet, the body composition of the mice was analyzed, measuring fat mass, lean mass and free water (Figure 18B,D). No major differences could be observed between WT and KO mice (Figure 18D).

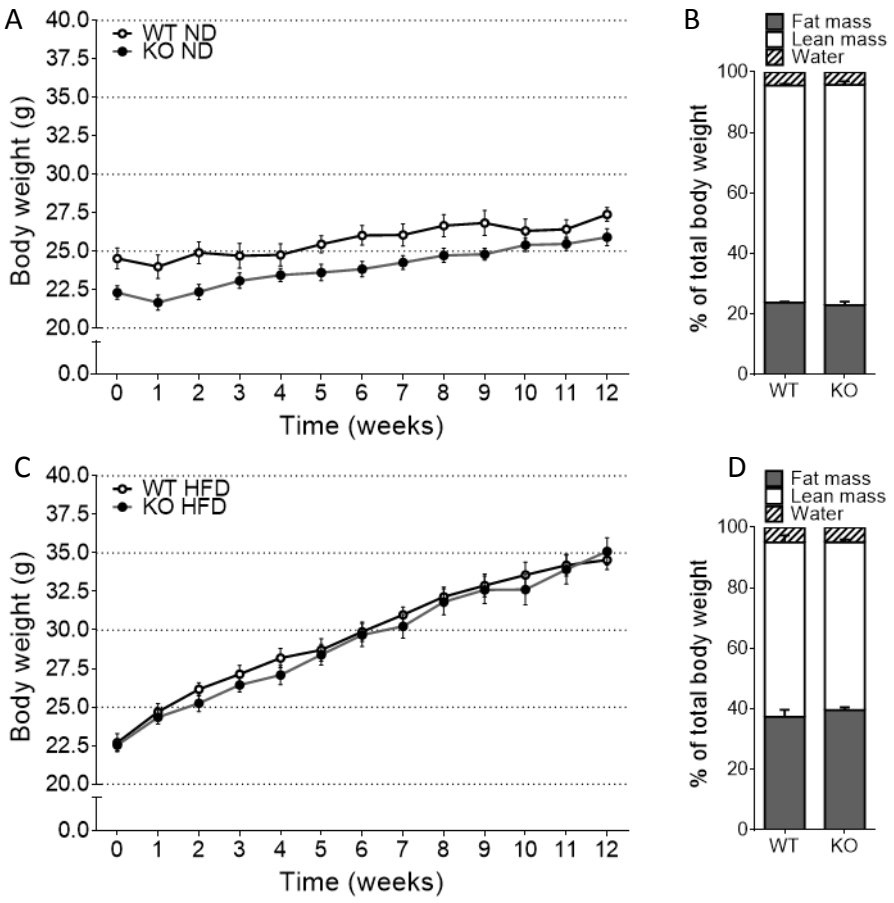

Figure 18: Body weight and body composition of WT and EBI2 KO mice under ND and HFD

(A,C) Body weight of WT and EBI2 KO mice during 12 weeks of ND (A) or HFD (C). (B,D) Fat mass, lean mass and free water of WT and EBI2 KO mice after 12 weeks of ND (B) or HFD (D) as percentage of total body weight. *n=12 per group.* Mean ± s.e.m. two-way ANOVA and t- test.

To investigate possible differences in adipose tissue depots, BAT, WATi and WATg were harvested (Figure 19A) and the weight recorded. The white adipose tissue depots showed significant increase in weight following HFD (~2 fold increase in WATi and ~3 fold increase in WATg), but no significant differences between WT and KO mice could be observed in any AT depots (ND: +11.3% in BAT KO vs. WT, -3.7% in WATi KO vs. WT, -13.8% in WATg KO vs. WT; HFD: +5.2% in BAT KO vs. WT, +4.9% in WATi KO vs. WT, +1.7% in WATg KO vs. WT) (Figure 19B).

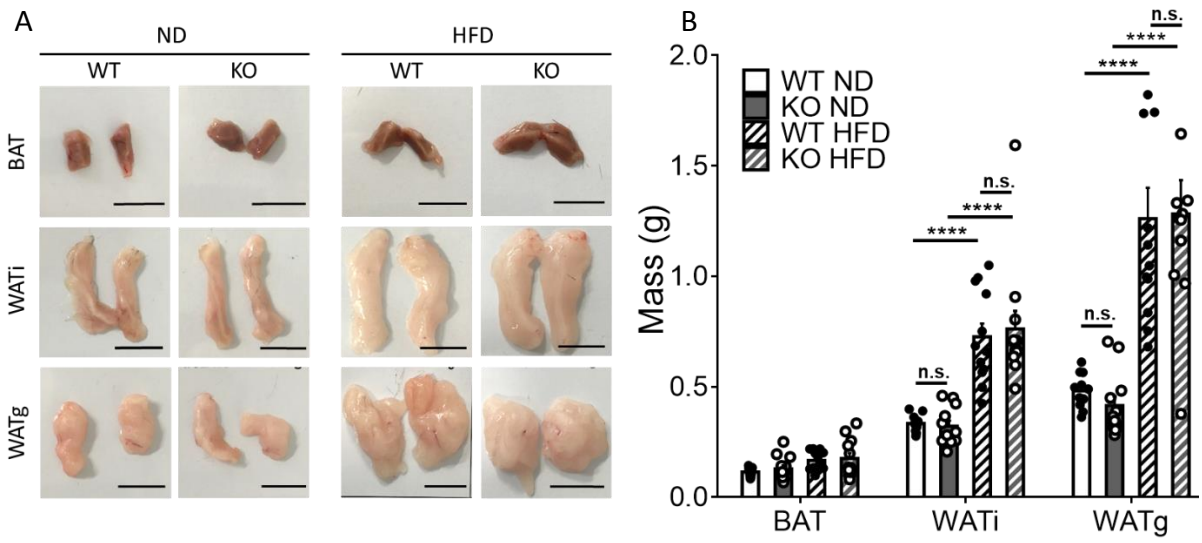

Figure 19: Adipose tissues in WT and EBI2 KO in ND and HFD

*(A) BAT (upper row), WATi (middle row) and WATg (bottom row) of WT and EBI2 KO after 12 weeks of ND or HFD. (B) Adipose tissues weight of WT and EBI2 KO mice after 12 weeks of ND or HFD. n=12 per group. Mean ± s.e.m. ANOVA, * p≤ 0.05, **p≤0.01, *** p≤0.001, **** p≤0.0001. Scale bar: 1 cm.*

Finally, possible differences in the morphology of adipocytes was investigated by histological analysis. The two genotypes showed similar morphology of adipocytes (Figure 20A), and no differences could be observed regarding the area of white adipocytes of WT and KO mice, on the same diet (Figure 20B,C). All together, these results suggest that the lack of EBI2 does not influence body weights and adipose tissue morphology in diet-induced obesity.

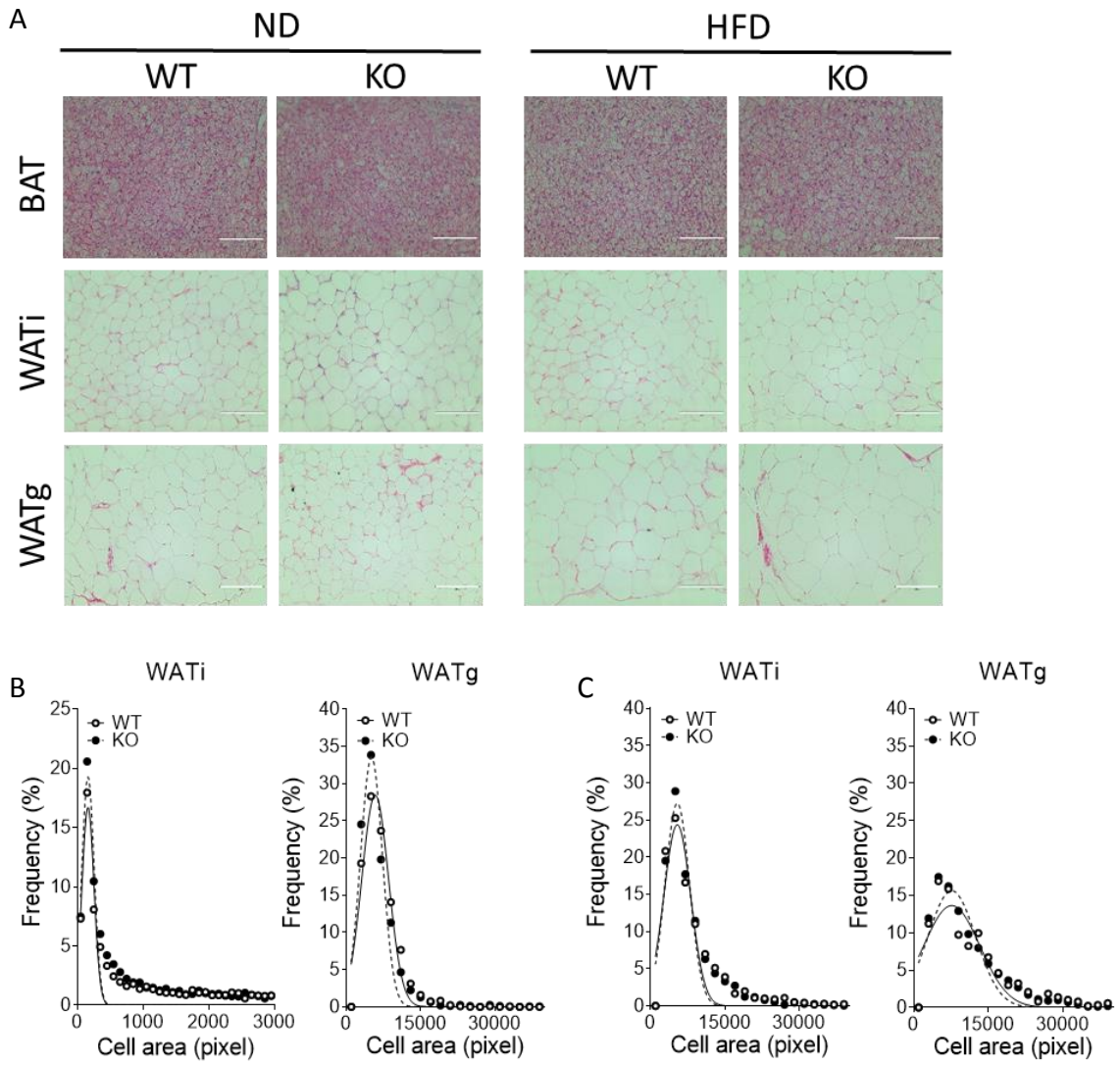

Figure 20: HE stainings of ATs from EBI2 KO mice after ND and HFD

(A*) HE staining of BAT (upper), WATi (middle) and WATg (bottom) from WT and EBI2 KO mice after 12 weeks of ND (left) or HFD (right). (B,C) Cell area distribution of adipocytes from WATi and WATg of ND (B) and HFD (C) fed mice. n=12 per group. Scale bar: 100 µm.*

4.4.2 | Loss of EBI2 affects UCP1 levels in BAT after HFD

To investigate possible influence of the lack of EBI2 on thermogenic abilities of the adipose tissues, the *Ucp1* levels were measured with RT-qPCR comparing WT and EBI2 KO mice, after 12 weeks (20 weeks old) of ND or HFD. A significant increase (+39.7%) in *Ucp1* was observed in BAT of HFD KO mice compared to HFD WT, whereas *Ucp1* expression was unaffected by EBI2 loss in the other adipose tissue depots (Figure 21A). Similar results were obtained with

immunohistochemistry on BAT and WATi (Figure 21B). Thus, the lack of EBI2 seems to influence the levels of *Ucp1* exclusively in BAT of HFD fed mice.

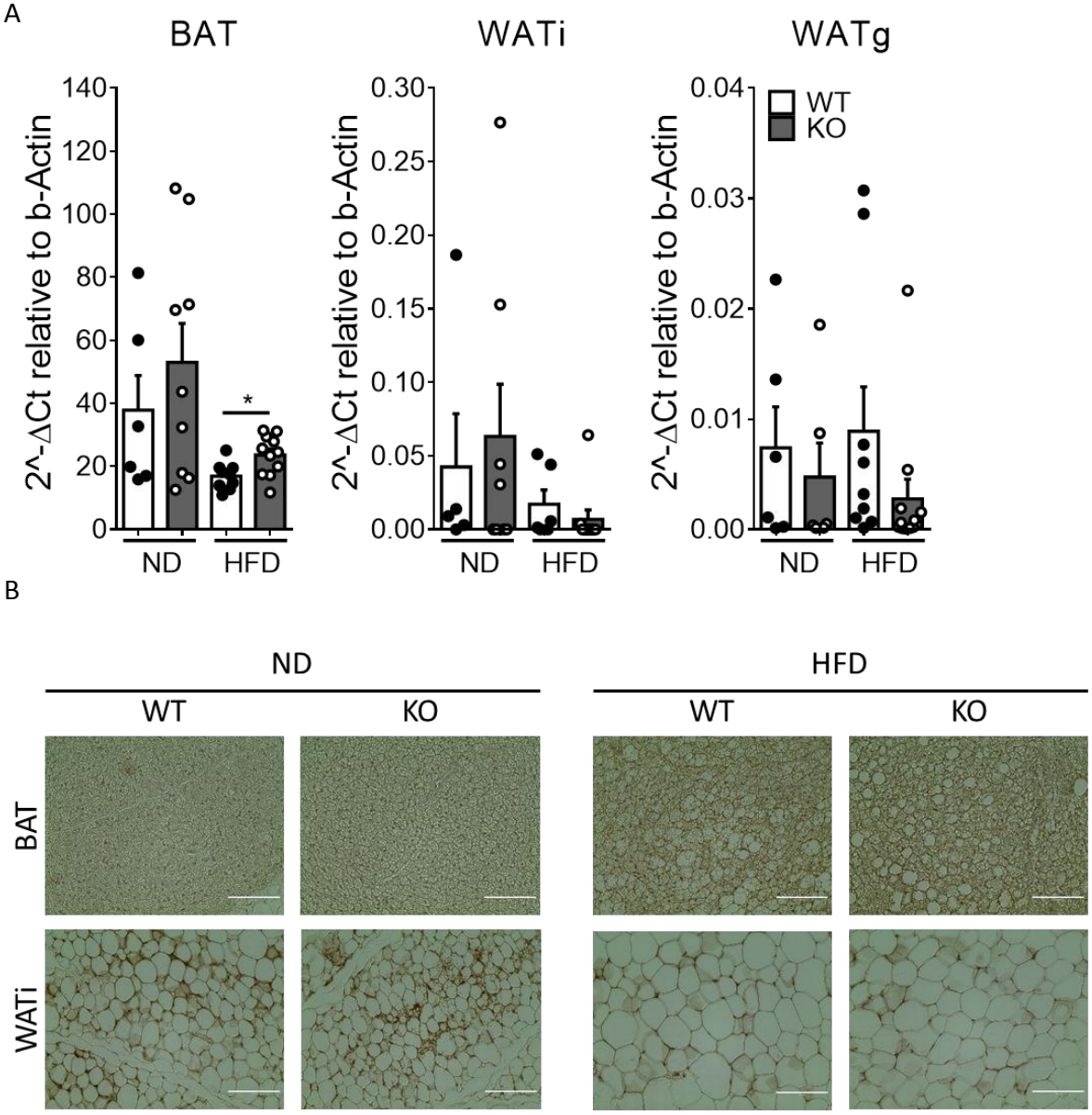

Figure 21: Ucp1 levels in adipose tissues

*(A) Ucp1expression relative to b-Actin in BAT (left), WATi (middle) and WATg (right) of WT and EBI2 KO mice after 12 weeks of ND or HFD. (B) DAB staining of UCP1 of BAT (above) and WATi (below) from WT and EBI2 KO mice after 12 weeks of ND or HFD. n=6-9. Mean ± s.e.m. t- test, * p≤ 0.05. Scale bar: 100 µM.*

4.4.3 | Loss of EBI2 decreases whole body metabolism in HFD fed mice but not under ND

The whole-body metabolism of WT and KO mice was characterized at the end of the 12 weeks of high fat or control diet. To this purpose, the VO_2 consumption, a measure for the energy expenditure, was recorded for 24h. Under ND, WT and EBI2 KO mice showed comparable energy expenditure (Figure 22A,B), both independently (Figure 22A) and in correlation with the body weight (Figure 22C). Differently, KO HFD mice had lower VO_2 consumption compared to WT, both during the day and the night time (Figure 23A,B). When analyzed in correlation to the body weight, the energy expenditure of EBI2 KO mice was significantly lower despite comparable body weight (Figure 23C), showing that the reduction in energy expenditure was not due to difference in the mass of the EBI2 KO mice.

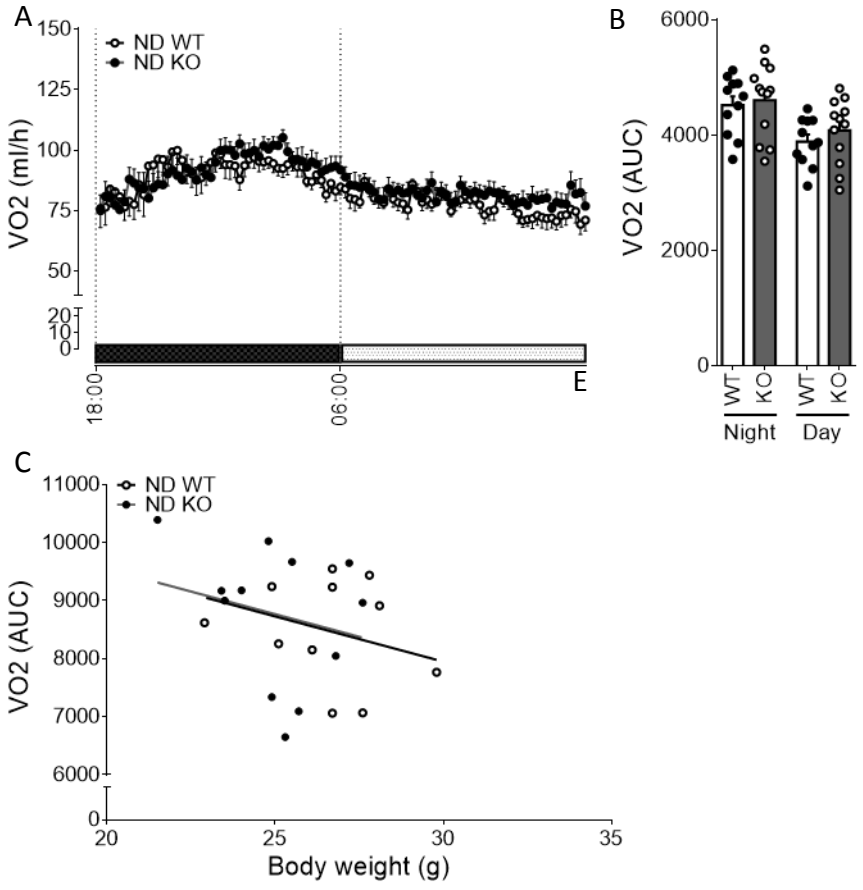

Figure 22: Whole-body metabolism of WT and EBI2 KO mice after 12 weeks of ND

(A,B) VO_2 consumption (ml/l) over 24 h (A) and as A.U.C of A (B) after 12 weeks of ND. (C) ANCOVA analysis of VO2 consumption (ml/l, AUC) over 24 h in relation to body weight. n=12 per group. Mean ± s.e.m.

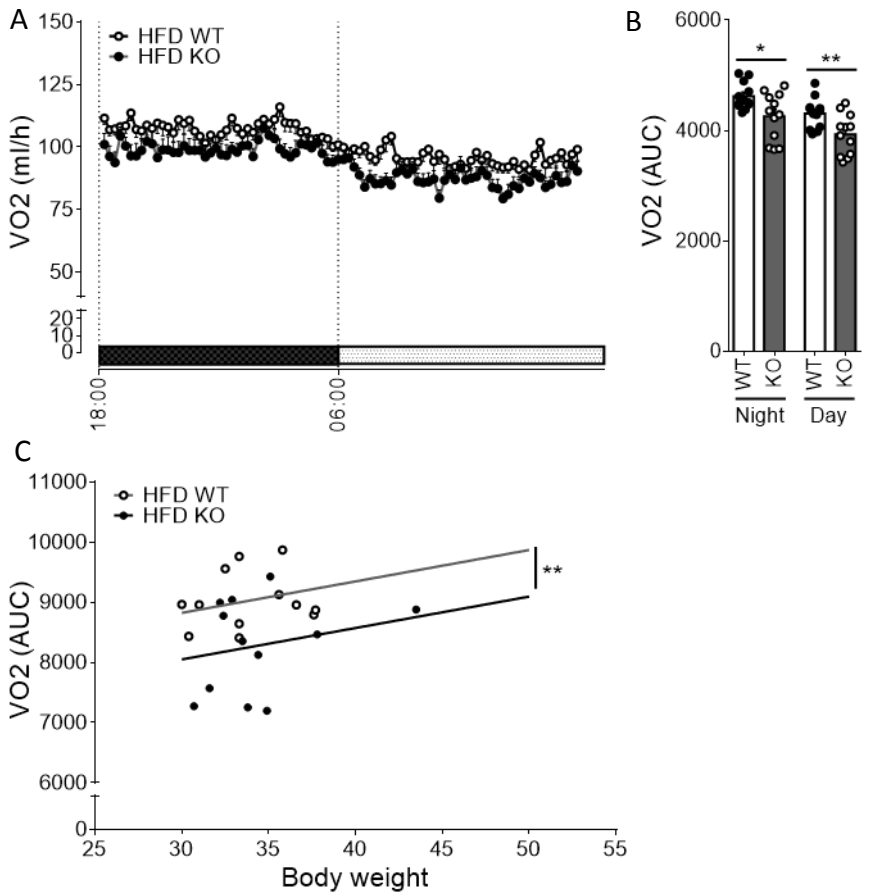

Figure 23: Whole-body metabolism of WT and EBI2 KO mice after 12 weeks of HFD

*(A,B) VO2 consumption (ml/l) over 24 h (A) and as A.U.C of A (B) after 12 weeks of HFD. (C) ANCOVA analysis of VO2 consumption (ml/l, AUC) over 24 h in relation to body weight. n=12 per group. Mean ± s.e.m. t-test, * p≤ 0.05.*

The reduction in the energy expenditure was moreover not due to reduced locomotor activity of KO mice compared to WT mice: indeed, KO mice showed a trend towards increased locomotor activity rather than decreased (Figure 24A). The lower energy expenditure was also not caused by an increased clearance of the lipids in the feces, since the energy content of feces from WT and KO mice was comparable (Figure 24B, in collaboration with Prof. Dr. Martin Klingenspor, Technical University of Munich), as well as the food consumption (Figure 24C).

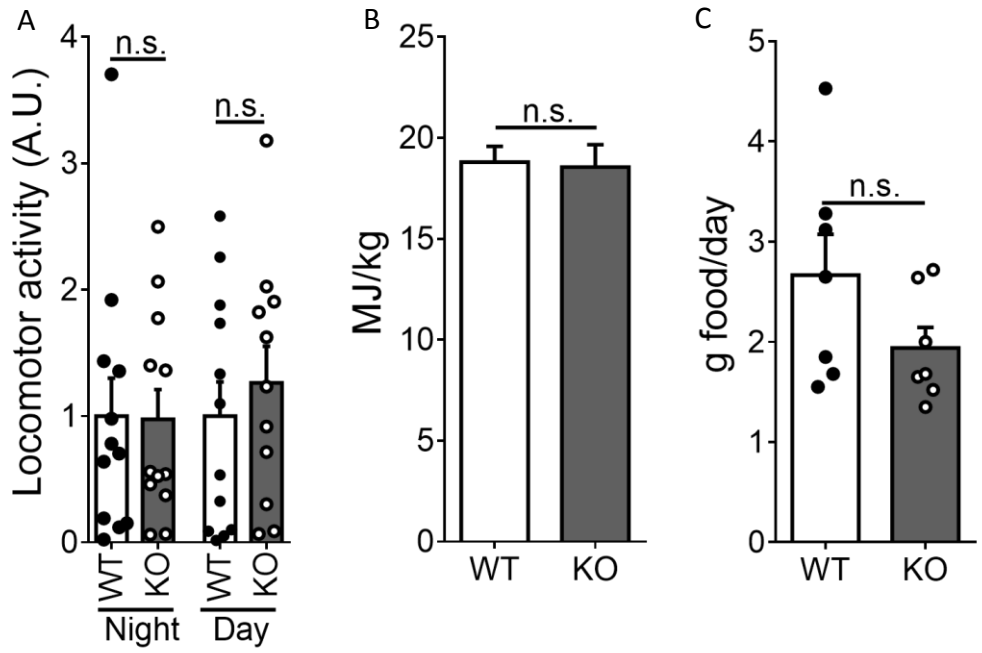

Figure 24: Locomotor activity, energy content of the feces and food intake after HFD

(A) Locomotor activity of WT and EBI2 KO mice after 12 weeks of HFD. (B) Energy content of the feces from WT and EBI2 KO mice after 12 weeks of HFD. (C) Food intake per day of WT and EBI2 KO mice after 12 weeks of HFD. n=12 per group. Mean ± s.e.m. t-test.

4.4.4 | Loss of EBI2 negatively affects glucose metabolism and blood cholesterol levels, without influencing NAFLD

Long-term exposure to a fat rich diet is known to cause type 2 diabetes (Hu et al., 2001; Ley et al., 2014). To assess the possible development of type 2 diabetes, a glucose tolerance test (GTT) was performed on lean and obese WT and EBI2 KO mice. No significant differences between WT and KO mice could be observed in blood glucose levels of lean mice after a single injection of glucose (8 µl/g body weight of 0.25 g/ml glucose solution in 0.9% NaCl, whereas obese EBI2 KO mice showed worse glucose tolerance to obese WT littermates (Figure 25B). Additionally, obese EBI2 KO mice had higher levels of blood glucose when fed *ad libitum* (Figure 25C).

Loss of EBI2 increased also the levels of circulating cholesterol after HFD, but not triglycerides and free fatty acids (Figure 25D).

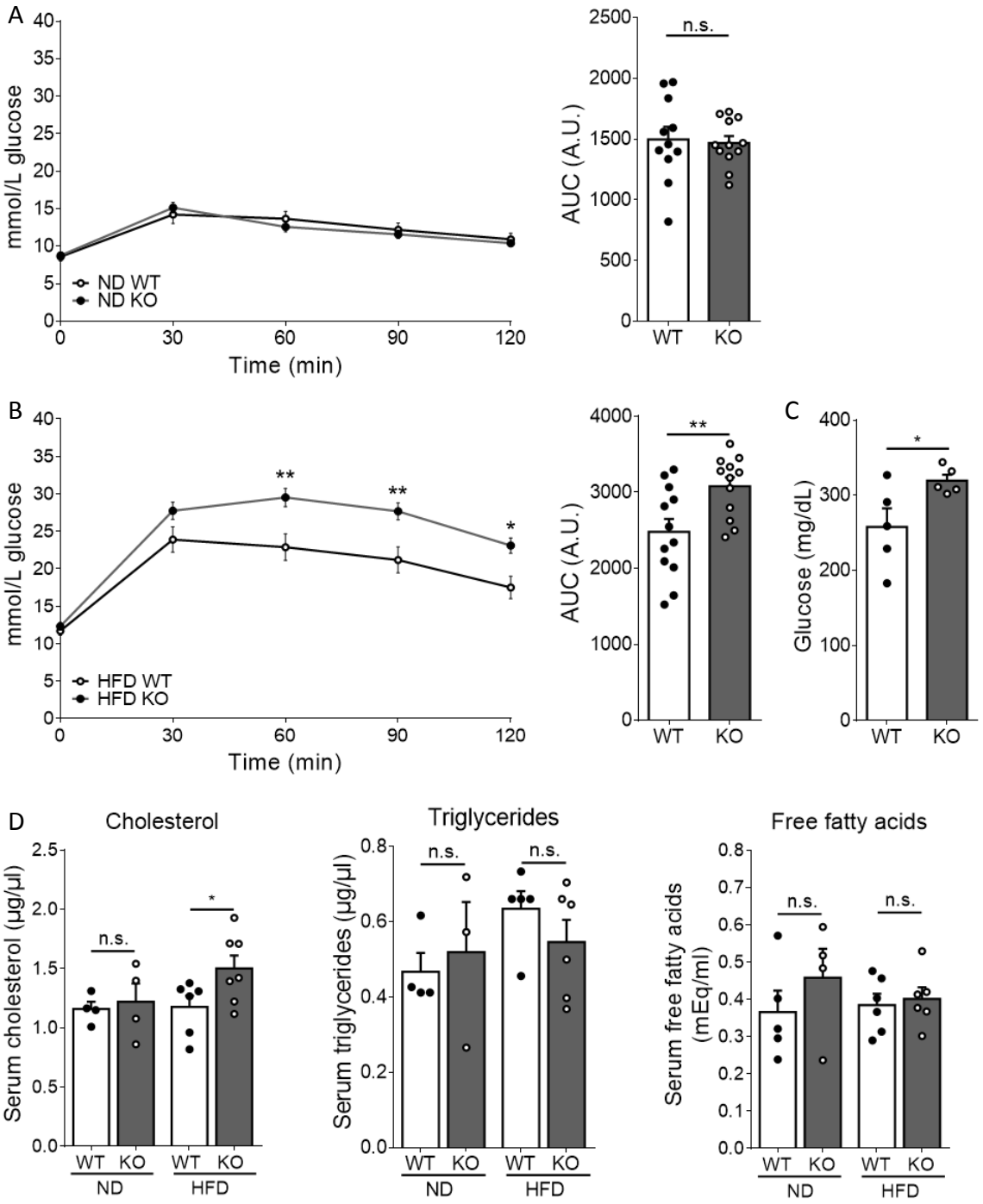

Figure 25: Glucose tolerance and serum lipids

*(A,B) Blood glucose (mmol/L) measured after injection of glucose (8 µl/g body weight of 0.25g/ml glucose solution in 0.9 % NaCl) i.p. in WT and EBI2 KO mice after 12 weeks of ND (A) or HFD (B). n=12 per group. (C) Blood glucose level of WT and EBI2 KO mice fed ad libitum. n=5. (D) Circulating cholesterol (left), triglycerides (middle) and free fatty acids in serum of WT and EBI2 KO mice after 12 weeks of ND or HFD. n=4-6. Mean ± s.e.m. two-way ANOVA, * p≤ 0.05, **p≤0.01*

Finally, loss of EBI2 did not significantly affect the development of NAFLD following HFD, as confirmed by histological analysis (Figure 26A), despite a reduction (not significant) in triglycerides (-30.0%) and free fatty acids (-15.7%) content in the liver (Figure 26B).

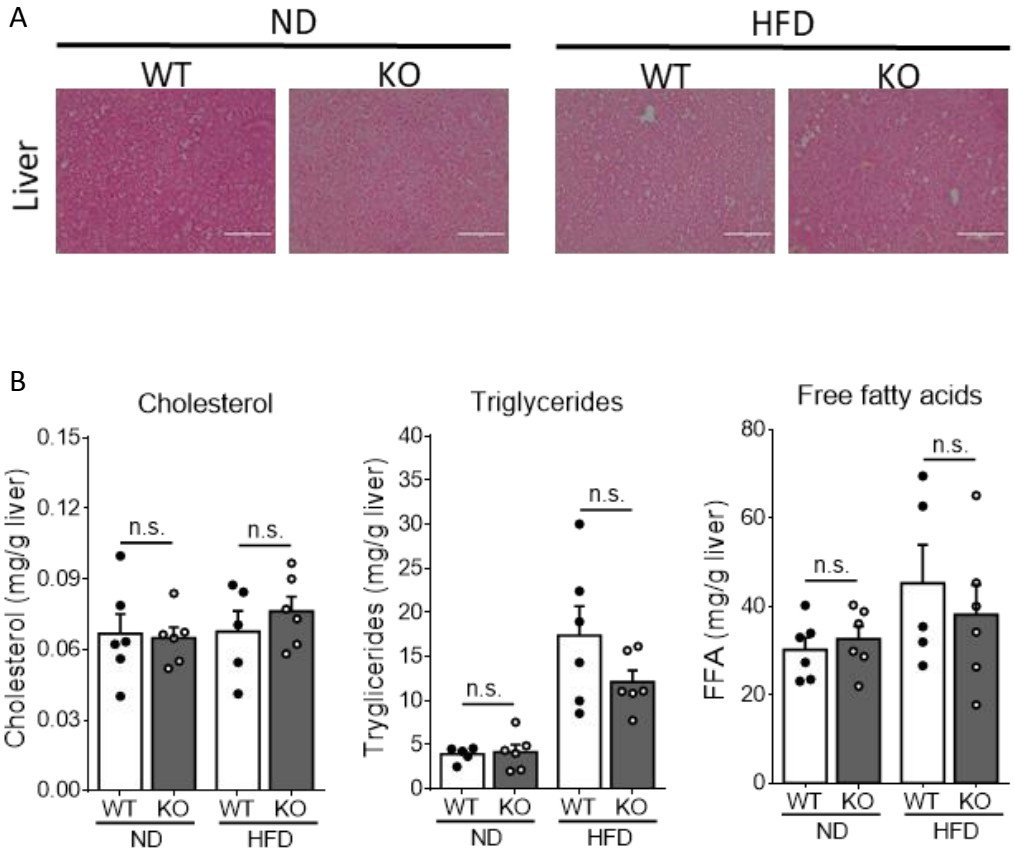

Figure 26: Effects of HFD on liver

(A) HE staining of liver from WT and EBI2 KO mice after 12 weeks of ND or HFD. (B) Cholesterol (left), triglycerides (middle) and free fatty acids (right) in liver of WT and EBI2 KO mice after 12 weeks of ND or HFD. n=6. Mean ± s.e.m.

4.5 | Effects of EBI2 KO during cold exposure

4.5.1 | Lack of EBI2 increases energy expenditure in acute cold exposure

Since the *in vitro* data showed that EBI2 affects the activity of BA, WT and EBI2 KO mice were exposed to cold temperature for 1 hour in order to cause a strong acute sympathetic activation of adipose tissue through NE release. During the 1 hour at 4°C, the energy expenditure of WT and EBI2 KO mice was characterized (Figure 27).

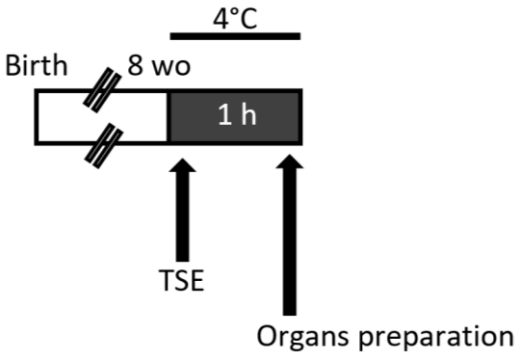

Figure 27: Short-term cold exposure experimental setup

Schematic representation of a short-term (1 h) cold exposure (4°C).

Consistently with the lipolysis data that showed a clear difference in the NE-induced effects (Figure 16) , the VO_2 consumption was 20% higher in EBI2 KO mice compared to WT (Figure 28A). However, EBI2 KO mice showed also a tendency towards greater locomotor activity than WT littermates when placed at 4°C (Figure 28B).

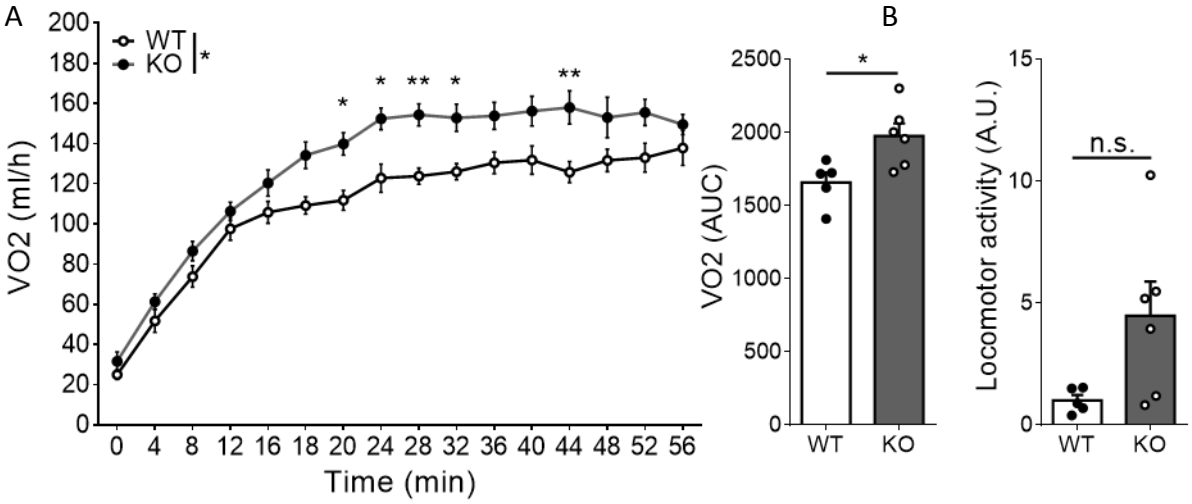

Figure 28: Whole body metabolism of WT and EBI2 KO mice during 1 hour of 4°C exposure

*(A) VO_2 consumption (ml/l) (left) and A.U.C (right) during 1 hour at 4°C. (B) Locomotor activity during 1 hour at 4°C. n=5-6 per group. Mean ± s.e.m. two-way ANOVA and t- test, * p≤ 0.05.*

When the mice were housed at normal housing temperature (i.e. 23°C) their energy expenditure was comparable between the two genotypes (Figure 29A), suggesting that the difference is triggered by the cold exposure. No differences could also be observed in the body weight of the

mice prior to cold exposure (Figure 29B). The levels of the main thermogenic and adipogenic genes showed no significant differences between WT and KO mice, as well as UCP1 (Figure 29C,D). Similarly, no significant differences were observed in the morphology of the adipocytes (Figure 29D).

Taken together, these results indicate that EBI2 is involved in regulating the metabolic response to an acute exposure to cold independently of preexisting differences in the metabolism at 23°C.

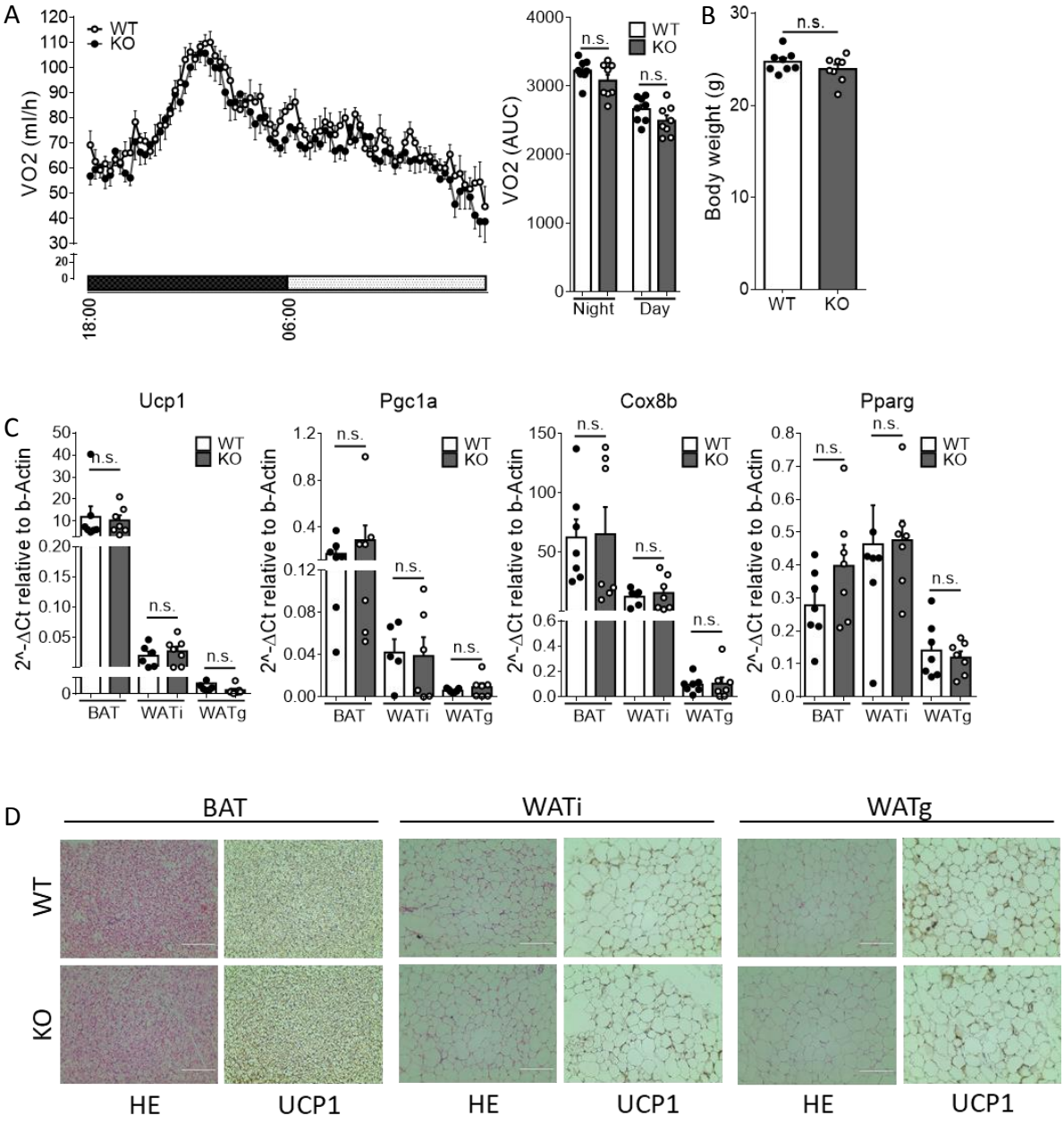

Figure 29: Whole-body metabolism of mice housed at 23°C

(A) VO_2 consumption (ml/l) (left) and A.U.C (right) during 24h at 23°C. (B) Body weight at 23°C (C) Thermogenic (Ucp1, Pgc1a, Cox8b) and adipogenic (Pparg) markers expression in ATs at 23°C. n=4. (D) HE and UCP1 staining of ATs at 23°C. Scale bar: 100 µM. n=7-8 per group. Mean ± s.e.m.

4.5.2 | Lack of EBI2 does not affect energy expenditure during long term cold exposure

Compared to standard housing temperature (23°C), EBI2 expression in WATi was significantly increased (4 fold increase) following 1 week at 4°C, whereas no significant differences were found in BAT (+47%) and WATg (-34%) (Figure 30). Therefore the role of EBI2 in browning, a process by which multilocular "beige" adipocytes arise within WAT, and especially WATi, following adrenergic stimulus, was further analyzed (Petrovic et al., 2010; Seale et al., 2008; Wu et al., 2012).

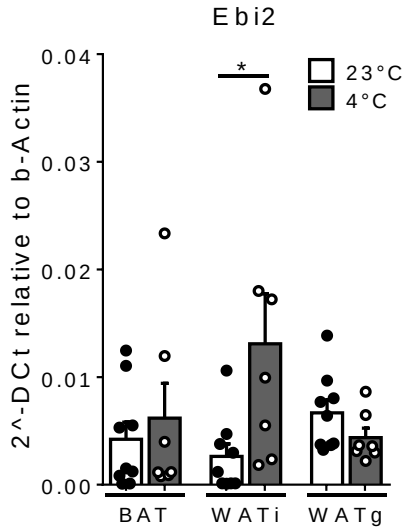

Figure 30: Ebi2 expression after 1 week of cold exposure

*Ebi2 expression in ATs of WT mice housed for 1 week at 23°C or 4°C. n=3. Mean ± s.e.m. t-test, * p≤ 0.05*

To investigate the effect of lack of EBI2 on cold-induced energy expenditure and WATi browning, 8 weeks old WT and EBI2 KO mice were acclimatized at 16°C for 3 days and subsequently housed at 4°C for 7 days. During the last day, the metabolism of the mice was characterized (Figure 31).

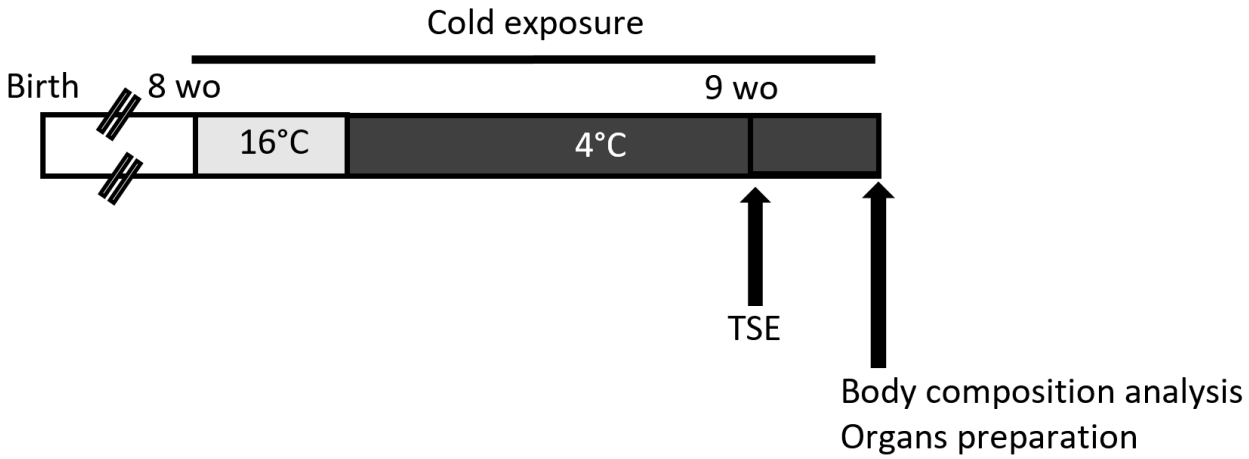

Figure 31: Long-term cold exposure experimental setup

Schematic representation of a long-term cold exposure (3 days of acclimatization at 16°C and 7 days at 4°C) followed by metabolic cages (TSE) measurements.

WT and EBI2 KO mice showed comparable VO_2 levels (Figure 32A). Adipogenic and thermogenic markers were comparable between the two genotypes, as showed at mRNA level (Figure 32B) and with UCP1 immunohistochemistry (Figure 32C). EBI2 KO mice weighed significantly more than WT littermates following cold exposure (+12%) (Figure 32D), due to higher white adipose tissue mass (+22.8% in WATi, +42.3% in WATg) (Figure 32E), despite no significant differences in whole body composition (Figure 32F). WT and EBI2 KO mice showed no differences in locomotor activity (Figure 32G).

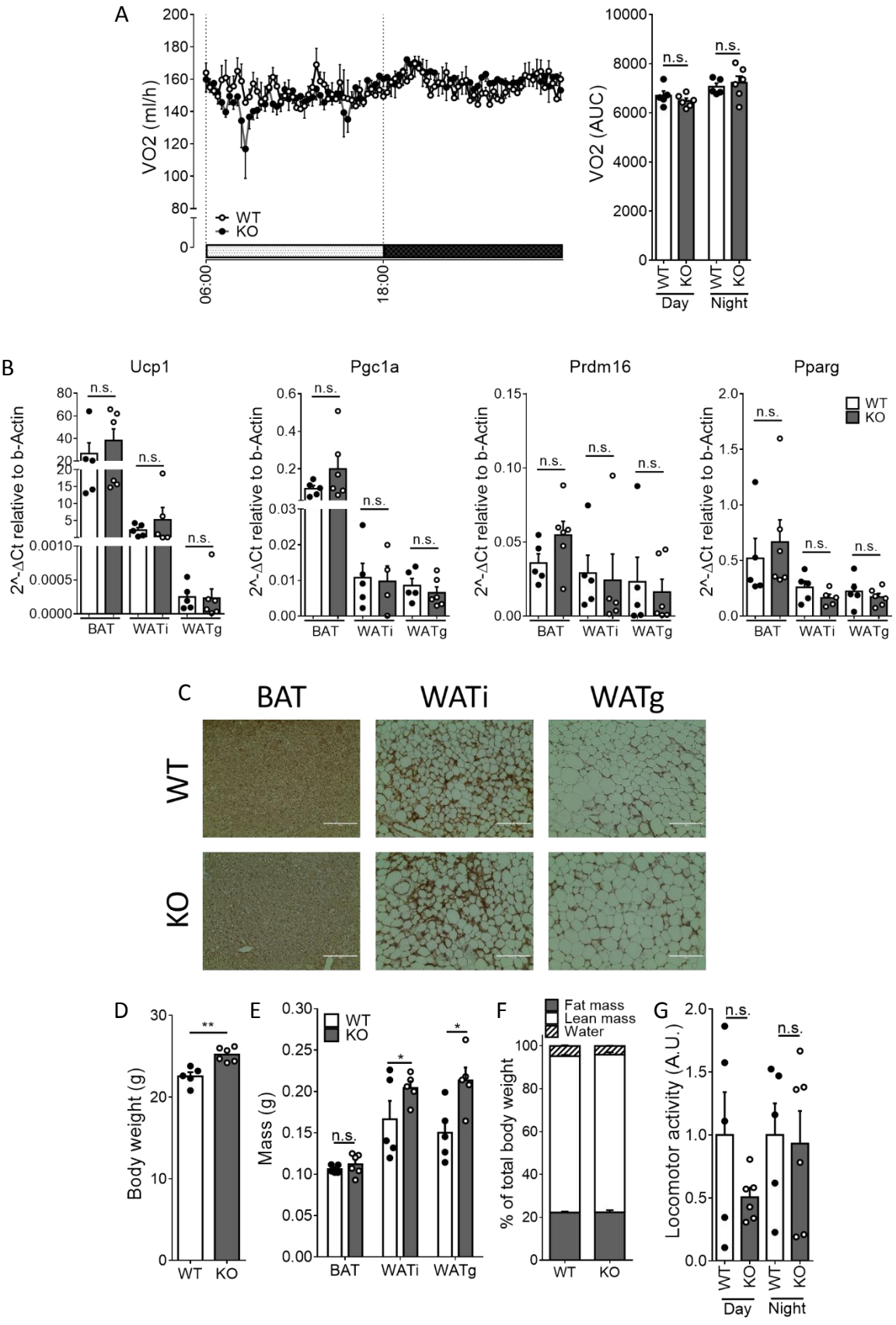
A
VO2 (ml/h)
WT
KO
06:00
18:00
VO2 (AUC)
n.s.
Day
Night
B
Ucp1
Pgc1a
Prdm16
Pparg
2^-ΔCt relative to b-Actin
BAT
WATi
WATg
C
BAT
WATi
WATg
WT
KO
D
Body weight (g)
E
Mass (g)
F
Fat mass
Lean mass
Water
% of total body weight
G
Locomotor activity (A.U.)

Figure 32: Whole body metabolism of WT and EBI2 KO mice after 7 days at 4°C

*(A) VO_2 consumption (ml/l) over 24 h (left) and as A.U.C (right) after 7 days at 4°C. (B) Ucp1, Pgc1a, Prdm16 and Pparg mRNA levels in adipose tissues after 7 days at 4°C. (C) UCP1 staining in adipose tissues after 7 days at 4°C. (D,E) Whole body (D) and adipose tissues weight (E) of WT and EBI2 KO mice after 7 days at 4°C. (F) Fat mass, lean mass and free water of WT and EBI2 KO mice after 7 days at 4°C. (G) Locomotor activity over 24 h after 7 days at 4°C. n=5-6 per group. Scale bar: 100 µm. Mean ± s.e.m. t- test, * p≤ 0.05.*

The morphology of adipocytes was analyzed with HE staining (Figure 33A): the adipocytes showed similar morphology between the two genotypes.

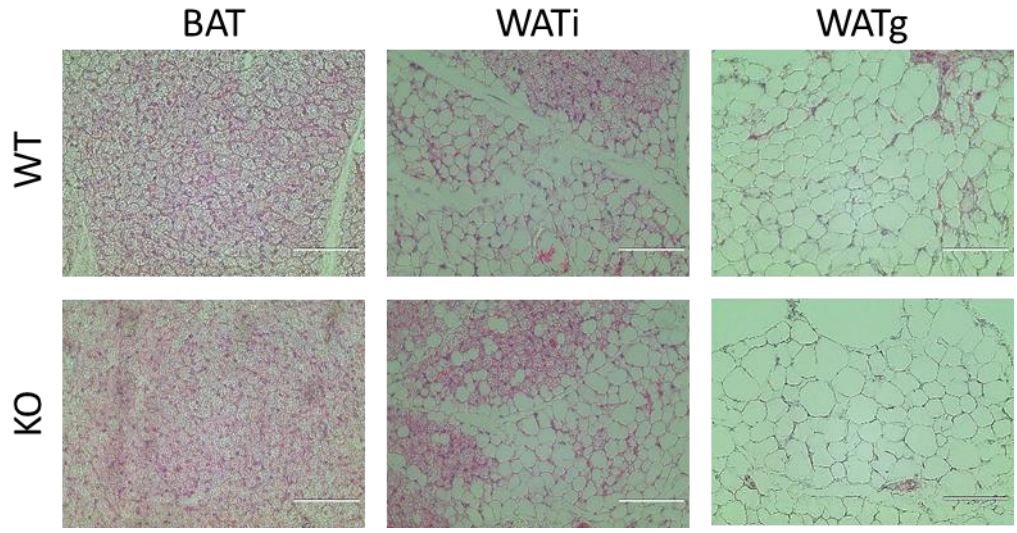

Figure 33: Adipocytes morphology after 1 week at 4°C

HE staining of adipose tissues of WT and EBI2 KO mice after 1 week at 4°C. Scale bar: 100 µm.

Analysis of β_3-adrenergic receptor (*Adrb3*) expression in adipose tissues of EBI2 WT and KO mice revealed interesting differences (Figure 34). When housed at 23°C, EBI2 KO mice exhibited higher expression of *Adrb3* in the thermogenic adipose tissues. However, after prolonged cold exposure *Adrb3* levels were reduced by 29% in BAT and by -43% in WATi of EBI2 KO mice, respectively (Figure 34), suggesting possible compensatory mechanisms involving β_3-adrenergic receptor after loss of EBI2.

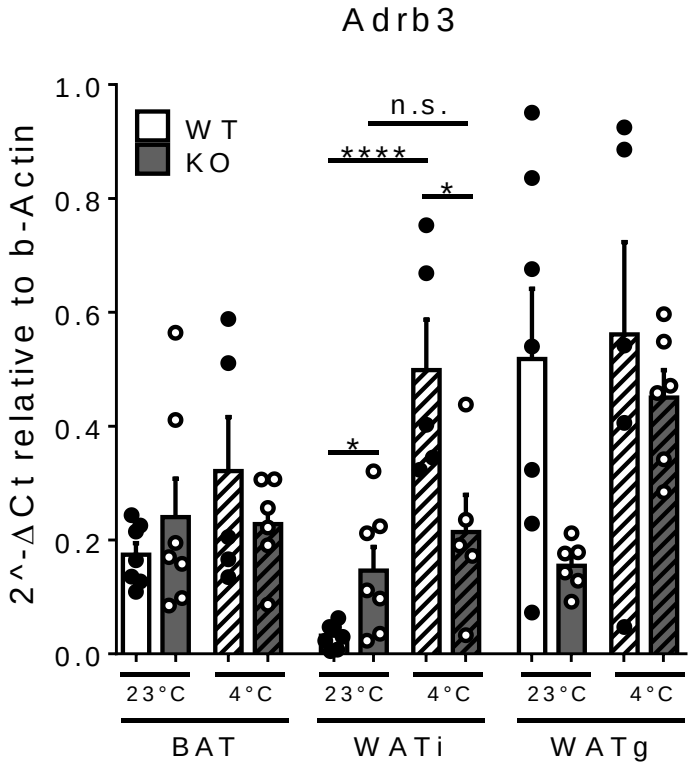

Figure 34: β_3-adrenergic receptor levels at 23°C and 4°C

*Adrb3 expression levels in ATs of EBI2 WT and KO mice housed at 23°C or after 1 week of cold exposure (4°C). Mean ± s.e.m. one-way ANOVA, * p≤ 0.05, **** p≤ 0.00001.*

4.6 | Effects of pharmacological activation of EBI2

4.6.1 | EBI2 acute activation decreases energy expenditure

Similarly to what was observed during cold exposure, EBI2 acute activation might regulate the energy expenditure. Thus, the metabolism of the 7α,25-OHC injected mice was characterized within the first hour after the first injection (i.p., 5 mg/kg, vehicle 0.9% NaCl and 10% DMSO) (Figure 35).

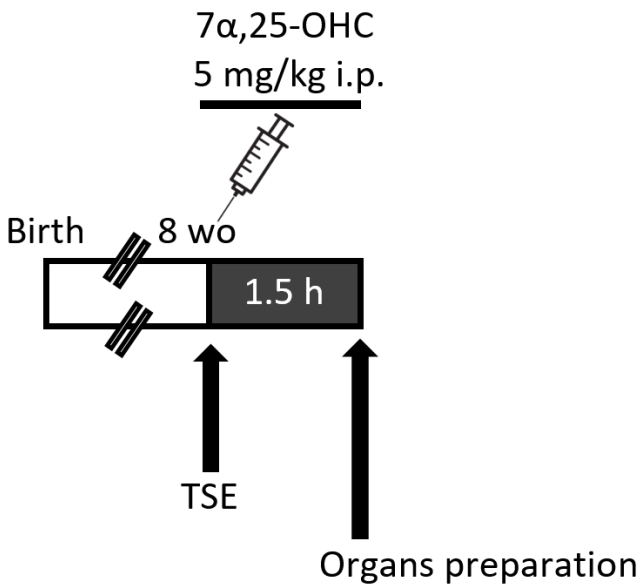

Figure 35: Single 7α,25-OHC injections experimental setup

Schematic representation of a single injection of 7α,25-OHC / vehicle and metabolic cages (TSE) measurement.

7α,25-OHC injection led to a significant decrease in VO_2 consumption (-13%) (Figure 36A), as expected by the activation of a $G_{\alpha i}$-coupled receptor. Also in this case, similarly to what observed during acute cold exposure, the locomotor activity was altered: 7α,25-OHC injected mice showed indeed a significant decrease in locomotor activity (Figure 36B), indicating that the acute metabolic effect of EBI2 activation might not be exclusively due to adipose tissue activity.

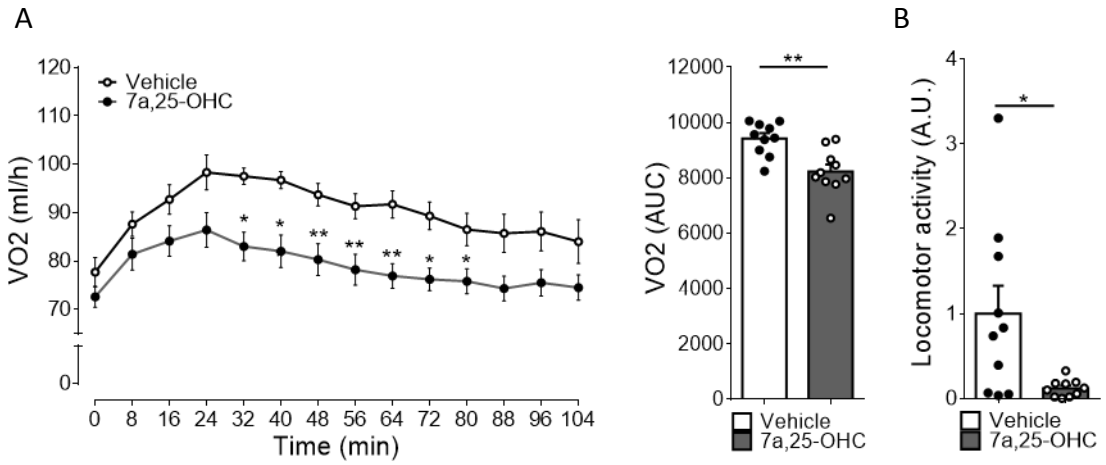

Figure 36: Whole body metabolism of WT mice following a single injection of 7α,25-OHC

*(A) VO_2 consumption (ml/l) (left) and as A.U.C (right) after a single injection of vehicle or 7α,25-OHC 5 mg/kg i.p. (B) Locomotor activity after a single injection of vehicle or 7α,25-OHC 5 mg/kg i.p. n=10 per group. Mean ± s.e.m. t-test, * p≤ 0.05, **p≤0.01*

To further validate that the effects induced by 7α,25-OHC was EBI2 dependent, the same treatment (Vehicle or 7α,25-OHC 5 mg/kg) was administrated to EBI2 KO mice, and their whole-body metabolism and locomotor activity characterized in the following 100 min. No differences could be observed in the energy expenditure (Figure 37A) nor in the locomotor activity (Figure 37B) of EBI2 KO mice injected with vehicle (DMSO) or 7α,25-OHC, indicating that the effects induced by 7α,25-OHC injection are EBI2-mediated.

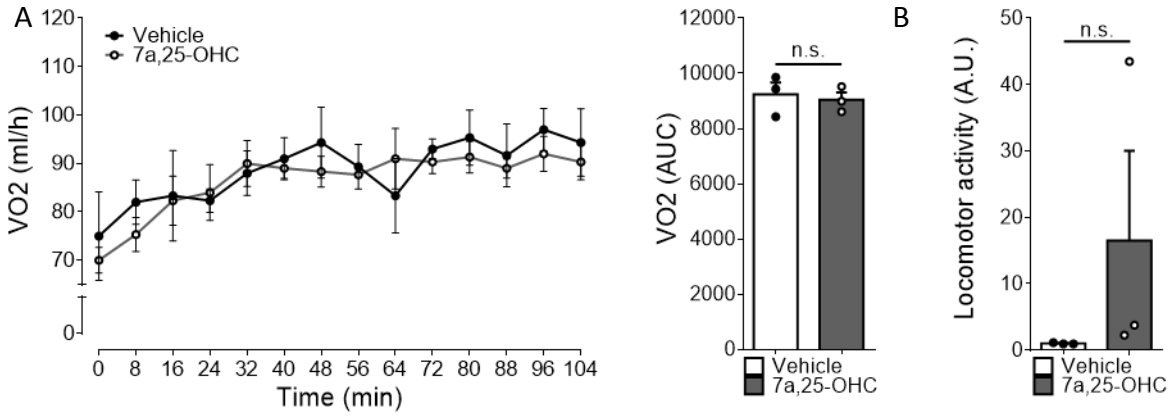

Figure 37: Whole body metabolism of KO mice following a single injection of 7α,25-OHC

(A) VO_2 consumption (ml/l) (left) and as A.U.C (right) after a single injection of vehicle or 7α,25-OHC 5 mg/kg i.p. (B) Locomotor activity after a single injection of vehicle or 7α,25-OHC 5 mg/kg i.p. n=3 per group. Mean ± s.e.m. t-test.

4.6.2 | Prolonged EBI2 activation does not affect metabolism

To assess whether prolonged EBI2 activation could influence the metabolism and energy expenditure, WT mice housed at 23°C were injected i.p. daily for 1 week with 5 mg/kg of 7α,25-OHC, the EBI2 endogenous ligand. A control group was injected with vehicle (0.9% NaCl, 10% DMSO). After the last (7th) injection, the metabolism of the mice was characterized (Figure 38).

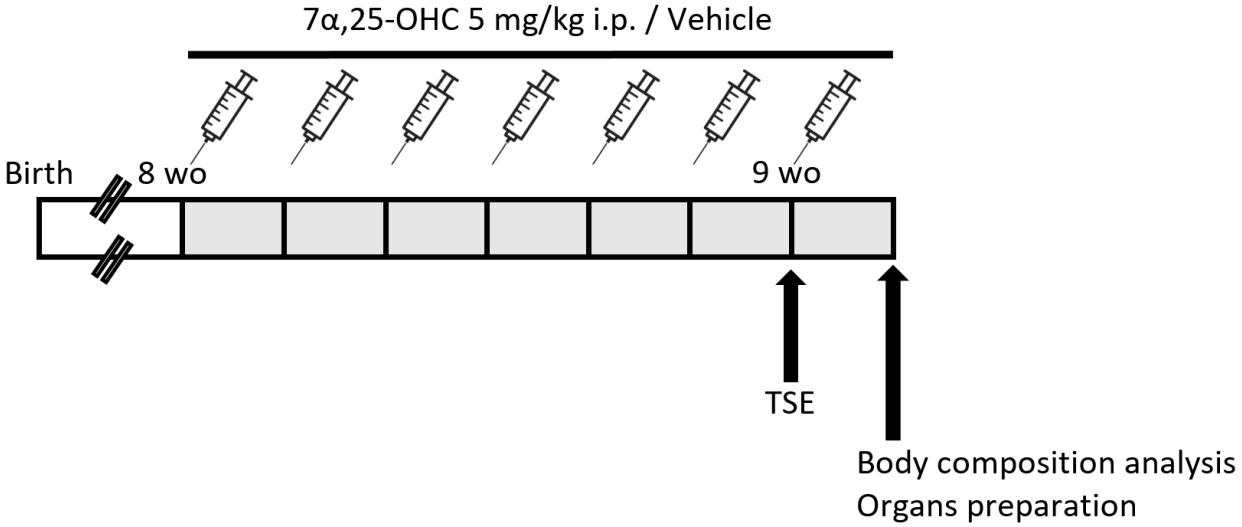

Figure 38: 1 week of 7α,25-OHC injections experimental setup

Schematic representation of 1 week of 7α,25-OHC / vehicle daily injections followed by metabolic cages (TSE) measurement.

Vehicle injected and 7α,25-OHC injected mice showed comparable VO_2 (Figure 39A), locomotor activity (Figure 39B), body weight (Figure 39C) as well as adipose tissues weight (Figure 39D), body composition (Figure 39E) and UCP1 mRNA expression (Figure 39F). The adipocytes of all the three adipose tissues showed similar morphology between the two groups (Figure 39G). Thus, prolonged EBI2 pharmacological activation seems not to influence the metabolism of mice.

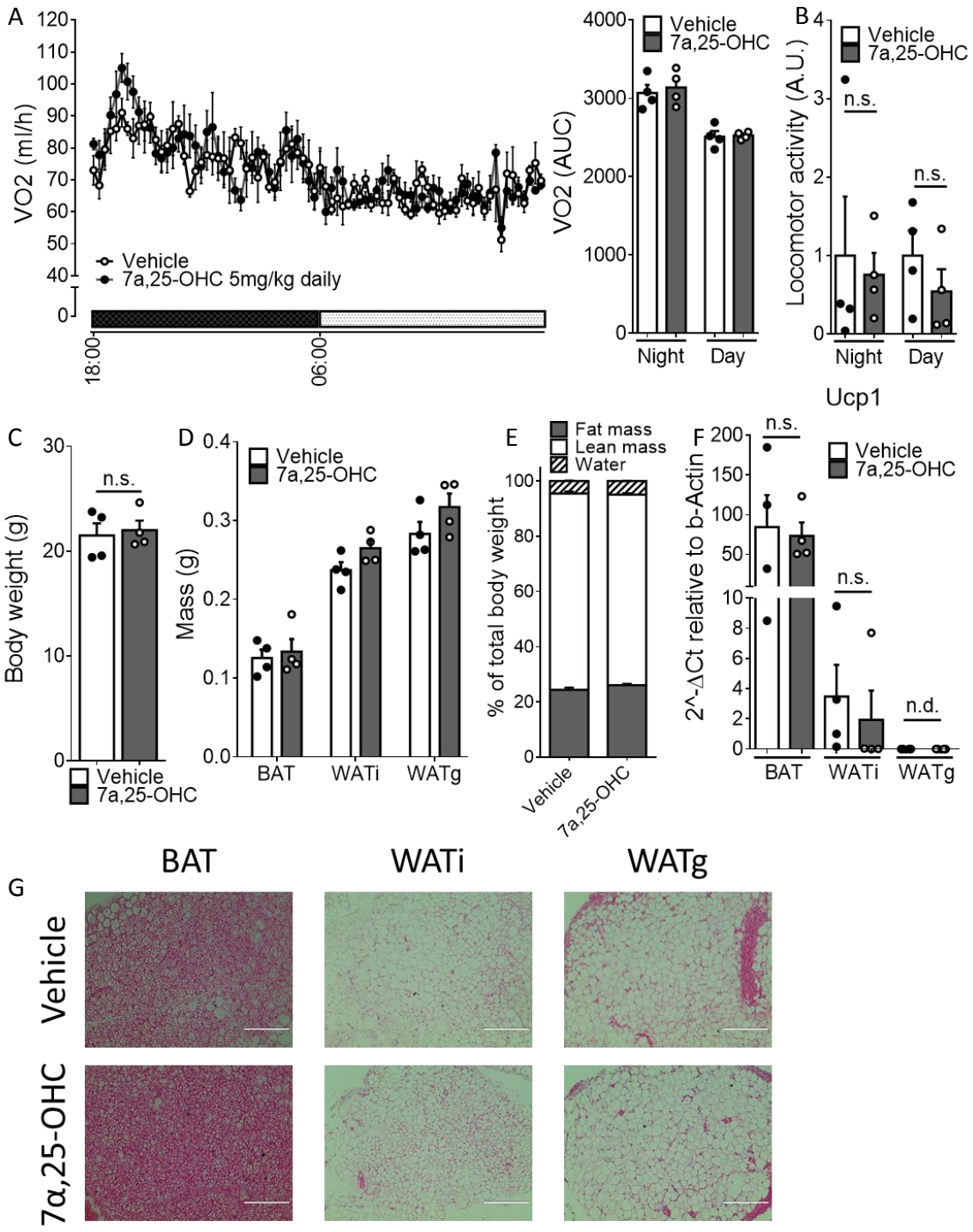

Figure 39: Whole body metabolism of WT mice treated for 7 days with 7α,25-OHC

(A) VO_2 consumption (ml/l) (left) and as A.U.C (right) after 7 days of vehicle or 7α,25-OHC injections i.p. 5 mg/kg/day. (B) Locomotor activity after 7 days of vehicle or 7α,25-OHC injections i.p. 5 mg/kg/day. (C) Body weight after 7 days of vehicle or 7α,25-OHC injections i.p. 5 mg/kg/day. (D) Adipose tissues weight after 7 days of vehicle or 7α,25-OHC injections i.p. 5 mg/kg/day. (F) Fat mass, lean mass and free water after 7 days of vehicle or 7α,25-OHC injections i.p. 5 mg/kg/day. (G) UCP1 mRNA expression in ATs of 7 days injected vehicle or 7α,25-OHC i.p. 5 mg/kg/day (G) HE staining of adipose tissues after 7 days of vehicle or 7α,25-OHC injections i.p. 5 mg/kg/day. n=4 per group. Scale bar: 100 µm (BAT), 200 µm (WATi, WATg). Mean ± s.e.m.

Long-term activation of a GPCR can lead to a transcriptional downregulation of receptor levels (Black et al., 2016; Von Zastrow, 2001), offering a possible explanation for the lack of an *in vivo* effect of 7α,25-OHC injection. To test this hypothesis, the mRNA levels of EBI2 were measured in adipose tissues after 1 week of vehicle or 7α,25-OHC treatment. However, no differences were observed in EBI2 transcriptional levels (Figure 40A). Similarly, there was no increase in HSD3B7, the enzyme involved in 7α,25-OHC degradation (Figure 40A). Thus, the lack of a EBI2 effect on metabolism following chronic activation is not due to EBI2 transcriptional downregulation nor to HSD3B7 mRNA upregulation.

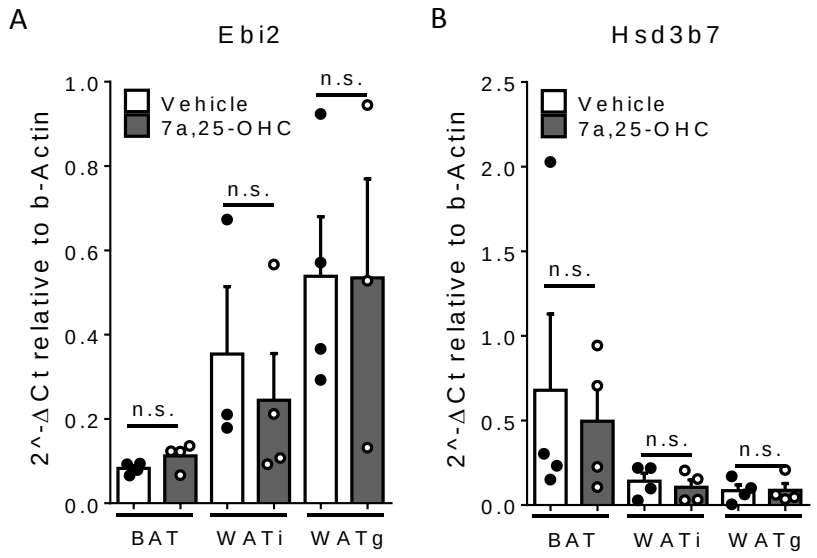

Figure 40: Ebi2 and Hsd3b7 expression after 7α,25-OHC injections

(A,B) EBI2 (A) and HSD3B7 (B) mRNA expression in ATs after 7 days of vehicle or 7α,25-OHC injections i.p. 5 mg/kg/day. n=4. Mean ± s.e.m.

5 | DISCUSSION

Oxysterols have originally been considered as intermediate metabolites between cholesterol and bile acids. However, in the last couple of decades, numerous studies have underlined their role as important mediators in many pathological conditions, such as atherosclerosis (Ares et al., 2000; Lizard et al., 1996; Yuan et al., 2000) and Alzheimer's disease (Leoni et al., 2003; Lütjohann et al., 2012). Recently, the levels of some oxysterols and the enzymes involved in their production were reported to be altered during obesity and metabolic syndrome (Guillemot-Legris et al., 2016b), suggesting a possible involvement of these molecules in the development of such pathologies.

In 2011, two independent research showed that a GPCR named Epstein-Barr virus-induced G-protein coupled receptor 2 (EBI2) or GPR183 was potently activated by some oxysterols, and its most potent endogenous ligand was discovered to be 7α,25-dihydroxycholesterol (7α,25-OHC) (Hannedouche et al., 2011; Liu et al., 2011). In the present study, EBI2 was found to be expressed in adipose tissues and adipocytes, and in particular in brown adipose tissue (BAT) and brown adipocytes (BA).

Therefore, this thesis investigated the role of EBI2 in adipose tissues, with particular focus on BA and BAT. To do that, a combined approach using pharmacological tools like the endogenous ligand 7α,25-OHC and the selective antagonist NIBR189, as well as a genetic approach involving EBI2 knockout mice were used *in vitro* and *in vivo*.

5.1 | EBI2 activation decreases the activity of brown adipocytes

One of the main features of brown adipocytes is the ability to produce heat in a process called non-shivering thermogenesis (NST). NST is stimulated, among other stimuli, by norepinephrine (NE) through β_3-adrenergic receptor, a $G_{\alpha s}$-coupled GPCR, which leads, via a signaling cascade involving cAMP and hormone sensitive lipase (HSL) phosphorylation, to triglycerides (TG) hydrolysis into free fatty acids (FFA) and glycerol. Contrarily to the β_3-adrenergic receptor, EBI2 was shown in this thesis to be a $G_{\alpha i}$-coupled GPCR in BA: EBI2 activation with its endogenous ligand 7α,25-OHC reduced NE-induced increase in intracellular cAMP. Consequently, NE-induced lipolysis was decreased by the treatment with 7α,25-OHC. In parallel, EBI2 activation decreased

the phosphorylation of HSL, an enzyme able to hydrolyze triglycerides in FFA. All these effects were mediated by EBI2, because they were blunted by the EBI2 selective antagonist NIBR189. EBI2 $G_{\alpha i}$-coupling was further proven by pertussis toxin treatment, which completely blunted 7α,25-OHC induced ERK1/2 phosphorylation in BA.

Also in WA EBI2 activation decreased NE-induced cAMP levels and lipolysis, albeit not significantly: however, it is important to notice that EBI2 mRNA was significantly higher in BA compared to WA, suggesting its role might be specific for thermogenically active adipocytes.

Importantly, EBI2 activation significantly decreased NE-induced lipolysis in *ex vivo* BAT explants from newborn mice, and the same tendency was observed in WATi from adult mice. However, no significant effects were observed on NE-induced lipolysis in WATg, indicating that EBI2 effect might be specific to thermogenic fat (i.e. BAT and WATi).

EBI2 activation in absence of a concomitant NE-stimulation did not decrease the intracellular cAMP pool, nor HSL phosphorylation or lipolysis, indicating that EBI2 does not affect the basal activity of brown adipocytes.

To investigate in detail how EBI2 activation influences the activity of BA, respirometry analysis was performed. Consistently with what observed on cAMP levels and lipolysis, 7α,25-OHC pre-treatment decreased the ability of the cells to increase their respiration in response to NE. Together with NE-induced respiration, the BA maximal respiratory capacity and the spare respiratory capacity, which indicate the ability of the cells to respond to increased energy demand or under stress, were significantly reduced by 7α,25-OHC pre-treatment. The mechanisms involving a reduction in maximal respiratory capacity and the spare respiratory capacity in adipocytes are so far poorly investigated (Alcalá et al., 2017; Keuper et al., 2014): however, previous studies, mostly conducted on endothelial cells, showed that such effects are strictly linked to cellular stress induced by reactive oxygen species (ROS) and impaired glucose homeostasis (Nannelli et al., 2018; Nguyen et al., 2016; Yetkin-Arik et al., 2019). To investigate whether this was the case also in BA, ROS production was measured over time in BA treated with NE and 7α,25-OHC. Consistently with previous studies (Chouchani et al., 2016; Lettieri-Barbato, 2019), NE treatment increased the ROS levels in BA, albeit not significantly, whereas 7α,25-OHC alone did not. Surprisingly, when BA were treated with both NE and 7α,25-OHC, the increase in

ROS levels was significantly higher than in the NE-treated cells, thus suggesting that the reduction in maximal respiration and spare respiratory capacity were due to increase in ROS production. Previous studies showed that ROS increase can activate UCP1 or induce its expression (Chouchani et al., 2016; Echtay and Brand, 2007), whereas others showed that the mechanisms through which ROS regulate energy expenditure can be independent of UCP1 (Nabben et al., 2011; Shabalina et al., 2010).

Chronic treatment of BA with 7α,25-OHC had no influence on thermogenic and adipogenic genes nor on lipid accumulation, suggesting that EBI2 exerts its effect acutely only. Whereas some GPCRs were shown to have a feedback mechanism upon ligand binding, by which the receptor expression is downregulated following receptor activation (Black et al., 2016; Von Zastrow, 2001), this was not the case of EBI2. Indeed, when mice were treated for 1 week with 7α,25-OHC, no EBI2 transcriptional downregulation was observed.

The effect of EBI2 loss on brown adipocytes was investigated using brown adipocytes isolated from WT and EBI2 KO littermates and differentiated *in vitro*. The lack of EBI2 did not affect the basal thermogenic ability of brown adipocytes, which showed comparable levels of thermogenic and adipogenic markers. WT and EBI2 KO BA had also comparable NE-induced lipolysis.
All together, these results indicate that EBI2 is able to decrease NE-induced brown adipocytes activation and thermogenic fat activity, without affecting adipocytes differentiation when EBI2 is chronically activated or genetically depleted.

5.2 | EBI2 regulates whole-body metabolism of mice in response to cold and upon pharmacological activation

An approach similar to the one used *in vitro* was used to investigate the role of EBI2 *in vivo*. First, WT mice were treated either every day for 1 week (chronic treatment) or with a single dose (acute treatment) of the EBI2 endogenous ligand 7α,25-OHC (5 mg/kg, i.p.), thus to mimic the conditions tested *in vitro*. All the experiments were performed at 23°C, a temperature that provides a mild adrenergic activation of ATs (Cui et al., 2016). Consistently with the *in vitro* data, the acute

activation of EBI2 by 7α,25-OHC injection decreased the whole-body metabolism of mice, resulting in decreased oxygen consumption and energy expenditure in the first hour following the injection, and reaching the basal level after 1.5 hour from the injection. This effect was mediated by EBI2 by injecting 7α,25-OHC in EBI2 KO mice, which showed energy expenditure comparable to the vehicle treated group.

Despite the significant decrease in the energy expenditure following acute injection of 7α,25-OHC, no changes in the energy expenditure of the mice were observed in the last 24 hours of chronic treatment (i.e. after 7 days of injections). The prolonged activation of EBI2 did not affect the adipose tissue morphology, nor the adipose tissue mass or body composition.

The mechanism by which the metabolism of mice was affected only in the first hour following 7α,25-OHC injection could be dependent on the short half-life of 7α,25-OHC in the organism. Even though the specific half-life of 7α,25-OHC was not investigated, previous studies reported that oxysterols have in general very short half-life, often shorter than 1 h (Björkhem, 2002; Meaney et al., 2001). To test whether EBI2 prolonged activation would lead, as for other GPCRs (Black et al., 2016; Von Zastrow, 2001), to a feedback mechanism causing EBI2 transcriptional downregulation, EBI2 mRNA was measured after chronic injections, but no differences were observed compared to vehicle treated mice. No changes were also observed in mRNA levels of HSD3B7, the enzyme involved in 7α,25-OHC degradation, after prolonged EBI2 activation.

A similar time-dependent mechanism was observed in EBI2 KO mice exposed to cold (4°C). When EBI2 KO mice were housed at 4°C for 1 h, they showed significantly higher energy expenditure compared to WT littermates, suggesting that EBI2 is involved in acute regulation of energy expenditure in cold-induced brown adipose tissue activation. Consistently, BAT from EBI2 KO mice showed higher *ex vivo* lipolysis than WT tissues in response to NE stimulus, and KO WATi had significantly higher basal lipolysis, thus supporting the idea of EBI2 regulating the activity of thermogenic fat.

Prolonged low temperatures are also known to induce “browning” of white adipose tissue (Nedergaard and Cannon, 2014). However, when the mice were gradually acclimatized to lower temperature (3 days at 16°C), and exposed to cold temperature (4°C) for 1 week, no significant

effect was observed on their oxygen consumption. Consistently, thermogenic genes levels were comparable between the two genotypes at both mRNA and protein level, indicating that EBI2 is not involved in cold-induced "browning" of white adipose tissue.

Prolonged cold exposure causes decrease of fat mass due to the increased need of producing heat to cope with the low temperature (Ravussin et al., 2014; Robidoux et al., 2004). EBI2 KO mice were able to conserve more white adipose tissue mass and body weight after 1 week of cold compared to WT. This result appears to be in contrast with the lack of a $G_{\alpha i}$-coupled receptor: indeed, mice lacking for such kind of receptor should be more sensitive to noradrenergic stimulus, and thus their adipose tissue consume more fat. However, the *in vitro* data showed that EBI2 activation leads to increased NE-induced ROS production. ROS production occurs at multiple sites of the electron transport chain, and leads to decrease in the mitochondrial proton gradient (Zhao et al., 2019), which is responsible for heat production in BA through UCP1. Thus, on the contrary, EBI2 loss could lead to increased efficiency of the electron transport chain, resulting in greater thermogenic capacity in response to cold and smaller adipose tissue loss. Another potential explanation to the comparable energy expenditure between WT and KO mice, as well as for the improved conservation of WAT in cold exposure EBI2 KO mice, comes from the levels of β_3-adrenergic receptor. Subcutaneous white adipose tissue (WATi), which is prone to "browning", was unable to increase β_3-adrenergic receptor expression following cold in EBI2 KO mice, suggesting a compensatory mechanism for the loss of EBI2. These reduced levels of *Adrb3* might also explain why EBI2 KO mice exhibit no significant changes in energy expenditure compared to WT mice: the loss of the inhibitory (EBI2) effect might be compensated by the reduced stimulatory (adrenergic β_3) signal. Moreover, this altered balance between $G_{\alpha i}/G_{\alpha s}$ signaling in brown/beige fat might be the basis why, EBI2 KO mice are able to conserve better the adipose tissue depots during prolonged cold.

Together with changes in the energy expenditure, acutely cold exposed EBI2 KO mice showed a tendency towards increased locomotor activity, whereas 7α,25-OHC injection caused a significant reduction in the locomotor activity compared to vehicle injected mice. No previous studies ever investigated this aspect, thus no further data are available to speculate whether this might be dependent on the nervous system, skeletal muscle, adipose tissue or other organs. However,

future experiments will be performed with tissue specific EBI2 KO mice to asses if the differences in energy expenditure are due exclusively to adipose tissue or if other organs and are involved.

5.3 | EBI2 loss affects metabolism in diet induced obesity without influencing body weight

Obesity and its comorbidities have become in the last few decades one of the main health concerns in developed countries, resulting in increased mortality rate and poor life quality (Di Angelantonio et al., 2016). Therefore, there is increased and urgent need to find new pharmacological therapies to counteract it. Since EBI2 activation was able to decrease lipolysis *in vitro*, the lack of EBI2 was hypothesized to increase energy expenditure and thus reduce weight gain during diet-induced obesity. However, EBI2 KO mice did not show any difference in body weight compared to WT mice when fed for 12 weeks with high fat diet. No differences were also observed in the total fat mass nor in the mass of the single adipose tissue depots.

EBI2 KO mice fed for 12 weeks with control diet (ND) showed no differences in energy expenditure compared to WT littermates. In contrast, obese EBI2 KO mice had decreased energy expenditure compared to WT littermate, despite an increase in UCP1 levels in BAT: this seems in contrast with the lack of a $G_{\alpha i}$-coupled receptor, which is supposed to reduce energy expenditure when stimulated. A possible explanation is that the lack of EBI2 eventually leads to the upregulation of another $G_{\alpha i}$-coupled receptor involved in regulation of energy expenditure in response to high fat diet, resulting in a decrease in energy expenditure in EBI2 KO mice. Previous works (El-Brolosy and Stainier, 2017) showed that the lack of a receptor can lead to the upregulation of a phylogenetically close one. A possible candidate for such mechanism in EBI2 KO mice is GPR18: GPR18 is indeed the EBI2 most phylogenetically close GPCR (Rosenkilde et al., 2006; Sanders et al., 2011), and was previously reported to be positively associated with obesity and T2D (Rajaraman et al., 2016).

A significant effect of EBI2 loss was observed in obesity-induced type 2 diabetes. EBI2 KO mice showed worse performance in the glucose tolerance test in comparison to WT mice, indicating stronger insulin resistance. Whether $G_{\alpha i}$-coupled receptors are able to influence the development

of type 2 diabetes is matter of debate: whereas the chemogenetic activation of $G_{\alpha i}$-coupled receptors in adipose tissue was shown to not influence glucose homeostasis (Caron et al., 2019), other research conducted on $G_{\alpha i}$-coupled receptors knockout mice showed opposite results (Dobbins et al., 2013; Girousse et al., 2013; Wallenius et al., 2017; Yang et al., 2015). Previous studies demonstrated that activation of $G_{\alpha i}$-coupled receptor during obesity is beneficial against development of type 2 diabetes because it reduces lipids mobilization (in particular free fatty acids) from adipose tissue, reducing their lipotoxicity (Wallenius et al., 2017). However, no differences have been observed in free fatty acids blood concentration between WT and EBI2 KO mice after high fat diet. Increased lipid mobilization from adipose tissue during obesity is known to induce Nonalcoholic Fatty Liver Disease (NAFLD), which is characterized by excess lipid uptake by the liver, and which has been linked to glucose intolerance and insulin resistance (Fabbrini et al., 2010). However, obese EBI2 KO mice showed a tendency towards decreased hepatic lipids compared to obese WY mice, suggesting that probably EBI2 influences insulin resistance via a different mechanism than lipid mobilization from adipose tissue and lipid uptake by the liver.

The lack of EBI2 might worsen the T2D induced by HFD because of its role in regulating ROS production. On one side, excessive ROS production has been positively linked to T2D development because of induction of adipocytes hypertrophy, increased lipid storage, decreased adiponectin expression and increased inflammation (Carrière et al., 2003; Lundgren et al., 2007; Murdolo et al., 2013; Wang et al., 2013, 2010). On the other side, decreased levels of ROS induced by administration of antioxidants were shown to induce insulin resistance and impair insulin signalling (Goldstein et al., 2005; Xu et al., 2012; Zhou et al., 2013).

Additionally, the loss of EBI2 might lead, as previously mentioned, to upregulation of GPR18, which was shown to be involved in development of T2D (Rajaraman et al., 2016).

Altogether, these data indicate that EBI2 loss negatively impact T2D, suggesting that treatment with the EBI2 ligand 7α,25-OHC could improve insulin resistance during obesity.

6 | REFERENCES

Aherne, W., and Hull, D. (1966). Brown adipose tissue and heat production in the newborn infant. J. Pathol. Bacteriol. *91*, 223–234.

Alcalá, M., Calderon-Dominguez, M., Bustos, E., Ramos, P., Casals, N., Serra, D., Viana, M., and Herrero, L. (2017). Increased inflammation, oxidative stress and mitochondrial respiration in brown adipose tissue from obese mice. Sci. Rep. *7*.

Allegretti, M., Cesta, M.C., and Locati, M. (2016). Allosteric modulation of chemoattractant receptors. Front. Immunol.

Amisten, S., Braun, O.O., Bengtsson, A., and Erlinge, D. (2008). Gene expression profiling for the identification of G-protein coupled receptors in human platelets. Thromb. Res. *122*, 47–57.

Di Angelantonio, E., Bhupathiraju, S.N., Wormser, D., Gao, P., Kaptoge, S., de Gonzalez, A.B., Cairns, B.J., Huxley, R., Jackson, C.L., Joshy, G., et al. (2016). Body-mass index and all-cause mortality: individual-participant-data meta-analysis of 239 prospective studies in four continents. Lancet *388*, 776–786.

Arch, J.R.S. (2008). The discovery of drugs for obesity, the metabolic effects of leptin and variable receptor pharmacology: Perspectives from β3- adrenoceptor agonists. Naunyn. Schmiedebergs. Arch. Pharmacol.

Ardecky, R., Sergienko, E., Zou, J., Ganji, S., Brown, B., Sun, Q., Ma, C.-T., Hood, B., Nguyen, K., Vasile, S., et al. (2010). Functional Antagonists of EBI-2.

Ares, M.P., Pörn-Ares, M.I., Moses, S., Thyberg, J., Juntti-Berggren, L., Berggren, P., Hultgårdh-Nilsson, A., Kallin, B., and Nilsson, J. (2000). 7beta-hydroxycholesterol induces Ca(2+) oscillations, MAP kinase activation and apoptosis in human aortic smooth muscle cells. Atherosclerosis *153*, 23–35.

Assimacopoulos-Jeannet, F., Brichard, S., Rencurel, F., Cusin, I., and Jeanrenaud, B. (1995). In vivo

effects of hyperinsulinemia on lipogenic enzymes and glucose transporter expression in rat liver and adipose tissues. Metabolism. *44*, 228–233.

Basith, S., Cui, M., Macalino, S.J.Y., Park, J., Clavio, N.A.B., Kang, S., and Choi, S. (2018). Exploring G protein-coupled receptors (GPCRs) ligand space via cheminformatics approaches: Impact on rational drug design. Front. Pharmacol.

Benned-Jensen, T., Smethurst, C., Holst, P.J., Page, K.R., Sauls, H., Sivertsen, B., Schwartz, T.W., Blanchard, A., Jepras, R., and Rosenkilde, M.M. (2011). Ligand modulation of the Epstein-Barr virus-induced seven-transmembrane receptor EBI2: identification of a potent and efficacious inverse agonist. J. Biol. Chem. *286*, 29292–29302.

Benned-Jensen, T., Madsen, C.M., Arfelt, K.N., Smethurts, C., Blanchard, A., Jepras, R., and Rosenkilde, M.M. (2013). Small molecule antagonism of oxysterol-induced Epstein-Barr virus induced gene 2 (EBI2) activation. FEBS Open Bio *3*, 156–160.

Birkenbach, M., Josefsen, K., Yalamanchili, R., Lenoir, G., and Kieff, E. (1993). Epstein-Barr virus-induced genes: first lymphocyte-specific G protein-coupled peptide receptors. J. Virol. *67*, 2209–2220.

Björkhem, I. (2002). Do oxysterols control cholesterol homeostasis? J. Clin. Invest. *110*, 725–730.

Black, J.B., Premont, R.T., and Daaka, Y. (2016). Feedback regulation of G protein-coupled receptor signaling by GRKs and arrestins. Semin. Cell Dev. Biol. *50*, 95–104.

Brown, A.J., and Jessup, W. (1999). Oxysterols and atherosclerosis. Atherosclerosis *142*, 1–28.

Cannon, B., and Nedergaard, J. (2004). Brown Adipose Tissue: Function and Physiological Significance. Physiol. Rev. *84*, 277–359.

Caron, A., Reynolds, R.P., Castorena, C.M., Michael, N.J., Lee, C.E., Lee, S., Berdeaux, R., Scherer, P.E., and Elmquist, J.K. (2019). Adipocyte Gs but not Gi signaling regulates whole-body glucose homeostasis. Mol. Metab. *27*, 11–21.

Carrière, A., Fernandez, Y., Rigoulet, M., Pénicaud, L., and Casteilla, L. (2003). Inhibition of preadipocyte proliferation by mitochondrial reactive oxygen species. FEBS Lett.

Carrière, A., Jeanson, Y., Berger-Müller, S., André, M., Chenouard, V., Arnaud, E., Barreau, C., Walther, R., Galinier, A., Wdziekonski, B., et al. (2014). Browning of white adipose cells by intermediate metabolites: An adaptive mechanism to alleviate redox pressure. Diabetes.

Cerione, R.A., Staniszewski, C., Benovic, J.L., Lefkowitz, R.J., Caron, M.G., Gierschik, P., Somers, R., Spiegel, A.M., Codina, J., and Birnbaumer, L. (1985). Specificity of the functional interactions of the beta-adrenergic receptor and rhodopsin with guanine nucleotide regulatory proteins reconstituted in phospholipid vesicles. J. Biol. Chem. *260*, 1493–1500.

Chalmin, F., Rochemont, V., Lippens, C., Clottu, A., Sailer, A.W., Merkler, D., Hugues, S., and Pot, C. (2015). Oxysterols regulate encephalitogenic CD4+ T cell trafficking during central nervous system autoimmunity. J. Autoimmun. *56*, 45–55.

Chang, T.-Y., Reid, P.C., Sugii, S., Ohgami, N., Cruz, J.C., and Chang, C.C.Y. (2005). Niemann-Pick type C disease and intracellular cholesterol trafficking. J. Biol. Chem. *280*, 20917–20920.

Chouchani, E.T., Kazak, L., Jedrychowski, M.P., Lu, G.Z., Erickson, B.K., Szpyt, J., Pierce, K.A., Laznik-Bogoslavski, D., Vetrivelan, R., Clish, C.B., et al. (2016). Mitochondrial ROS regulate thermogenic energy expenditure and sulfenylation of UCP1. Nature.

Clapham, D.E., and Neer, E.J. (1997). G protein βγ subunits. Annu. Rev. Pharmacol. Toxicol. *37*, 167–203.

Clapham, J.C., and Arch, J.R.S. (2007). Thermogenic and metabolic antiobesity drugs: Rationale and opportunities. Diabetes, Obes. Metab.

Cousin, B., Cinti, S., Morroni, M., Raimbault, S., Ricquier, D., Pénicaud, L., and Casteilla, L. (1992). Occurrence of brown adipocytes in rat white adipose tissue: molecular and morphological characterization. J. Cell Sci. *103 (Pt 4)*, 931–942.

Cui, X., Nguyen, N.L.T., Zarebidaki, E., Cao, Q., Li, F., Zha, L., Bartness, T., Shi, H., and Xue, B. (2016).

Thermoneutrality decreases thermogenic program and promotes adiposity in high-fat diet-fed mice. Physiol. Rep. *4*.

Cypess, A.M., Lehman, S., Williams, G., Tal, I., Rodman, D., Goldfine, A.B., Kuo, F.C., Palmer, E.L., Tseng, Y.-H., Doria, A., et al. (2009). Identification and Importance of Brown Adipose Tissue in Adult Humans. N. Engl. J. Med. *360*, 1509–1517.

Cypess, A.M., Weiner, L.S., Roberts-Toler, C., Elía, E.F., Kessler, S.H., Kahn, P.A., English, J., Chatman, K., Trauger, S.A., Doria, A., et al. (2015). Activation of human brown adipose tissue by a β3-adrenergic receptor agonist. Cell Metab.

Deng, X., Sun, S., Wu, J., Kuei, C., Joseph, V., Liu, C., and Mani, N.S. (2016). Fluoro analogs of bioactive oxy-sterols: Synthesis of an EBI2 agonist with enhanced metabolic stability. Bioorg. Med. Chem. Lett. *26*, 4888–4891.

Dhanasekaran, N., and Dermott, J.M. (1996). Signaling by the G12 class of G proteins. Cell. Signal. *8*, 235–245.

Dobbins, R.L., Shearn, S.P., Byerly, R.L., Gao, F.F., Mahar, K.M., Napolitano, A., Nachbaur, G.J., and Le Monnier de Gouville, A.-C. (2013). GSK256073, a selective agonist of G-protein coupled receptor 109A (GPR109A) reduces serum glucose in subjects with type 2 diabetes mellitus. Diabetes, Obes. Metab. *15*, 1013–1021.

Drake, M.T., Shenoy, S.K., and Lefkowitz, R.J. (2006). Trafficking of G Protein–Coupled Receptors. Circ. Res. *99*, 570–582.

Dranka, B.P., Hill, B.G., and Darley-Usmar, V.M. (2010). Mitochondrial reserve capacity in endothelial cells: The impact of nitric oxide and reactive oxygen species. Free Radic. Biol. Med.

Echtay, K.S., and Brand, M.D. (2007). 4-Hydroxy-2-nonenal and uncoupling proteins: An approach for regulation of mitochondrial ROS production. In Redox Report, p.

Eishingdrelo, H. (2013). Minireview: Targeting GPCR Activated ERK Pathways for Drug Discovery. Curr. Chem. Genomics Transl. Med.

El-Brolosy, M.A., and Stainier, D.Y.R. (2017). Genetic compensation: A phenomenon in search of mechanisms. PLoS Genet. *13*.

Emgård, J., Kammoun, H., García-Cassani, B., Chesné, J., Parigi, S.M., Jacob, J.-M., Cheng, H.-W., Evren, E., Das, S., Czarnewski, P., et al. (2018). Oxysterol Sensing through the Receptor GPR183 Promotes the Lymphoid-Tissue-Inducing Function of Innate Lymphoid Cells and Colonic Inflammation. Immunity *48*, 120-132.e8.

Fabbrini, E., Sullivan, S., and Klein, S. (2010). Obesity and nonalcoholic fatty liver disease: Biochemical, metabolic, and clinical implications. Hepatology *51*, 679–689.

Fedorenko, A., Lishko, P.V., and Kirichok, Y. (2012). Mechanism of Fatty-Acid-Dependent UCP1 Uncoupling in Brown Fat Mitochondria. Cell *151*, 400–413.

Ferré, P., and Foufelle, F. (2007). SREBP-1c Transcription Factor and Lipid Homeostasis: Clinical Perspective. Horm. Res. Paediatr. *68*, 72–82.

Frayn, K.N. (2002). Adipose tissue as a buffer for daily lipid flux. Diabetologia *45*, 1201–1210.

Garcia-Marcos, M., Ghosh, P., and Farquhar, M.G. (2015). GIV/Girdin transmits signals from multiple receptors by triggering trimeric G protein activation. J. Biol. Chem. *290*, 6697–6704.

Gatto, D., Wood, K., Caminschi, I., Murphy-Durland, D., Schofield, P., Christ, D., Karupiah, G., and Brink, R. (2013). The chemotactic receptor EBI2 regulates the homeostasis, localization and immunological function of splenic dendritic cells. Nat. Immunol. *14*, 446–453.

Ge, H., Li, X., Weiszmann, J., Wang, P., … H.B.-, and 2008, undefined Activation of G protein-coupled receptor 43 in adipocytes leads to inhibition of lipolysis and suppression of plasma free fatty acids. Academic.Oup.Com.

Gessier, F., Preuss, I., Yin, H., Rosenkilde, M.M., Laurent, S., Endres, R., Chen, Y.A., Marsilje, T.H., Seuwen, K., Nguyen, D.G., et al. (2014). Identification and Characterization of Small Molecule Modulators of the Epstein–Barr Virus-Induced Gene 2 (EBI2) Receptor. J. Med. Chem. *57*, 3358–3368.

Gesta, S., Tseng, Y.-H., and Kahn, C.R. (2007). Developmental origin of fat: tracking obesity to its source. Cell *131*, 242–256.

Girousse, A., Tavernier, G., Valle, C., Moro, C., Mejhert, N., Dinel, A.L., Houssier, M., Roussel, B., Besse-Patin, A., Combes, M., et al. (2013). Partial Inhibition of Adipose Tissue Lipolysis Improves Glucose Metabolism and Insulin Sensitivity Without Alteration of Fat Mass. PLoS Biol. *11*.

Goldstein, B.J., Kalyankar, M., and Wu, X. (2005). Redox paradox: Insulin action is facilitated by insulin-stimulated reactive oxygen species with multiple potential signaling targets. Diabetes.

González-Muniesa, P., Mártinez-González, M.A., Hu, F.B., Després, J.P., Matsuzawa, Y., Loos, R.J.F., Moreno, L.A., Bray, G.A., and Martinez, J.A. (2017). Obesity. Nat. Rev. Dis. Prim.

Guillemot-Legris, O., Mutemberezi, V., Cani, P.D., and Muccioli, G.G. (2016a). Obesity is associated with changes in oxysterol metabolism and levels in mice liver, hypothalamus, adipose tissue and plasma. Sci. Rep.

Guillemot-Legris, O., Mutemberezi, V., and Muccioli, G.G. (2016b). Oxysterols in Metabolic Syndrome: From Bystander Molecules to Bioactive Lipids. Trends Mol. Med. *22*, 594–614.

Haemmerle, G., Zimmermann, R., Hayn, M., Theussl, C., Waeg, G., Wagner, E., Sattler, W., Magin, T.M., Wagner, E.F., and Zechner, R. (2002). Hormone-sensitive lipase deficiency in mice causes diglyceride accumulation in adipose tissue, muscle, and testis. J. Biol. Chem. *277*, 4806–4815.

Hanlon, C.D., and Andrew, D.J. (2015). Outside-in signaling - A brief review of GPCR signaling with a focus on the Drosophila GPCR family. J. Cell Sci. *128*, 3533–3542.

Hannedouche, S., Zhang, J., Yi, T., Shen, W., Nguyen, D., Pereira, J.P., Guerini, D., Baumgarten, B.U., Roggo, S., Wen, B., et al. (2011). Oxysterols direct immune cell migration via EBI2. Nature *475*, 524–527.

Harms, M., and Seale, P. (2013). Brown and beige fat: development, function and therapeutic potential. Nat. Med. *19*, 1252–1263.

Hauser, A.S., Chavali, S., Masuho, I., Jahn, L.J., Martemyanov, K.A., Gloriam, D.E., and Babu, M.M. (2018). Pharmacogenomics of GPCR Drug Targets. Cell *172*, 41-54.e19.

Heinig, M., Petretto, E., Wallace, C., Bottolo, L., Rotival, M., Lu, H., Li, Y., Sarwar, R., Langley, S.R., Bauerfeind, A., et al. (2010). A trans-acting locus regulates an anti-viral expression network and type 1 diabetes risk. Nature *467*, 460–464.

Hellmér, J., Marcus, C., Sonnenfeld, T., and Arner, P. (1992). Mechanisms for differences in lipolysis between human subcutaneous and omental fat cells. J. Clin. Endocrinol. Metab. *75*, 15–20.

Higgins, J.B., and Casey, P.J. (1994). In vitro processing of recombinant G protein gamma subunits. Requirements for assembly of an active beta gamma complex. J. Biol. Chem. *269*, 9067–9073.

Hoffmann, L.S., Etzrodt, J., Willkomm, L., Sanyal, A., Scheja, L., Fischer, A.W.C., Stasch, J.P., Bloch, W., Friebe, A., Heeren, J., et al. (2015). Stimulation of soluble guanylyl cyclase protects against obesity by recruiting brown adipose tissue. Nat. Commun. *6*.

Hu, F.B., Liu, S., and van Dam, R.M. (2001). Diet and risk of Type II diabetes: the role of types of fat and carbohydrate. Diabetologia *44*, 805–817.

Ikeda, S.R. (1996). Voltage-dependent modulation of N-type calcium channels by G-protein βγ subunits. Nature *380*, 255–258.

Ikeda, K., Maretich, P., and Kajimura, S. (2018). The Common and Distinct Features of Brown and Beige Adipocytes. Trends Endocrinol. Metab.

Iuliano, L. (2011). Pathways of cholesterol oxidation via non-enzymatic mechanisms. Chem. Phys. Lipids *164*, 457–468.

Jeanson, Y., Carrière, A., and Casteilla, L. (2015). A New Role for Browning as a Redox and Stress Adaptive Mechanism? Front. Endocrinol. (Lausanne). *6*, 158.

Jia, J., Conlon, T.M., Sarker, R.S., Taşdemir, D., Smirnova, N.F., Srivastava, B., Verleden, S.E.,

Güneş, G., Wu, X., Prehn, C., et al. (2018). Cholesterol metabolism promotes B-cell positioning during immune pathogenesis of chronic obstructive pulmonary disease. EMBO Mol. Med. *10*.

Jiang, X., Sidhu, R., Porter, F.D., Yanjanin, N.M., Speak, A.O., te Vruchte, D.T., Platt, F.M., Fujiwara, H., Scherrer, D.E., Zhang, J., et al. (2011). A sensitive and specific LC-MS/MS method for rapid diagnosis of Niemann-Pick C1 disease from human plasma. J. Lipid Res. *52*, 1435–1445.

Keuper, M., Jastroch, M., Yi, C.X., Fischer-Posovszky, P., Wabitsch, M., Tschöp, M.H., and Hofmann, S.M. (2014). Spare mitochondrial respiratory capacity permits human adipocytes to maintain ATP homeostasis under hypoglycemic conditions. FASEB J. *28*, 761–770.

Kharitonenkov, A., Shiyanova, T.L., Koester, A., Ford, A.M., Micanovic, R., Galbreath, E.J., Sandusky, G.E., Hammond, L.J., Moyers, J.S., Owens, R.A., et al. (2005). FGF-21 as a novel metabolic regulator. J. Clin. Invest.

Kir, S., White, J.P., Kleiner, S., Kazak, L., Cohen, P., Baracos, V.E., and Spiegelman, B.M. (2014). Tumour-derived PTH-related protein triggers adipose tissue browning and cancer cachexia. Nature.

Knudsen, J.G., Murholm, M., Carey, A.L., Biensø, R.S., Basse, A.L., Allen, T.L., Hidalgo, J., Kingwell, B.A., Febbraio, M.A., Hansen, J.B., et al. (2014). Role of IL-6 in exercise training- and cold-induced UCP1 expression in subcutaneous white adipose tissue. PLoS One.

Larsen, T.M., Toubro, S., Van Baak, M.A., Gottesdiener, K.M., Larson, P., Saris, W.H.M., and Astrup, A. (2002). Effect of a 28-d treatment with L-796568, a novel β 3-adrenergic receptor agonist, on energy expenditure and body composition in obese men. Am. J. Clin. Nutr.

Leoni, V., Masterman, T., Patel, P., Meaney, S., Diczfalusy, U., and Björkhem, I. (2003). Side chain oxidized oxysterols in cerebrospinal fluid and the integrity of blood-brain and blood-cerebrospinal fluid barriers. J. Lipid Res. *44*, 793–799.

Lettieri-Barbato, D. (2019). Redox control of non-shivering thermogenesis. Mol. Metab.

Ley, S.H., Hamdy, O., Mohan, V., and Hu, F.B. (2014). Prevention and management of type 2

diabetes: dietary components and nutritional strategies. Lancet *383*, 1999–2007.

Li, G., Xie, C., Lu, S., Nichols, R.G., Tian, Y., Li, L., Patel, D., Ma, Y., Brocker, C.N., Yan, T., et al. (2017). Intermittent Fasting Promotes White Adipose Browning and Decreases Obesity by Shaping the Gut Microbiota. Cell Metab.

Li, Z., Jiang, H., Xie, W., Zhang, Z., Smrcka, A. V., and Wu, D. (2000). Roles of PLC-β2 and -β3 and PI3kγ in chemoattractant-mediated signal transduction. Science (80-.). *287*, 1046–1049.

Liu, C., Wu, J., Zhu, J., Kuei, C., Yu, J., … J.S.-J. of B., and 2009, U. (2009). Lactate inhibits lipolysis in fat cells through activation of an orphan G-protein-coupled receptor, GPR81. ASBMB *284*, 2811–2822.

Liu, C., Yang, X. V., Wu, J., Kuei, C., Mani, N.S., Zhang, L., Yu, J., Sutton, S.W., Qin, N., Banie, H., et al. (2011). Oxysterols direct B-cell migration through EBI2. Nature *475*, 519–523.

Lizard, G., Deckert, V., Dubrez, L., Moisant, M., Gambert, P., and Lagrost, L. (1996). Induction of apoptosis in endothelial cells treated with cholesterol oxides. Am. J. Pathol. *148*, 1625–1638.

Logothetis, D.E., Kurachi, Y., Galper, J., Neer, E.J., and Clapham, D.E. (1987). The βγ subunits of GTP-Binding proteins activate the muscarinic K+ channel in heart. Nature *325*, 321–326.

Lundgren, M., Svensson, M., Lindmark, S., Renström, F., Ruge, T., and Eriksson, J.W. (2007). Fat cell enlargement is an independent marker of insulin resistance and “hyperleptinaemia.” Diabetologia.

Luo, L., and Liu, M. (2016). Adipose tissue in control of metabolism. J. Endocrinol. *231*, R77–R99.

Lupattelli, G., De Vuono, S., and Mannarino, E. (2011). Patterns of cholesterol metabolism: Pathophysiological and therapeutic implications for dyslipidemias and the metabolic syndrome. Nutr. Metab. Cardiovasc. Dis. *21*, 620–627.

Lütjohann, D., Meichsner, S., and Pettersson, H. (2012). Lipids in Alzheimer’s disease and their potential for therapy. Clin. Lipidol. *7*, 65–78.

Luttrell, L.M., Ferguson, S.S., Daaka, Y., Miller, W.E., Maudsley, S., Della Rocca, G.J., Lin, F., Kawakatsu, H., Owada, K., Luttrell, D.K., et al. (1999). Beta-arrestin-dependent formation of beta2 adrenergic receptor-Src protein kinase complexes. Science *283*, 655–661.

van Marken Lichtenbelt, W.D., Vanhommerig, J.W., Smulders, N.M., Drossaerts, J.M.A.F.L., Kemerink, G.J., Bouvy, N.D., Schrauwen, P., and Teule, G.J.J. (2009). Cold-Activated Brown Adipose Tissue in Healthy Men. N. Engl. J. Med. *360*, 1500–1508.

Meaney, S., Hassan, M., Sakinis, A., Lütjohann, D., Von Bergmann, K., Wennmalm, Å., Diczfalusy, U., and Björkhem, I. (2001). Evidence that the major oxysterols in human circulation originate from distinct pools of cholesterol: a stable isotope study Supplementary key words CYP7A • CYP27 • CYP46 • brain choles-terol • 18 O study.

Montague, C.T., Prins, J.B., Sanders, L., Digby, J.E., and O'Rahilly, S. (1997). Depot- and sex-specific differences in human leptin mRNA expression: implications for the control of regional fat distribution. Diabetes *46*, 342–347.

Moonen, M.P.B., Nascimento, E.B.M., and van Marken Lichtenbelt, W.D. (2019). Human brown adipose tissue: Underestimated target in metabolic disease? Biochim. Biophys. Acta - Mol. Cell Biol. Lipids.

Murdolo, G., Piroddi, M., Luchetti, F., Tortoioli, C., Canonico, B., Zerbinati, C., Galli, F., and Iuliano, L. (2013). Oxidative stress and lipid peroxidation by-products at the crossroad between adipose organ dysregulation and obesity-linked insulin resistance. Biochimie.

Nabben, M., Shabalina, I.G., Moonen-Kornips, E., Van Beurden, D., Cannon, B., Schrauwen, P., Nedergaard, J., and Hoeks, J. (2011). Uncoupled respiration, ROS production, acute lipotoxicity and oxidative damage in isolated skeletal muscle mitochondria from UCP3-ablated mice. Biochim. Biophys. Acta - Bioenerg.

Nannelli, G., Terzuoli, E., Giorgio, V., Donnini, S., Lupetti, P., Giachetti, A., Bernardi, P., and Ziche, M. (2018). ALDH2 activity reduces mitochondrial oxygen reserve capacity in endothelial cells and induces senescence properties. Oxid. Med. Cell. Longev. *2018*.

Napolitano, L., and Fawcett, D. (1958). The fine structure of brown adipose tissue in the newborn mouse and rat. J. Biophys. Biochem. Cytol. *4*, 685–692.

Nedergaard, J., and Cannon, B. (2014). The browning of white adipose tissue: Some burning issues. Cell Metab. *20*, 396–407.

Nedergaard, J., Bengtsson, T., and Cannon, B. (2007). Unexpected evidence for active brown adipose tissue in adult humans. Am. J. Physiol. Endocrinol. Metab. *293*, E444-52.

Nevius, E., Pinho, F., Dhodapkar, M., Jin, H., Nadrah, K., Horowitz, M.C., Kikuta, J., Ishii, M., and Pereira, J.P. (2015). Oxysterols and EBI2 promote osteoclast precursor migration to bone surfaces and regulate bone mass homeostasis. J. Exp. Med. *212*, 1931–1946.

Nguyen, H.M., Mejia, E.M., Chang, W., Wang, Y., Watson, E., On, N., Miller, D.W., and Hatch, G.M. (2016). Reduction in cardiolipin decreases mitochondrial spare respiratory capacity and increases glucose transport into and across human brain cerebral microvascular endothelial cells. J. Neurochem. *139*, 68–80.

Novershtern, N., Subramanian, A., Lawton, L.N., Mak, R.H., Haining, W.N., McConkey, M.E., Habib, N., Yosef, N., Chang, C.Y., Shay, T., et al. (2011). Densely interconnected transcriptional circuits control cell states in human hematopoiesis. Cell *144*, 296–309.

Oakley, R.H., Laporte, S.A., Holt, J.A., Caron, M.G., and Barak, L.S. (2000). Differential affinities of visual arrestin, βarrestin1, and βarrestin2 for G protein-coupled receptors delineate two major classes of receptors. J. Biol. Chem. *275*, 17201–17210.

Ory, D.. (2000). Niemann-Pick type C: A disorder of cellular cholesterol trafficking. Biochim. Biophys. Acta - Mol. Cell Biol. Lipids *1529*, 331–339.

Palczewski, K., Buczyłko, J., … M.K.-J. of B., and 1991, undefined (1991). Mechanism of rhodopsin kinase activation. ASBMB.

Pereira, J.P., Kelly, L.M., Xu, Y., and Cyster, J.G. (2009). EBI2 mediates B cell segregation between the outer and centre follicle. Nature *460*, 1122–1126.

Petrovic, N., Walden, T.B., Shabalina, I.G., Timmons, J.A., Cannon, B., and Nedergaard, J. (2010). Chronic peroxisome proliferator-activated receptor γ (PPARγ) activation of epididymally derived white adipocyte cultures reveals a population of thermogenically competent, UCP1-containing adipocytes molecularly distinct from classic brown adipocytes. J. Biol. Chem. *285*, 7153–7164.

Preuss, I., Ludwig, M.-G., Baumgarten, B., Bassilana, F., Gessier, F., Seuwen, K., and Sailer, A.W. (2014). Transcriptional regulation and functional characterization of the oxysterol/EBI2 system in primary human macrophages. Biochem. Biophys. Res. Commun. *446*, 663–668.

Rajaraman, G., Simcocks, A., Hryciw, D.H., Hutchinson, D.S., and McAinch, A.J. (2016). G protein coupled receptor 18: A potential role for endocannabinoid signaling in metabolic dysfunction. Mol. Nutr. Food Res. *60*, 92–102.

Ravussin, Y., Xiao, C., Gavrilova, O., and Reitman, M.L. (2014). Effect of intermittent cold exposure on brown fat activation, obesity, and energy Homeostasis in mice. PLoS One *9*.

Reunert, J., Fobker, M., Kannenberg, F., Du Chesne, I., Plate, M., Wellhausen, J., Rust, S., and Marquardt, T. (2016). Rapid Diagnosis of 83 Patients with Niemann Pick Type C Disease and Related Cholesterol Transport Disorders by Cholestantriol Screening. EBioMedicine *4*, 170–175.

Rial, E., Poustie, A., and Nicholls, D.G. (1983). Brown-adipose-tissue mitochondria: the regulation of the 32 000-Mr uncoupling protein by fatty acids and purine nucleotides. Eur. J. Biochem. *137*, 197–203.

Ribas, G.S., Pires, R., Coelho, J.C., Rodrigues, D., Mescka, C.P., Vanzin, C.S., Biancini, G.B., Negretto, G., Wayhs, C.A.Y., Wajner, M., et al. (2012). Oxidative stress in Niemann-Pick type C patients: a protective role of N-butyl-deoxynojirimycin therapy. Int. J. Dev. Neurosci. *30*, 439–444.

Robidoux, J., Martin, T.L., and Collins, S. (2004). β-3 adrenergic receptor and regulation of energy expenditure : A Family Affair. Annu. Rev. Pharmacol. Toxicol. *44*, 297–323.

Van Rooyen, D.M., Gan, L.T., Yeh, M.M., Haigh, W.G., Larter, C.Z., Ioannou, G., Teoh, N.C., and Farrell, G.C. (2013). Pharmacological cholesterol lowering reverses fibrotic NASH in obese,

diabetic mice with metabolic syndrome. J. Hepatol. *59*, 144–152.

Rosenkilde, M.M., Benned-Jensen, T., Andersen, H., Holst, P.J., Kledal, T.N., Lüttichau, H.R., Larsen, J.K., Christensen, J.P., and Schwartz, T.W. (2006). Molecular pharmacological phenotyping of EBI2. An orphan seven-transmembrane receptor with constitutive activity. J. Biol. Chem. *281*, 13199–13208.

Russell, D.W. (2003). The enzymes, regulation, and genetics of bile acid synthesis. Annu. Rev. Biochem. *72*, 137–174.

Rutkowska, A., Preuss, I., Gessier, F., Sailer, A.W., and Dev, K.K. (2015). EBI2 regulates intracellular signaling and migration in human astrocyte. Glia *63*, 341–351.

Rutkowska, A., Shimshek, D.R., Sailer, A.W., and Dev, K.K. (2018). EBI2 regulates pro-inflammatory signalling and cytokine release in astrocytes. Neuropharmacology *133*, 121–128.

Sanders, M.P.A., Fleuren, W.W.M., Verhoeven, S., van den Beld, S., Alkema, W., de Vlieg, J., and Klomp, J.P.G. (2011). Ss-TEA: Entropy based identification of receptor specific ligand binding residues from a multiple sequence alignment of class A GPCRs. BMC Bioinformatics *12*.

Schlein, C., Talukdar, S., Heine, M., Fischer, A.W., Krott, L.M., Nilsson, S.K., Brenner, M.B., Heeren, J., and Scheja, L. (2016). FGF21 lowers plasma triglycerides by accelerating lipoprotein catabolism in white and brown adipose tissues. Cell Metab.

Seale, P., Bjork, B., Yang, W., Kajimura, S., Chin, S., Kuang, S., Scimè, A., Devarakonda, S., Conroe, H.M., Erdjument-Bromage, H., et al. (2008). PRDM16 controls a brown fat/skeletal muscle switch. Nature *454*, 961–967.

Shabalina, I.G., Hoeks, J., Kramarova, T. V., Schrauwen, P., Cannon, B., and Nedergaard, J. (2010). Cold tolerance of UCP1-ablated mice: A skeletal muscle mitochondria switch toward lipid oxidation with marked UCP3 up-regulation not associated with increased basal, fatty acid- or ROS-induced uncoupling or enhanced GDP effects. Biochim. Biophys. Acta - Bioenerg.

Shabalina, I.G., Vrbacký, M., Pecinová, A., Kalinovich, A. V., Drahota, Z., Houštěk, J., Mráček, T.,

Cannon, B., and Nedergaard, J. (2014). ROS production in brown adipose tissue mitochondria: The question of UCP1-dependence. Biochim. Biophys. Acta - Bioenerg.

Shen, Z.-J., Hu, J., Esnault, S., Dozmorov, I., and Malter, J.S. (2015). RNA Seq profiling reveals a novel expression pattern of TGF-β target genes in human blood eosinophils. Immunol. Lett. *167*, 1–10.

Shen, Z.-J., Hu, J., Kashi, V.P., Kelly, E.A., Denlinger, L.C., Lutchman, K., McDonald, J.G., Jarjour, N.N., and Malter, J.S. (2017). Epstein-Barr Virus–induced Gene 2 Mediates Allergen-induced Leukocyte Migration into Airways. Am. J. Respir. Crit. Care Med. *195*, 1576–1585.

Stephens, L.R., Eguinoa, A., Erdjument-Bromage, H., Lui, M., Cooke, F., Coadwell, J., Smrcka, A.S., Thelen, M., Cadwallader, K., Tempst, P., et al. (1997). The Gβγ/sensitivity of a PI3K is dependent upon a tightly associated adaptor, p101. Cell *89*, 105–114.

Tan, C.Y., and Vidal-Puig, A. (2008). Adipose tissue expandability: the metabolic problems of obesity may arise from the inability to become more obese. Biochem. Soc. Trans. *36*, 935–940.

Tang, W.J., and Gilman, A.G. (1991). Type-specific regulation of adenylyl cyclase by G protein βγ subunits. Science (80-.). *254*, 1500–1503.

Tint, G.S., Pentchev, P., Xu, G., Batta, A.K., Shefer, S., Salen, G., and Honda, A. (1998). Cholesterol and oxygenated cholesterol concentrations are markedly elevated in peripheral tissue but not in brain from mice with the Niemann-Pick type C phenotype. J. Inherit. Metab. Dis. *21*, 853–863.

Tremblay-Franco, M., Zerbinati, C., Pacelli, A., Palmaccio, G., Lubrano, C., Ducheix, S., Guillou, H., and Iuliano, L. (2015). Effect of obesity and metabolic syndrome on plasma oxysterols and fatty acids in human. Steroids *99*, 287–292.

Tseng, Y.H., Kokkotou, E., Schulz, T.J., Huang, T.L., Winnay, J.N., Taniguchi, C.M., Tran, T.T., Suzuki, R., Espinoza, D.O., Yamamoto, Y., et al. (2008). New role of bone morphogenetic protein 7 in brown adipogenesis and energy expenditure. Nature.

Vanier, M.T., Gissen, P., Bauer, P., Coll, M.J., Burlina, A., Hendriksz, C.J., Latour, P., Goizet, C.,

Welford, R.W.D., Marquardt, T., et al. (2016). Diagnostic tests for Niemann-Pick disease type C (NP-C): A critical review. Mol. Genet. Metab. *118*, 244–254.

Villarroya, F., Peyrou, M., and Giralt, M. (2017). Transcriptional regulation of the uncoupling protein-1 gene. Biochimie *134*, 86–92.

Virtanen, K.A., Lidell, M.E., Orava, J., Heglind, M., Westergren, R., Niemi, T., Taittonen, M., Laine, J., Savisto, N.-J., Enerbäck, S., et al. (2009). Functional Brown Adipose Tissue in Healthy Adults. N. Engl. J. Med. *360*, 1518–1525.

Vögler, O., Barceló, J.M., Ribas, C., and Escribá, P. V. (2008). Membrane interactions of G proteins and other related proteins. Biochim. Biophys. Acta - Biomembr. *1778*, 1640–1652.

De Vries, L., Zheng, B., Fischer, T., Elenko, E., and Farquhar, M.G. (2000). The Regulator of G Protein Signaling Family. Annu. Rev. Pharmacol. Toxicol. *40*, 235–271.

Wajchenberg, B.L. (2000). Subcutaneous and Visceral Adipose Tissue: Their Relation to the Metabolic Syndrome. Endocr. Rev. *21*, 697–738.

Wallenius, K., Thalén, P., Björkman, J.-A., Johannesson, P., Wiseman, J., Böttcher, G., Fjellström, O., and Oakes, N.D. (2017). Involvement of the metabolic sensor GPR81 in cardiovascular control. JCI Insight *2*.

Wang, C.H., Wang, C.C., Huang, H.C., and Wei, Y.H. (2013). Mitochondrial dysfunction leads to impairment of insulin sensitivity and adiponectin secretion in adipocytes. FEBS J.

Wang, T., Si, Y., Shirihai, O.S., Si, H., Schultz, V., Corkey, R.F., Hu, L., Deeney, J.T., Guo, W., and Corkey, B.E. (2010). Respiration in adipocytes is inhibited by reactive oxygen species. Obesity.

Wanke, F., Moos, S., Croxford, A.L., Heinen, A.P., Gräf, S., Kalt, B., Tischner, D., Zhang, J., Christen, I., Bruttger, J., et al. (2017). EBI2 Is Highly Expressed in Multiple Sclerosis Lesions and Promotes Early CNS Migration of Encephalitogenic CD4 T Cells. Cell Rep. *18*, 1270–1284.

Wettschureck, N., and Offermanns, S. (2005). Mammalian G Proteins and Their Cell Type Specific

Functions. Physiol. Rev. *85*, 1159–1204.

Wooten, J.S., Wu, H., Raya, J., Perrard, X.D., Gaubatz, J., and Hoogeveen, R.C. (2014). The Influence of an Obesogenic Diet on Oxysterol Metabolism in C57BL/6J Mice. Cholesterol *2014*.

Worthmann, A., John, C., Rühlemann, M.C., Baguhl, M., Heinsen, F.A., Schaltenberg, N., Heine, M., Schlein, C., Evangelakos, I., Mineo, C., et al. (2017). Cold-induced conversion of cholesterol to bile acids in mice shapes the gut microbiome and promotes adaptive thermogenesis. Nat. Med.

Wu, J., Boström, P., Sparks, L.M., Ye, L., Choi, J.H., Giang, A.H., Khandekar, M., Virtanen, K.A., Nuutila, P., Schaart, G., et al. (2012). Beige adipocytes are a distinct type of thermogenic fat cell in mouse and human. Cell *150*, 366–376.

Wyss, A., Raselli, T., Perkins, N., Ruiz, F., Schmelczer, G., Klinke, G., Moncsek, A., Roth, R., Spalinger, M.R., Hering, L., et al. (2019). The EBI2-oxysterol axis promotes the development of intestinal lymphoid structures and colitis. Mucosal Immunol. *12*, 733–745.

Xu, J., Kulkarni, S.R., Donepudi, A.C., More, V.R., and Slitt, A.L. (2012). Enhanced Nrf2 activity worsens insulin resistance, impairs lipid accumulation in adipose tissue, and increases hepatic steatosis in leptin-deficient mice. Diabetes.

Yang, T., Gao, X., Sandberg, M., Zollbrecht, C., Zhang, X.M., Hezel, M., Liu, M., Peleli, M., Lai, E.Y., Harris, R.A., et al. (2015). Abrogation of adenosine A1 receptor signalling improves metabolic regulation in mice by modulating oxidative stress and inflammatory responses. Diabetologia *58*, 1610–1620.

Yetkin-Arik, B., Vogels, I.M.C., Neyazi, N., van Duinen, V., Houtkooper, R.H., van Noorden, C.J.F., Klaassen, I., and Schlingemann, R.O. (2019). Endothelial tip cells in vitro are less glycolytic and have a more flexible response to metabolic stress than non-tip cells. Sci. Rep. *9*.

Yin, H., Xu, L., and Porter, N.A. (2011). Free Radical Lipid Peroxidation: Mechanisms and Analysis. Chem. Rev. *111*, 5944–5972.

Young, P., Arch, J.R.S., and Ashwell, M. (1984). Brown adipose tissue in the parametrial fat pad of

the mouse. FEBS Lett. *167*, 10–14.

Yuan, X.M., Li, W., Brunk, U.T., Dalen, H., Chang, Y.H., and Sevanian, A. (2000). Lysosomal destabilization during macrophage damage induced by cholesterol oxidation products. Free Radic. Biol. Med. *28*, 208–218.

Von Zastrow, M. (2001). Endocytosis and downregulation of G protein-coupled receptors. In Parkinsonism and Related Disorders, pp. 265–271.

Zhao, R.Z., Jiang, S., Zhang, L., and Yu, Z. Bin (2019). Mitochondrial electron transport chain, ROS generation and uncoupling (Review). Int. J. Mol. Med. *44*, 3–15.

Zhou, J., Huang, K., and Lei, X.G. (2013). Selenium and diabetes - Evidence from animal studies. Free Radic. Biol. Med.

Zimmermann, R., Strauss, J.G., Haemmerle, G., Schoiswohl, G., Birner-Gruenberger, R., Riederer, M., Lass, A., Neuberger, G., Eisenhaber, F., Hermetter, A., et al. (2004). Fat Mobilization in Adipose Tissue Is Promoted by Adipose Triglyceride Lipase. Science (80-.). *306*, 1383–1386.

Zingaretti, M.C., Crosta, F., Vitali, A., Guerrieri, M., Frontini, A., Cannon, B., Nedergaard, J., and Cinti, S. (2009). The presence of UCP1 demonstrates that metabolically active adipose tissue in the neck of adult humans truly represents brown adipose tissue. FASEB J. *23*, 3113–3120.

Zmysłowski, A., and Szterk, A. (2017). Current knowledge on the mechanism of atherosclerosis and pro-atherosclerotic properties of oxysterols. Lipids Health Dis. *16*, 188.

7 | SUMMARY

Weight-related diseases are common and often fatal conditions characterized by an imbalance between energy intake and energy expenditure. Obesity and weight gain related diseases such as type 2-diabetes have reached in the last decades pandemic levels. Importantly, excessive weight loss characterizes a broad spectrum of pathological conditions, from cancer cachexia to anorexia-nervosa.

Adipose tissue activity is positively regulated by $G_{\alpha s}$-coupled receptors such as β3-adrenergic receptors, causing an intracellular increase of cAMP and the following stimulation of lipolysis and energy expenditure. Oppositely, activation of $G_{\alpha i}$-coupled receptors causes inhibition of cAMP production and lipolysis. Among $G_{\alpha i}$-coupled receptors, the Epstein-Barr virus-induced G protein-coupled receptor 2 (EBI2) was found to be highly expressed on adipocytes and adipose tissues; however, its possible role in regulating energy expenditure and adipose tissue function has not been investigated so far. In this study, the effect of EBI2 and its ligand 7α,25-dihydroxycholesterol (7α,25-OHC) was studied on adipocytes, adipose tissue and whole-body metabolism.

EBI2 stimulation was able to potently decrease activation of brown adipocytes, decreasing intracellular cAMP levels and counteracting norepinephrine-induced lipolysis. *In vivo*, EBI2 deletion increased energy expenditure in response to an acute cold stimulus. EBI2 acute activation following *in vivo* injection of 7α,25-OHC potently influenced the energy expenditure in mice, dramatically decreasing oxygen consumption. The data on the long-term effects of EBI2 loss or stimulation are less clear, and require further studies.

Thus, EBI2 is involved in regulating acutely adipose tissue activity and energy expenditure, and in the long term in the development of type 2-diabetes.

8 | PUBLICATIONS AND ABSTRACTS

Publications

Schmidleithner L., Thabet Y., Schönfeld E., Köhne M., Sommer D., Abdullah Z., Sadlon T., Osei-Sarpong C., Subbaramaiah K., Copperi F., Haendler K., Varga T., Schanz O., Bourry S., Bassler K., Krebs W., Peters A.E., Baumgart A.K., Schneeweiss M., Klee K., Schmidt S.V., Nüssing S., Sander J., Ohkura N., Waha A., Sparwasser T., Wunderlich F.T., Förster I., Ulas T., Weighardt H., Sakaguchi S., Pfeifer A., Blüher M., Dannenberg A.J., Ferreirós N., Muglia L.J., Wickenhauser C., Barry S.C., Schultze J.L., Beyer M. (2019). Enzymatic Activity of HPGD in Treg Cells Suppresses Tconv Cells to Maintain Adipose Tissue Homeostasis and Prevent Metabolic Dysfunction. Immunity. 21;50(5):1232-1248.e14.

Campa C.C., Silva R.L., Margaria J.P., Pirali T., Mattos M.S., Kraemer L.R., Reis D.C, Grosa G., Copperi F., Dalmarco E.M., Lima-Júnior R.C.P., Aprile S., Sala V., Dal Bello F., Prado D.S., Alves-Filho J.C., Medana C., Cassali G.D., Tron G.C., Teixeira M.M., Ciraolo E., Russo R.C., Hirsch E. (2018). Inhalation of the prodrug PI3K inhibitor CL27c improves lung function in asthma and fibrosis. Nat Commun. 12;9(1):5232.

Campa C.C., Margaria J.P., Derle A., Del Giudice M., De Santis M.C., Gozzelino L., Copperi F., Bosia C., Hirsch E. (2018) Rab11 activity and PtdIns(3)P turnover removes recycling cargo from endosomes. Nat Chem Biol. 14(8):801-810.

Campa C.C., Germena G., Ciraolo E., Copperi F., Sapienza A., Franco I., Ghigo A., Camporeale A., Di Savino A., Martini M., Perino A., Megens R.T., Kurz A.R., Scheiermann C., Sperandio M., Gamba A., Hirsch E. (2016) Rac signal adaptation controls neutrophil mobilization from the bone marrow. Sci Signal. 9(459):ra124.